Cell Lysis and Consumption during Cannibalistic Growth of *Bacillus subtilis* 168

Dissertation

der Mathematisch-Naturwissenschaftlichen Fakultät

der Eberhard Karls Universität Tübingen

zur Erlangung des Grades eines

Doktors der Naturwissenschaften

(Dr. rer. nat.)

vorgelegt von

Maraike Müller

aus Göppingen

Tübingen

2024

Gedruckt mit Genehmigung der Mathematisch-Naturwissenschaftlichen Fakultät der Eberhard Karls Universität Tübingen.

Tag der mündlichen Qualifikation:	06.05.2024
Dekan:	Prof. Dr. Thilo Stehle
1. Berichterstatter/-in:	apl. Prof. Dr. Christoph Mayer
2. Berichterstatter/-in:	Prof. Dr. Karl Forchhammer

Faber est suae quisque fortunae.

Appius Claudius Caecus

Erklärung

Ich erkläre hiermit, dass ich die zur Promotion eingereichte Arbeit selbständig verfasst, nur die angegebenen Quellen und Hilfsmittel benutzt und Stellen, die wörtlich oder inhaltlich nach den Werken anderer Autoren entnommen sind, als solche gekennzeichnet habe.

……

Unterschrift

Tübingen, den

Table of contents

Summary

Bacillus subtilis is a Gram-positive organism that forms long-lasting endospores under unfavorable environmental conditions, such as nutrient limitation. As sporulation is a time and energy-consuming developmental process, *B. subtilis* seeks to delay entry into sporulation until absolutely necessary. In a survival strategy called cannibalism a subpopulation of cells, the “cannibals”, secrete two proteinaceous toxins, SKF and SDP, to attack sibling cells. These toxins induce cell death and lysis in the prey cell, which involves endogenous, cell wall lytic enzymes (i.e. autolysins). Ultimately, the cannibals feed on the nutrients released by the decay of prey cells and sporulation of *B. subtilis* is delayed. Thus, a cell population is sacrificed for the sake of survival of the species.

The first aim of this study was to investigate the role of autolysins in cannibalism and to identify which autolysins are required for prey lysis. The focus was set on the major autolysins of *B. subtilis* LytC, LytD, LytE, and LytF as it was reported that a mutant lacking all four autolysins fails to lyse during sporulation. Cannibalistic behavior was monitored with agar diffusion experiments using toxin-expressing and autolysin-defective cells as well as isolated SDP toxin, along with fluorescence microscopy of labeled strains. The role of specific autolysins was shown to be highly dependent on preculturing conditions, and no particular autolysin appeared to be absolutely essential.

The second aim was to investigate the flow of nutrients from lysed prey cells to the cannibals, with an emphasis on the salvage of cell wall fragments. Therefore, a cell wall labeling strain was generated in this study, which can serve as a tool to study cell wall decay and consumption during cannibalism. *B. subtilis* degrades and recycles its own peptidoglycan cell wall also during vegetative growth, when the cell wall undergoes a steady remodeling and turnover. Known to be important in this process is the *N*-acetyl-muramic acid (MurNAc) recycling operon, which encodes the genes required for the salvage of the cell wall sugar MurNAc. In this operon next to the exo-*N*-acetylgluco-saminidase *nagZ* and the *N*-acetylmuramyl-L-alanine amidase *amiE*, a gene of previously unknown function *ybbC* (*namZ*) is located. We identified *ybbC* as the coding gene for a novel peptidoglycan recycling enzyme that functions as unique exo-lytic β-*N*-acetyl-muramidase (named NamZ). The enzyme was characterized by HPLC-MS analyses of culture supernatants of *B. subtilis* mutants, showing differences in the cell wall fragment releases as well as fragment release upon peptidoglycan digestions using combinations of purified NagZ, AmiE and NamZ enzymes. A biochemical characterization using the

chromogenic substrate pNP-MurNAc as well as the purified minimal natural substrate MurNAc-GlcNAc, reveled that NamZ is identical to an enzyme reported in earlier studies ((Del Rio and Berkeley 1976); DOI: 10.1111/j.1432-1033.1976.tb10382.x) that was not linked to a coding gene. NamZ is the founding member of a novel family of glycosyl hydrolases, now classified as GH171 within the “carbohydrate-active enzymes” CAZy-database (www.cazy.GH171.html) and involved in the sequential hydrolysis of peptidoglycan from the non-reducing end, in concert with the exo-lytic *N*-acetylglucosaminidase NagZ and the exo-acting amidase AmiE. The role of NamZ and the entire MurNAc recycling cluster during sporulation still remains enigmatic.

Zusammenfassung

Bacillus subtilis ist ein Gram-positiver Organismus, der unter ungünstigen Umweltbedingungen, wie beispielsweise Nährstoffmangel, langlebige Endosporen bildet. Da die Sporenbildung ein zeit- und energieaufwändiger Entwicklungsprozess ist, versucht *B. subtilis*, den Eintritt in die Sporenbildung so lange hinauszuzögern, bis es absolut notwendig ist In einer Überlebensstrategie, die als Kannibalismus bezeichnet wird, produziert eine Subpopulation von Zellen, die „Kannibalen“, zwei Protein-Toxine, SKF und SDP, um Geschwisterzellen anzugreifen. Diese Toxine induzieren den Zelltod und die Lyse in der Opferzelle, an der endogene, Zellwand-lytische Enzyme (z.B. Autolysine) beteiligt sind. Letztlich ernähren sich die Kannibalen von den Nährstoffen, die durch den Zerfall der Opferzellen freigesetzt werden, und die Sporulation von *B. subtilis* wird verzögert. Dadurch wird eine Zellpopulation für das Überleben der Art geopfert.

Das erste Ziel dieser Arbeit war es, die Rolle der Autolysine im Kannibalismus zu untersuchen und herauszufinden, welche Autolysine für die Lyse der Opfer erforderlich sind. Der Schwerpunkt lag auf den Hauptautolysinen LytC, LytD, LytE und LytF von *B. subtilis*, da berichtet wurde, dass eine Mutante, der alle vier Autolysine fehlen, während der Sporulation nicht lysiert. Das kannibalistische Verhalten wurde mit Agardiffusionsexperimenten unter Verwendung von Toxin-exprimierenden und Autolysin-defekten Zellen sowie isoliertem SDP-Toxin und Fluoreszenzmikroskopie von markierten Stämmen untersucht. Es zeigte sich, dass die Rolle spezifischer Autolysine scheint in hohem Maße von den Vorkulturbedingungen abhängig zu sein, und kein bestimmtes Autolysin scheint absolut wesentlich zu sein.

Das zweite Ziel war die Untersuchung des Nährstoffflusses von lysierten Opferzellen zu den Kannibalen, wobei der Schwerpunkt auf der Verwertung von Zellwandfragmenten lag. Daher wurde in dieser Arbeit ein Zellwandmarkierungsstamm generiert, der als Werkzeug zur Untersuchung des Zellwandabbaus und -verbrauchs bei Kannibalismus dienen kann. *B. subtilis* baut seine eigene Zellwand aus Peptidoglykan ab recycelt sie auch während des vegetativen Wachstums, bei dem die Zellwand einem ständigen Umbau und Umsatz unterliegt. Eine wichtige Rolle bei diesem Prozess spielt das *N*-Acetylmuraminsäure (MurNAc)-Recycling-Operon, das für die Gene kodiert, die für die Verwertung des Zellwandzuckers MurNAc erforderlich sind. In diesem Operon befindet sich neben der Exo-*N*-Acetylglukosaminidase *nagZ* und der *N*-Acetylmuramyl-L-Alanin-Amidase *amiE* ein Gen mit bisher unbekannter Funktion *ybbC* (*namZ*). Wir konnten *ybbC* als das

kodierende Gen für ein neuartiges Peptidoglykan-Recycling-Enzym identifizieren, das als einzigartige Exo-lytische β-N-Acetylmuramidase (NamZ) fungiert. Das Enzym wurde mittels HPLC-MS-Analysen von Kulturüberständen von *B. subtilis*-Mutanten charakterisiert, die Unterschiede in der Freisetzung von Zellwandfragmenten, sowie in der Freisetzung von Fragmenten bei Peptidoglykanverdau unter Verwendung von Kombinationen der gereinigten Enzyme NagZ, AmiE und NamZ zeigten. Eine biochemische Charakterisierung unter Verwendung des chromogenen Substrats pNP-MurNAc, sowie des gereinigten minimalen natürlichen Substrats MurNAc-GlcNAc ergab, dass NamZ mit einem Enzym identisch ist, über das in früheren Studien berichtet wurde ((Del Rio and Berkeley 1976); DOI: 10.1111/j.1432-1033.1976.tb10382.x), welches aber nicht mit einem kodierenden Gen assoziiert war. NamZ ist das Gründungsmitglied einer neuen Familie von Glykosylhydrolasen, die jetzt als GH171 in der CAZy-Datenbank für „kohlenhydrataktive Enzyme“ (www.cazy.GH171.html) klassifiziert ist und zusammen mit der Exo-lytischen *N*-Acetylglukosaminidase NagZ und der Exo-aktiven Amidase AmiE an der sequenziellen Hydrolyse von Peptidoglykan vom nicht-reduzierenden Ende beteiligt ist. Die Rolle von NamZ und des gesamten MurNAc-Recycling-Clusters bei der Sporulation ist nach wie vor rätselhaft.

1 Introduction

1.1 *Bacillus subtilis*, a model organism of cell differentiation

Bacillus subtilis is a rod-shaped, aerobe, Gram-positive bacterium, which is found prevalent in soils. It is a well-studied model organism, examined in laboratories particularly to understand the molecular mechanisms of cell differentiation (Priest 1993). *B. subtilis* is a survivalist and withstands harsh environmental conditions such as nutrient limitation as well as changes in pH or temperature. One strategy to ensure survival during nutrient limitation is the formation of long-lasting endospores. In this process, a subpopulation of cells that first senses the deprival of supplements, like carbon, nitrogen, and phosphate, activates the global regulator Spo0A by phosphorylation via a phosphorelay (Piggot and Hilbert 2004, Claverys and Havarstein 2007). To trigger the sporulation process in these cells, Spo0A-P must accumulate to higher concentrations. Endospore formation is a developmental process of no return that involves autolytic processes and a major remodeling of the cell envelope (Figure 1) (Smith *et al.* 1996, Dworkin and Losick 2005, Vollmer *et al.* 2008b). This developmental process occurs during biofilm growth (Lewis 2000) and is preceded by the cannibalism of sibling cells (González-Pastor *et al.* 2003).

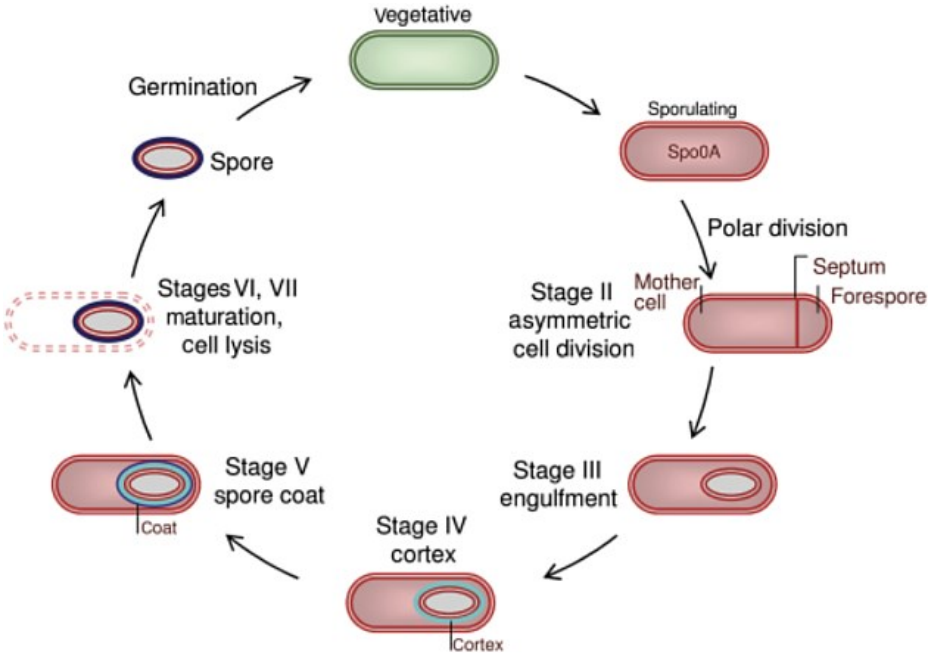

Figure 1 | Sporulation process and spore formation of *B. subtilis*. A vegetative growing cell initiates sporulation by expression and phosphorylation of the regulator Spo0A. First, the asymmetric septum is built, from which a forespore and a mother cell is formed. Second, the forespore is engulfed and the spore cortex assembles. Afterwards, the spore coat is built, the spore matures, and the spore is released by lysis of the mother cell. When conditions become more favorable again, the spore germinates and turns into a vegetatively growing cell. The figure was modified after (González-Pastor 2011).

Cannibalism, i.e. the feeding on sibling cells, is another strategy used by *B. subtilis* to overcome nutrient limitation, thereby delaying entry into the more extensive sporulation process. Cannibalism involves autolytic processes and is based on the heterogeneity of a starving cell population, where some cells recognize the nutrient limitation earlier than others (González-Pastor *et al.* 2003). Cells that sense nutrient limitation activate/phosphorylate the global regulator Spo0A (González-Pastor *et al.* 2003). In contrast to activation of the sporulation process, cannibalism is triggered by lower levels of Spo0A-P in the cells and causes the expression of genes that are responsible for the formation and secretion of cannibalism toxins as well as the expression of immunity factors (Figure 2) (Ellermeier *et al.* 2006, Liu *et al.* 2010, González-Pastor 2011). Cannibalism is a developmental process that constitutes an insufficiently understood phase of bacterial growth, the decay or decline phase, in which cell numbers are drastically reduced (as opposed to the exponential phase). In particular, the role of cell wall lytic enzymes in cell lysis (autolysins) as well as the cell wall degradation in prey cells and recovery routes used by the cannibal cells remain unclear.

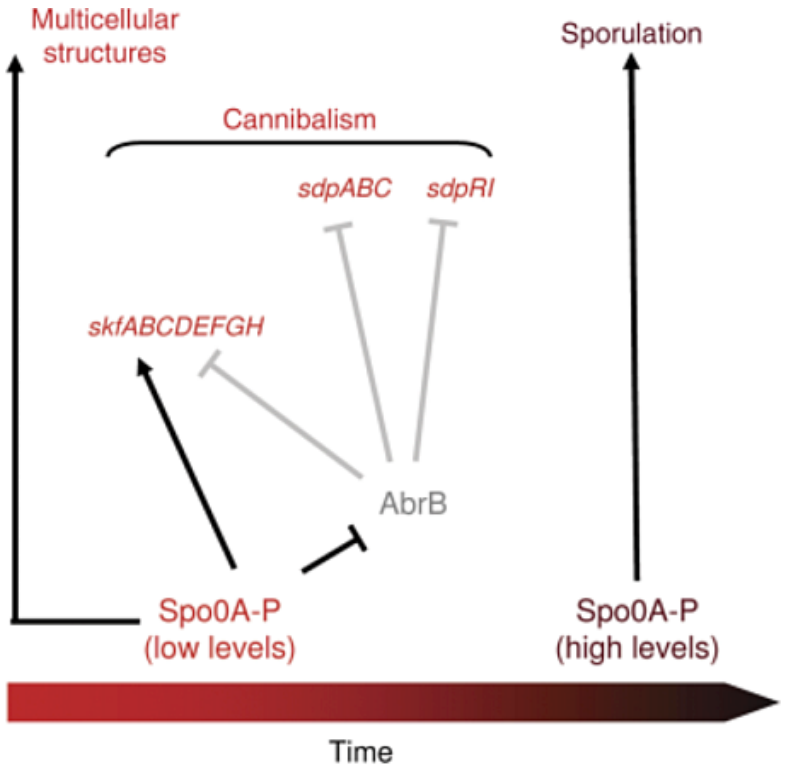

Figure 2 | Different levels of Spo0A regulate different cell fates. Low levels of Spo0A-P activate the formation of multicellular structures, for example in biofilms and the expression of cannibalism operons *(skfABCDEFGH*, *sdpABC* and *sdpRI)* and inhibit the repressor AbrB. Thereby, the *skf* operon is activated directly and indirectly. Both *sdp* operons are indirectly activated by the inhibition of AbrB. On the contrary, high levels of Spo0A-P initiate sporulation. The figure was taken from (González-Pastor 2011).

1.2 The bacterial cell wall

1.2.1 Structure of the peptidoglycan

Bacteria are surrounded by a cell envelope, which is essential for the viability and stability of the cells and preserves the shape and the integrity (Koch and Doyle 1985, Glauner *et al.* 1988, Barrett *et al.* 2007). The cell envelope undergoes a dramatic remodeling during cell growth, cell division and cell differentiation (e.g. sporulation) (Egan *et al.* 2017). A rigid sack-like structure (sacculus), called murein or peptidoglycan, is responsible for protection of the cells against turgor pressure and modulates translocation of molecules (Atrih *et al.* 1999, Cloud-Hansen *et al.* 2006, Walter and Mayer 2019). The peptidoglycan is built up from the saccharides *N*-acetylmuramic acid (MurNAc) and *N*-acetylglucosamine (GlcNAc) and peptides (Figure 3).

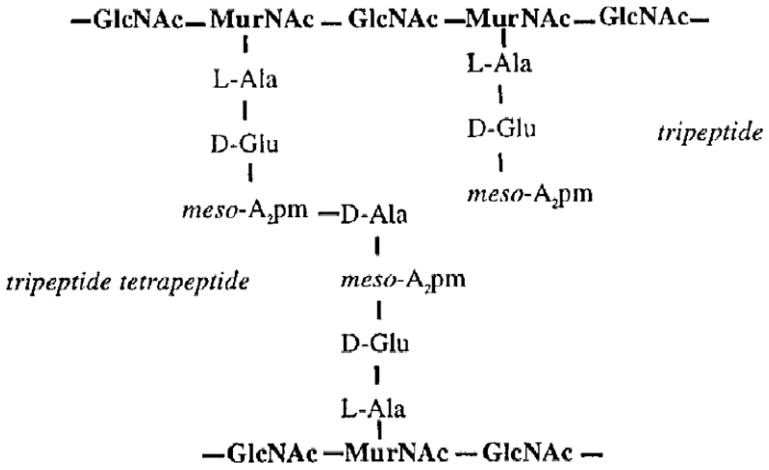

Figure 3 | Peptidoglycan structure of *B. subtilis*. The peptidoglycan backbone consists of the alternating sugars *N*-acetylglucosamine (GlcNAc) and *N*-acetylmuramic acid (MurNAc) which are linked via a β–1,4–glycosidic bond. The sugar chains are cross-linked through peptides, which are bound to the D-lactoyl group of MurNAc residues. The peptide stems consist of L-alanine-D-glutamic acid-*meso*-diaminopimelic acid-D-alanine-(D-alanine) (L-Ala-γ-D-Glu-*m*-DAP-D-Ala-(D-Ala). Cross-linking is built between the *m*-DAP at position 3 and the D-Ala at position 4. The figure was taken from (Atrih and Foster 1999).

The MurNAc and GlcNAc residues are linked by β-1,4-glycosidic bonds, resulting in long glycan strands. These are cross-linked through peptides, which are bound to the D-lactoyl group of MurNAc residues. Despite the high amount of cross-linkage, its net-shapes structure and the stabilizing properties, the peptidoglycan network is a very dynamic structure which gets constantly synthesized, modified and hydrolyzed during bacterial growth (Rogers 1974, Höltje and Glauner 1990, Doyle and Marquis 1994, Cloud-Hansen *et al.* 2006, Hayhurst *et al.* 2008, Walter and Mayer 2019). The peptide stem of the two model organisms *E. coli* and *B. subtilis* consists of L-alanine-D-glutamic

acid-*meso*-diaminopimelic acid-D-alanine-(D-alanine) (L-Ala-γ-D-Glu-*m*-DAP-D-Ala-(D-Ala)) (Schleifer and Kandler 1972, Vollmer *et al.* 2008a), whereas the *m*-DAP is amidated in *B. subtilis* (Warth and Strominger 1971). Cross-linking of peptide stems occurs between the carboxyl group of the D-Ala at position 4 of the donor peptide chain and the amino group of the diaminopimelic acid at position 3 of the acceptor peptide chain end. The cross-linking or transpeptidation reaction is driven by hydrolysis of the peptide bond of the donor peptide chain between the D-Ala at position 4 and the terminal D-Ala at position 5 in a transpeptidation reaction (Atrih *et al.* 1999, Vollmer *et al.* 2008b), catalyzed by the so-called penicillin-binding proteins (Cho *et al.* 2016).

The glycan strands carry a 1,6-anhydro-*N*-acetylmuramic acid (anhMurNAc) residue at the terminal reducing end, which is a MurNAc with an intra-molecular glycosidic bond between the C1 and C6 (Glauner *et al.* 1988, Vollmer and Bertsche 2008). MurNAc residues are proposed on the non-reducing end of native glycan strands (Atrih *et al.* 1999). The glycan strands of peptidoglycan can be further modified by *O*-acetylation of MurNAc, de-*N*-acetylation of MurNAc and GlcNAc or by phosphorylation, which represents the linkage of peptidoglycan and wall teichoic acids (WTA) (Schleifer and Kandler 1972, Atrih *et al.* 1999, Brown *et al.* 2013). In *B. subtilis* a high number of the muropeptide residues are de-*N*-acetylated and therefore, are present as deacetylated glucosamine (GlcN) and muramic acid (MurN). The mechanism of deacetylation provides resistance against hydrolysis by lysozyme (Atrih *et al.* 1999, Psylinakis *et al.* 2005). Responsible for the deacetylation of the MurNAc in PGN are the *N*-acetylmuramic acid deacetylases PdaC (Kobayashi *et al.* 2012) and PdaA (Fukushima *et al.* 2005). The latter plays a role in the formation of muramic δ-lactam, a spore specific peptidoglycan residue (Fukushima *et al.* 2005). Additionally, the peptides can also be modified by amidation, like D-Glu (occasionally in *B. subtilis*) or *m*-DAP (around 99% in *B. subtilis*) on the free carboxyl group (Atrih *et al.* 1999, Foster and Popham 2002, Vollmer *et al.* 2008b).

Depending on the composition of the envelope structure and thickness of the peptidoglycan layer, bacteria can be classified as Gram-negative and Gram-positive organisms (Figure 4) (Reith and Mayer 2011).

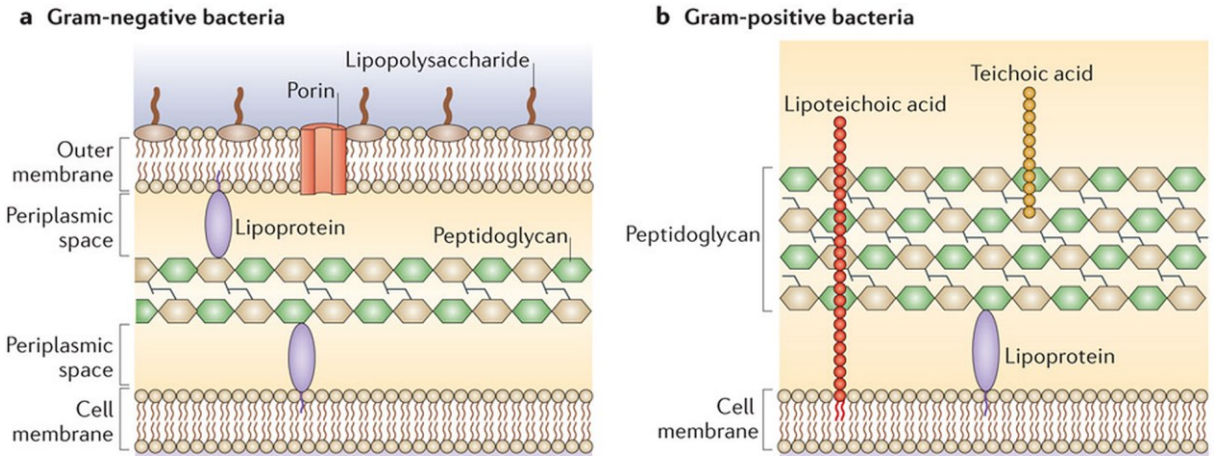

Figure 4 | Cell envelope structures of Gram-negative and Gram-positive bacteria. (a) The Gram-negative cell wall is built up by three different layers: A cell membrane or cytoplasmic membrane, which surrounds the cytoplasm, an outer membrane, containing membrane proteins and lipopolysaccharides, and in-between the periplasm where the thin peptidoglycan layer is sited. The peptidoglycan layer is connected to the cell membrane and the outer membrane by lipoproteins. **(b)** The Gram-positive cell wall is built up by two different layers: a cell membrane or cytoplasmic membrane, which surrounds the cytoplasm and where the lipoteichoic acids (LTA) are attached, and a thick peptidoglycan layer, where wall teichoic acids (WTA) are covalently attached. As in Gram-negatives, the peptidoglycan layer is linked to the cell membrane by lipoproteins. The figure was taken from (Brown *et al.* 2015).

The Gram-negative cell envelope consists of two lipid layers, the inner (cytoplasmic) membrane and the outer membrane, creating a periplasmic space in which the peptidoglycan is located. The outer membrane contains phospholipids on the inner leaflet as well as glycolipids (lipopolysaccharides) on the outer leaflet and serves as a selective permeability barrier to protect the cells. Between the inner and the outer membrane, a unique compartment is established, the periplasmic space, which accounts for approximately 20% of the cell volume and contains extra-cytoplasmic proteins essential for peptidoglycan synthesis and remodeling. In the periplasm the peptidoglycan is embedded as a thin layer in Gram-negatives and is connected to the outer membrane by a lipoprotein (Lpp or Braun's lipoprotein) which stabilizes the outer membrane. The inner membrane is a phospholipid bilayer surrounding the cytoplasm (Braun 1975, Silhavy *et al.* 2010, Brown *et al.* 2015).

In contrast, the cell envelope of Gram-positive organisms lacks an outer membrane and consists of a thick peptidoglycan layer (30 to 100 nm) (Silhavy *et al.* 2010) which covers the cytoplasmic membrane. The Gram-positive peptidoglycan is permeated by long anionic polymers, called teichoic acids. The cell wall of *B. subtilis* contains 46% peptidoglycan and 54% teichoic acids per cell dry weight (Graham and Beveridge 1994). WTA are covalently linked to the MurNAc residue of the peptidoglycan at the

C6 hydroxyl via a phosphodiester bond. Lipoteichoic acids (LTA) are linked by diacylglycerol to the cytoplasmic membrane (Figure 4) (Silhavy *et al.* 2010, Brown *et al.* 2015).

The WTA of *B. subtilis* carry a linkage unit bound to the peptidoglycan consisting of *N*-acetylglucosamine-1-phosphate-*N*-acetylmannosamine (GlcNAc-ManNAc) and one to three glycerol phosphates (Brown *et al.* 2013). Attached to the linkage unit is a chain of up to 40 sn-glycerol-3-phosphate repeating units, resulting in an anionic polymer with a negative charge. The glycerol phosphate units can be modified by α-glucose or D-alanyl esters. The latter introduces a positive charge to the peptidoglycan network due to its protonated state. Thus, peptidoglycan and teichoic acids form a polyanionic matrix, that has an immense impact in maintenance of cation homeostasis, regulation of autolysins and flow of ions, nutrients, and proteins to and from the cytoplasmic membrane (Neuhaus and Baddiley 2003, Bhavsar *et al.* 2004, Rice and Bayles 2008, Brown *et al.* 2013). Furthermore, due to their positive charge the WTA are responsible for controlling autolysin activity and are involved in the formation of a buffer zone between the surrounding and the cytoplasmic membrane, comparable to the periplasm in Gram-negative organisms (Rice and Bayles 2008). The thick peptidoglycan layer of Gram-positives is comparable to a net-like structure that serves as a molecular sieve to protect the cells (Doyle and Marquis 1994, Demchick and Koch 1996).

The structure of *B. subtilis* peptidoglycan varies in dependance of its location. The cylindrical side of the cell shows on the outer surface a disorientated, gel-like peptidoglycan with large, deep pores, whereas on the inner surface, the cylindrical side of the cell shows a dense, organized peptidoglycan with circumferentially orientated strands. On the outer surface, the cell poles consist of a dense peptidoglycan arranged in concentric rings, whereas on the inner surface, the cell poles and the division septum show dense, randomly oriented glycan strands (Figure 5) (Pasquina-Lemonche *et al.* 2020).

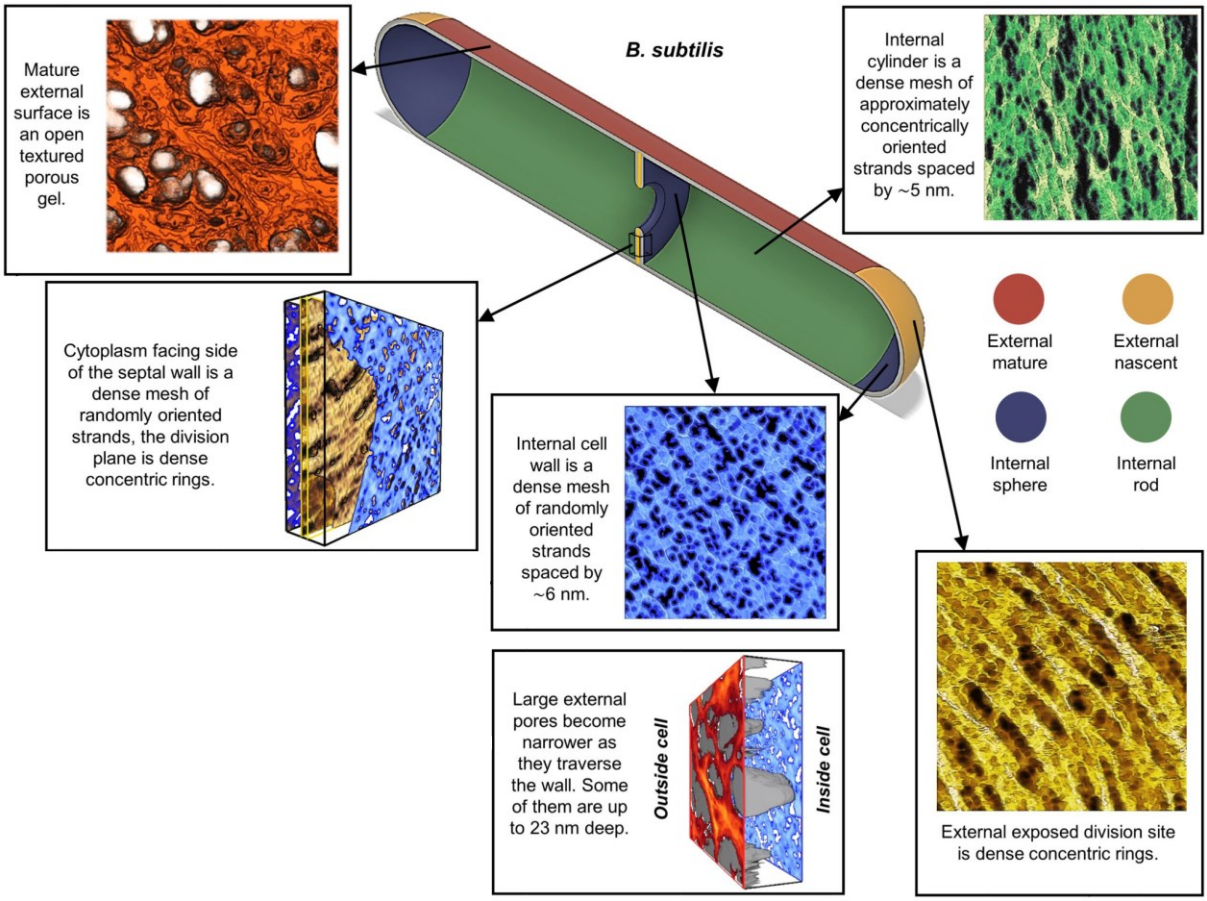

Figure 5 | *B. subtilis* peptidoglycan architecture. The structure of the rod-shaped *B. subtilis* peptidoglycan is dependent on the location around the cell. On the outer surface, the cylindrical side of the cell shows a disoriented, gel-like peptidoglycan with large, deep pores (colored in red), whereas on the inner surface, the cylindrical side of the cell shows a dense, organized peptidoglycan with circumferentially oriented strands (colored in green). On the outer surface, the cell poles consist of a dense peptidoglycan arranged in concentric rings (colored in yellow), while on the inner surface, the cell poles and the dividing septum have dense, randomly oriented glycan strands (colored in blue). The figure was modified after (Pasquina-Lemonche *et al.* 2020).

1.2.2 Synthesis and turnover of the peptidoglycan

The peptidoglycan is a dynamic structure as it gets constantly synthesized, remodeled, and hydrolyzed during cell growth (Vermassen *et al.* 2019). Synthesis of the peptidoglycan is a complex process involving three steps. Firstly, the formation of soluble precursors in the cytoplasm, secondly the synthesis of membrane-bound Lipid II, which is translocated through the cytoplasmic membrane, and thirdly, the polymerization of Lipid II into the existing glycan chains in the cell wall. The cytoplasmic step comprises the generation of UDP-GlcNAc from fructose-6-phosphate by the action of GlmS (a glucosamine-6-phosphate-synthase), GlmM (a phospho-glucosamine mutase) and GlmU (a glucosamine-1-phosphate acetyltransferase / *N*-acetylglucosamine-1-phosphate uridyltransferase), the conversion of UDP-GlcNAc to

UDP-MurNAc by MurA (a UDP-*N*-acetylglucosamine 1-carboxyvinyltransferase) and MurB (a UDP-*N*-acetylenolpyruvoylglucosamine reductase) and the attachment of the peptide stem to UDP-MurNAc by the Mur-ligases MurC, MurD, MurE and MurF leading to UDP-MurNAc-pentapeptide (Atrih *et al.* 1999, van Heijenoort 2001, El Zoeiby *et al.* 2003, Barreteau *et al.* 2008). UDP-MurNAc-pentapeptide is then coupled to a C_{55}-undecaprenyl phosphate carrier lipid by MraY (a phospho-*N*-acetylmuramoyl pentapeptide-transferase), thereby anchored in the cytoplasmic membrane, generating Lipid I. Afterwards, MurG (a UDP-*N*-acetylglucosamine-*N*-acetylmuramyl-(pentapeptide)-pyrophosphoryl-undecaprenol *N*-acetylglucosamine transferase) transfers UDP-GlcNAc to Lipid I leading to the formation of Lipid II which is flipped across the membrane by MurJ (a flippase) to be polymerized into the cell wall (Mengin-Lecreulx *et al.* 1991, Bouhss *et al.* 2004, Do *et al.* 2020). The polymerization of Lipid II into the existing glycan chains involves the action of penicillin-binding proteins (PBPs) together the SEDS (shape, elongation, division and sporulation) complex (Cho *et al.* 2016, Meeske *et al.* 2016). Glycosyltransferases of the SEDS complex connect the reducing end of the growing glycan strand to the GlcNAc of Lipid II by forming a β-1,4-glycosidic bond. Cross-linking of the glycan strand is performed by transpeptidases. The last D-alanine of the pentapeptide is cleaved off from the donor peptide stem and the C-terminus of the other D-Ala crosslinks with the N-terminus of the *m*-DAP of the acceptor peptide stem (Atrih *et al.* 1999, Carballido-Lopez and Formstone 2007, Kim *et al.* 2014, Cho *et al.* 2016, Meeske *et al.* 2016, Do *et al.* 2020).

Gram-positive rod-shaped bacteria, like *B. subtilis*, grow accordingly to the inside-to-outside growth model, which means that peptidoglycan moves from the place of synthesis at the cytoplasmic membrane to the outside. Thereby it gets more and more stretched, and finally it is hydrolyzed and released (Koch and Doyle 1985, Vollmer *et al.* 2008b, Wheeler *et al.* 2015). This process, known as the turnover of peptidoglycan, is essential for balanced cell enlargement and division. Thereby, about 20% of the cell wall is hydrolyzed per generation (De Boer *et al.* 1981, Jolliffe *et al.* 1981). The release of peptidoglycan fragments involves the action of peptidoglycan hydrolases, which need to be regulated strictly to ensure bacterial survival. There are different classes of hydrolases as glycosidases and peptidases categorized depending on their hydrolytic bond specificity (Figure 6) (Smith *et al.* 1996, Smith *et al.* 2000, Vollmer *et al.* 2008b, Do *et al.* 2020).

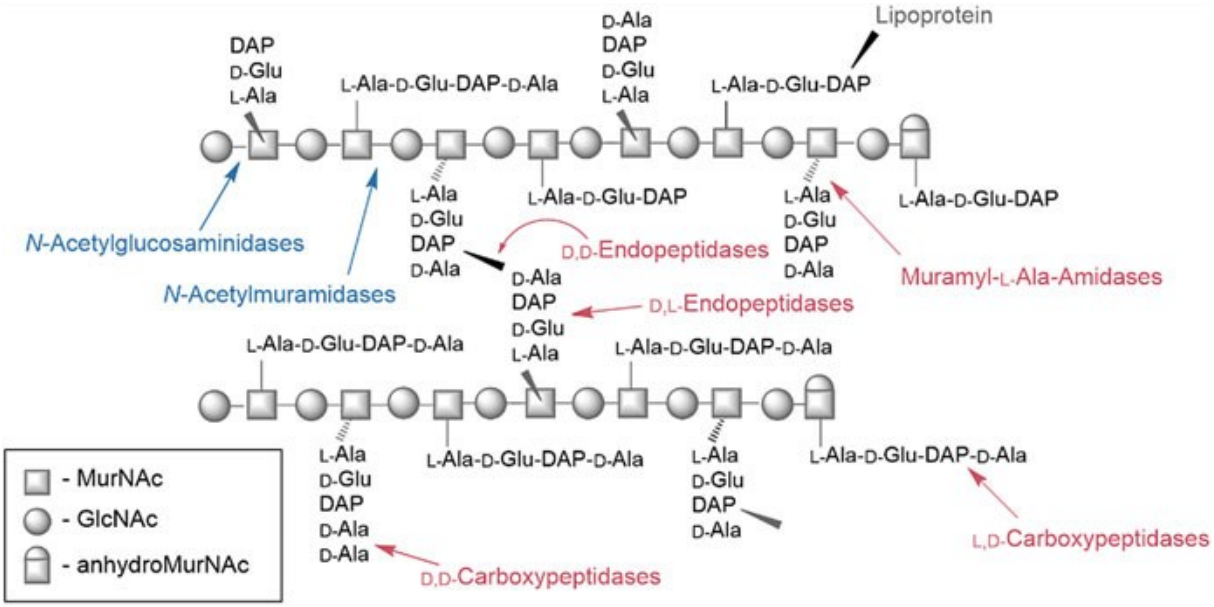

Figure 6 | Peptidoglycan hydrolases and their respective cleavage sites. Depending on their activity, hydrolases are classified as glycosidases (blue) and peptidases (red). *N*-acetylmuramidases and *N*-acetylglucosaminidases belong to the class of glycosidases and cleave in-between glycan strands. *N*-acetylmuramidases specifically cleave MurNAc-GlcNAc substrates, whereas *N*-acetylglucosaminidases are specific for GlcNAc-MurNAc substrates. Amidases, carboxypeptidases, and endopeptidases pertain to the class of peptidases and are responsible for the cleavage of the peptide stem. Muramyl-L-Ala-amidases are specific for cleavage between a MurNAc residue and the peptide stem, carboxypeptidases specifically cleave in-between the peptide stem, depending on whether they have a L,D or a D,D specificity and endopeptidases cleave the cross-links between to different peptide stems as well as in-between the peptide stem, depending on whether they have a L,D or a D,D specificity. The arrows represent the sites of hydrolysis. The figure was taken from (Walter and Mayer 2019).

Glycosidases cleave the β-1,4-glycosidic bonds connecting the cell wall saccharides. These include *N*-acetylmuramidases (muramidases), *N*-acetylglucosaminidases (glucosaminidases) and lytic transglycosylases. The first cleaves the glycosidic bond between MurNAc and GlcNAc, the second splits the linkage between GlcNAc and MurNAc and the last cleaves non-hydrolytically the bond between MurNAc and GlcNAc, thus converting MurNAc to anhMurNAc (Figure 6) (Mayer *et al.* 2019).

Whereas peptidases cleave the linkage within the peptide stem. There are *N*-acetylmuramyl-L-alanine amidases (amidases), carboxypeptidases and endopeptidases. Amidases release the peptides from the D-lactoyl moiety of the MurNAc residue. For carboxypeptidases, there are two different cleavage mechanisms. On the one hand, DD-carboxypeptidases that cleave exolytic the linkage between the terminal D-alanine and the D-alanine at position 4, converting pentapeptide into tetrapeptide and on the other hand, LD-carboxypeptidases that cleave the bond between the D-alanine at position 4 and the *m*-DAP at position 3, forming tripeptide from tetrapeptide. Lastly, endopeptidases cleave

other amide linkages within the peptide stem or interpeptide bridges (Figure 6) (Smith *et al.* 1996, Smith *et al.* 2000, Scheurwater *et al.* 2008, Vollmer *et al.* 2008b, Do *et al.* 2020).

1.2.3 Recycling of turnover products

The degradation of the peptidoglycan (turnover) releases huge amounts of fragments (muropeptides) involving the action of various autolysins, produced by the growing bacteria, which cleave the different bonds between the single building blocks of the cell wall (Vermassen *et al.* 2019). The recovery of products emerged by turnover of the cell wall to use them as energy source or for the synthesis of new peptidoglycan is known as “peptidoglycan recycling” (Uehara and Park 2008, Mayer 2012). This metabolic process was first discovered for the Gram-negative organism *E. coli*, which breaks down and reuses over 60% of its peptidoglycan per generation (Goodell 1985, Park and Uehara 2008, Johnson *et al.* 2013). In Gram-negative bacteria, the peptidoglycan recycling takes place synchronous to the turnover process (Höltje 1998), where peptidoglycan gets degraded by the action of lytic transglycosylases, releasing anhydro-muropeptides, GlcNAc-anhMurNAc-tri-, -tetra-, and -pentapeptides, whereas GlcNAc-anhMurNAc-tetrapeptide is the main product. Turnover products are kept in the periplasm, due to the presence of the outer membrane (Litzinger *et al.* 2010). The uptake from the periplasm into the cytoplasm is carried out via the permease AmpG. Cytoplasmatically, anhydro-muropeptides get further degraded by hydrolases. The anhMurNAc-L-alanine amidase AmpD releases the peptide stem from the anhMurNAc residue. The peptide chain is cleaved additionally by a LD-carboxypeptidase, creating a D-alanine and a tripeptide, which gets directly shuttled into peptidoglycan synthesis by Mpl, a murein peptide ligase. Mpl attaches tripeptide to UDP-MurNAc yielding UDP-MurNAc-tripeptide. Residual GlcNAc-anhMurNAc gets cleaved by the action of an exo-*N*-acetylglucosaminidase NagZ, releasing single amino sugars GlcNAc and anhMurNAc. GlcNAc gets phosphorylated by the *N*-acetyl-D-glucosamine kinase NagK to GlcNAc-6-phosphate (GlcNAc-6P) and de-acetylated by the *N*-acetylglucosamine-6-phosphate deacetylase NagA, yielding glucosamine-6-phosphate (GlcN-6P). This serves as substrate for the glucosamine-6-phosphate deaminase NagB leading to fructose-6-phosphate (Frc-6P), which enters either peptidoglycan synthesis or glycolysis. The second released amino sugar, anhMurNAc, is the substrate for the anhydro-*N*-acetylmuramic acid kinase AnmK, leading to the formation of MurNAc-6-phosphate (MurNAc-6P). By the action of the *N*-acetylmuramic acid 6-phosphate

etherase MurQ MurNAc-6P is converted to GlcNAc-6P which is the substrate for NagA as described above. Additionally, external MurNAc can be incorporated by the phosphotransferase system (PTS) transporter MurP. Thereby, MurNAc is phosphorylated to MurNAc-6P, serving as substrate for MurQ (Hadi *et al.* 2008, Jaeger and Mayer 2008, Uehara and Park 2008, Reith and Mayer 2011).

For the Gram-positive organism *B. subtilis*, turnover rates of up to 50% of the sacculus per generation are reported (Park and Uehara 2008, Borisova *et al.* 2016). Shed components are transported into the cell via specific transporters and channeled into peptidoglycan *de novo* biosynthesis or enter basic metabolic pathways, like glycolysis (Uehara and Park 2008, Litzinger *et al.* 2010, Do *et al.* 2020). In Gram-positive bacteria, peptidoglycan turnover and recycling are much less understood and apparently differs from Gram-negatives. Firstly, Gram-positives miss an outer membrane as barrier, which leads to some loss of turnover products (Mauck and Glaser 1970, Mauck *et al.* 1971). Secondly, lytic transglycosylases and thus the release of anhydro-muropeptides play a minor role in peptidoglycan recycling in Gram-positives, whereas muramidases and *N*-acetylglucosaminidases are widespread (Reith and Mayer 2011). Next, no orthologs for the *E. coli* recycling proteins AmpG, AmpD and AnmK could be identified (Litzinger *et al.* 2010). Lastly, peptidoglycan recycling occurs not at the same time as turnover but rather after a delay in transition and stationary growth phase when nutrients begin to be limiting (Borisova *et al.* 2016). Nevertheless, orthologs of the key-enzyme in peptidoglycan recycling, the etherase MurQ, were found in almost all Gram-positive bacteria, indicating that peptidoglycan recycling is a common mechanism amongst Gram-positives (Jaeger and Mayer 2008). An operon with orthologous genes to the *E. coli* recycling genes was identified for *B. subtilis*. This operon is encoded by six genes. Within, an ortholog encoding for the *N*-acetylmuramic acid 6-phosphate etherase MurQ together with orthologs of the transcriptional MurNAc-6P-sensitive repressor MurR and the phosphotransferase system (PTS) transporter MurP were found. Furthermore, the *N*-acetylmuramyl-L-alanine amidase AmiE and the exo-*N*-acetylglucosaminidase NagZ are encoded in this operon (Figure 7) (Litzinger *et al.* 2010, Mayer *et al.* 2019).

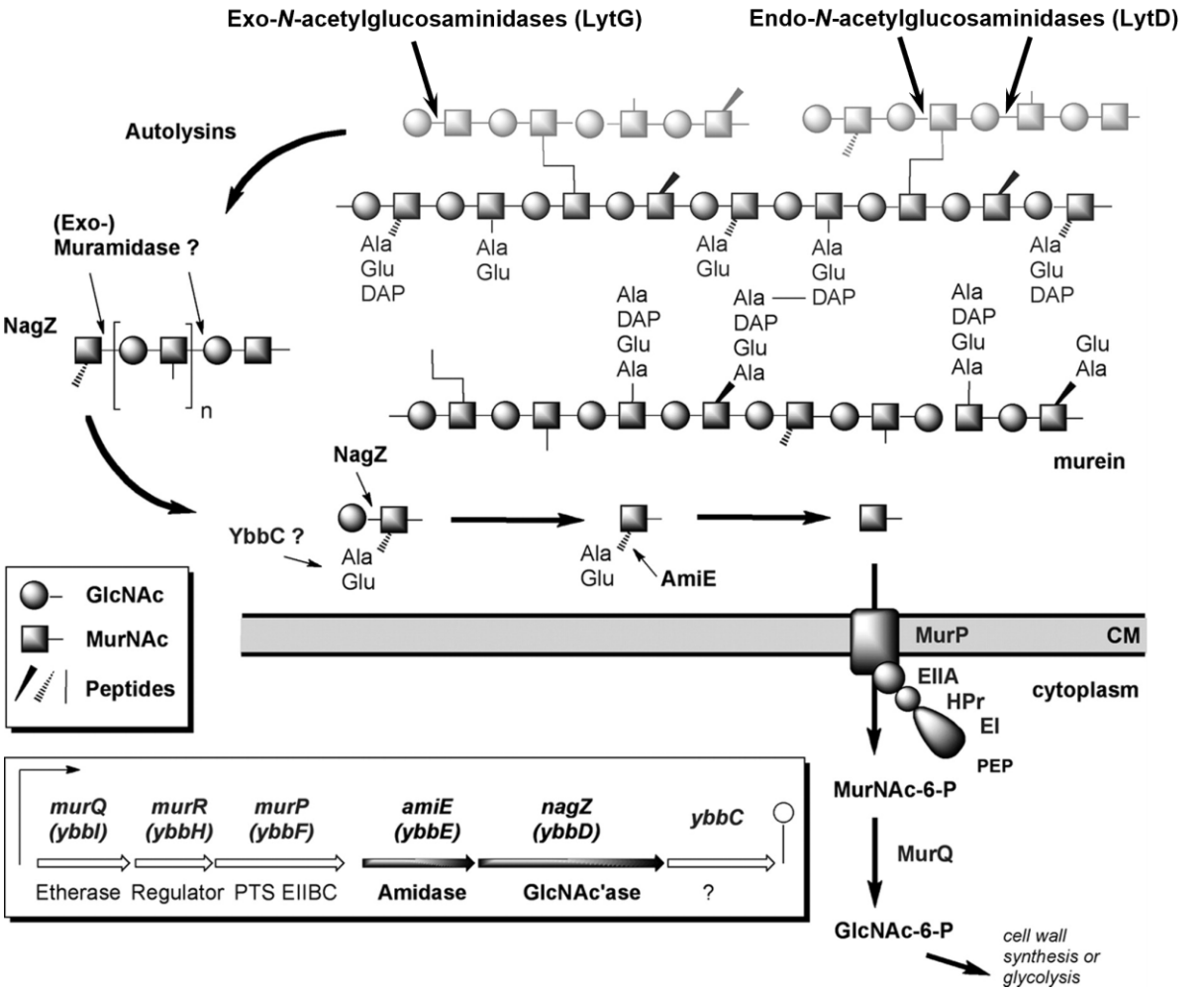

Figure 7 | Scheme of peptidoglycan turnover and MurNAc recycling in *B. subtilis*. Autolysins, like endo-acting *N*-acetylglucosaminidases and *N*-acetylmuramidases, cleave the peptidoglycan, thereby generating GlcNAc-MurNAc-peptides. Generation of single cell wall sugars is managed by the action of exo-acting hydrolases, like the *N*-acetylglucosaminidase NagZ (YbbD), which chips off GlcNAc from the non-reducing ends of a peptidoglycan fragment, resulting in GlcNAc and MurNAc-peptides. The latter serve as substrate for the amidase AmiE (YbbE), subsequently cleaving the peptide stem off from the D-lactoyl group of the MurNAc residue, resulting in MurNAc and peptides. MurNAc is then incorporated in the cell by the PTS transporter MurP (YbbF) and gets thereby phosphorylated into MurNAc-6P. The etherase MurQ (YbbI) uses MurNAc-6P as a substrate, converting it to GlcNAc-6P, which is shuttled either in cell wall synthesis or glycolysis. Furthermore, the regulator *murR* (*ybbH*) and a gene of unknown function, *ybbC*, are encoded in the operon responsible for the recycling of MurNAc. The figure was modified after (Litzinger *et al.* 2010).

The peptidoglycan turnover in *B. subtilis* involves the cleavage of peptidoglycan by glycosidases. *N*-acetylmuramidases and *N*-acetylglucosaminidases are distinguished between exo- and endo-acting enzymes. Endo-acting hydrolases cleave in-between the glycan backbone: endo-*N*-acetylmuramidases generate muropeptides harboring GlcNAc at the non-reducing end, whereas endo-*N*-acetylglucosaminidases, like LytD, generate muropeptides harboring MurNAc at the non-reducing end. In contrast, exo-acting hydrolases chip off single amino sugars from the non-reducing end of a glycan

strand or peptidoglycan fragments: exo-*N*-acetylglucosaminidases, like NagZ, cleave the β-1,4-glycosidic bond between GlcNAc-MurNAc, whereas exo-*N*-acetylmuramidases cleave the β-1,4-glycosidic bond between MurNAc-GlcNAc (Figure 7). Therefore, to generate single cell wall sugars, endo-acting hydrolases must fragmentate the peptidoglycan and cleave it into GlcNAc-MurNAc-peptide and MurNAc-GlcNAc-peptides. It was shown that GlcNAc-MurNAc-peptides serve as substrate for the major exo-*N*-acetylglucosaminidase NagZ, which is encoded in the recycling operon. It cleaves the glycosidic bond between the GlcNAc at the non-reducing end and the MurNAc at the reducing end, generating GlcNAc and MurNAc-peptides. The next gene of the operon, AmiE, hydrolyzes the *N*-acetylmuramyl-L-Ala bond of the MurNAc-peptides, releasing MurNAc and peptides (Litzinger *et al.* 2010). Additionally, it was found that *B. subtilis* possesses an exo-*N*-acetylmuramidase, which is active on MurNAc at the non-reducing end of a glycan chain and would act as counterpart to NagZ. An enzyme with this specificity was described, but the encoding gene remained unknown (Del Rio *et al.* 1973, Del Rio and Berkeley 1976). After fragmentation of the peptidoglycan into muropeptides by the action of endo-*N*-acetylglucosaminidases, MurNAc-GlcNAc-peptides serve as substrate for the activity of an amidase, like AmiE. After the peptides are released, MurNAc-GlcNAc serves as a substrate for the unknown exo-*N*-acetylmuramidase, which cleaves the glycosidic bond between the MurNAc at the non-reducing end and the GlcNAc at the reducing end, generating single amino sugars. A potential candidate for the role of the exo-*N*-acetylmuramidase described by Del Rio and colleagues would be *ybbC*, which is encoded in the recycling operon of *B. subtilis* next to *amiE* and *nagZ* (Litzinger *et al.* 2010).

Finally, released GlcNAc and MurNAc are incorporated by PTS transporters, and thereby phosphorylated simultaneously. MurP is responsible for the transport of MurNAc. The uptake leads to the formation of MurNAc-6P, generating the substrate for MurQ, which converts MurNAc-6P to GlcNAc-6P (Figure 7). The uptake of GlcNAc from released peptidoglycan fragments is mediated by NagP. Thereby, the amino sugar GlcNAc is taken up into the cells, phosphorylated simultaneously and forming GlcNAc-6P. By the *N*-acetylglucosamine-6-phosphate deacetylase NagA, GlcNAc-6P is de-acetylated to GlcN-6P, serving as a substrate for the glucosamine-6-phosphate deaminase NagB, yielding in Frc-6P, which can either enter peptidoglycan *de novo* synthesis or glycolysis (Figure 7) (Litzinger *et al.* 2010).

Peptidoglycan recycling in Gram-positives is not only a mechanism to re-use turnover products in glycolysis or *de novo* synthesis, but also plays an important role in survival fitness as, especially when growth gets static under nutrient limitation and the beginning of sporulation (Dworkin and Losick 2005, Borisova *et al.* 2016).

1.3 Role of autolysins and autolysis

Bacteria possess a variety of potentially lytic enzymes, responsible for the hydrolysis of peptidoglycan that may cause cell lysis if not controlled in their activities. Autolysins are involved in vegetative cell growth, cell division and particularly cell differentiation processes. Furthermore, autolysins are also required for motility and natural competence, enabling bacteria to adapt to changing environmental conditions (Jolliffe *et al.* 1981, Smith *et al.* 1996) Importance of certain autolysins has been illustrated by investigations of mutants. Strains missing major autolysins show e.g. defects in growth as they are not able to separate properly and, instead, grow as chains (Doyle and Koch 1987). To be beneficial for the cells, autolysins must be strictly regulated and coordinated spatiotemporally (see Table 1; (Smith *et al.* 2000)).

Table 1 | Functions of *B. subtilis* autolysins (adapted from Smith *et al.* 2000)

Protein	Activity	Function	Location	Expression	Reference
			beta-lactamase family		
PbpE	Endopeptidase	Penicillin-binding protein PBP4*	Cell membrane	Induced by cell wall stress	(Popham and Setlow 1993)
PbpX	Endopeptidase	Penicillin-binding protein X	During vegetative growth: septum during sporulation: asymmetric septa and prespore		(Scheffers *et al.* 2004)
			CwlJ-family		
CwlJ	Cell wall hydrolase	Depolymerization of cortex peptidoglycan during germination	Inner spore coat?	Late during sporulation in the mother cell	(Bagyan and Setlow 2002, Amon *et al.* 2020)
			DUF1343-family		
NamZ	Exo-*N*-acetyl-muramidase	Cleavage of muro-peptides derived from peptidoglycan		Late exponential and early stationary phase?	this study and (Müller *et al.* 2021)
			Glycosyl-hydrolase 3 family		
NagZ	Exo-*N*-acetyl-glucosaminidase	Cleavage of muro-peptides derived from peptidoglycan, but not from whole peptidoglycan	Cell wall-associated	Late exponential and early stationary phase	(Litzinger *et al.* 2010)

Protein	Activity	Function	Location	Expression	Reference
			Glycosyl-hydrolase 18 family		
YaaH	*N*-acetyl-glucosaminidase	Protection of the spore, survival of ethanol stress	Inner spore coat	During sporulation in the mother cell	(Kodama *et al.* 1999, Höper *et al.* 2005, McKenney and Eichenberger 2012)
YdhD	Spore coat glycosylase	Cell wall hydrolysis	Spore wall	During sporulation in the mother cell	(Kodama *et al.* 2000)
YkvQ					
YkzR					
YvbX					
			Glycosyl-hydrolase 73 family		
LytD	Endo-*N*-acetyl-glucosaminidase	Cell separation, cell wall turnover	Cell wall	Vegetative growth	(Margot *et al.* 1994, Rashid *et al.* 1995, Horsburgh *et al.* 2003b, Chen *et al.* 2009)
LytG	Endo-*N*-acetyl-glucosaminidas	Cell wall turnover	Cell wall	Vegetative growth	(Horsburgh *et al.* 2003b)
			***N*-acetylmuramoyl-L-alanine amidase 2 family**		
CwlA	*N*-acetylmuramoyl-L-alanine amidase	*skin*-mediated lysis?		Apparently silent	(Foster 1991, Kuroda *et al.* 1991, Foster 1993)
CwlH	*N*-acetylmuramoyl-L-alanine amidase	Cleavage of mother cell peptidoglycan to release the endospore		Late during sporulation in the mother cell	(Nugroho *et al.* 1999)
XlyA	*N*-acetylmuramoyl-L-alanine amidase	PBSX prophage mediated lysis		PBSX induction	(Longchamp *et al.* 1994)

Protein	Activity	Function	Location	Expression	Reference
XlyB	*N*-acetylmuramoyl-L-alanine amidase	PBSX prophage mediated lysis		PBSX induction	(Visweswaran *et al.* 2014)
BlyA	*N*-acetylmuramoyl-L-alanine amidase	SP-β mediated lysis		SP-β induction	(Regamey and Karamata 1998)
			***N*-acetylmuramoyl-L-alanine amidase 3 family**		
CwlC	*N*-acetylmuramoyl-L-alanine amidase	Mother cell lysis	Cell wall of the mother cell	Late during sporulation in the mother cell	(Kuroda *et al.* 1993, Smith and Foster 1995, Shida *et al.* 2000)
CwlD	*N*-acetylmuramoyl-L-alanine amidase	Spore germination, formation of muramic δ-lactam structure in the spore cortex	Spore cortex	Sporulation	(Sekiguchi *et al.* 1995, Gilmore *et al.* 2004)
LytC	*N*-acetylmuramoyl-L-alanine amidase	Mother cell lysis, cell separation, cell wall turnover, cell lysis, flagellar function	Cell wall	Vegetative growth and sporulation	(Lazarevic *et al.* 1992, Margot and Karamata 1992, Yamamoto *et al.* 2003)
YqiI	Cell wall hydrolase	Cell wall metabolism			(Fischer and Bremer 2012)
YrvJ	Cell wall hydrolase	Cell wall metabolism?			
			Peptidase C40 family		
CwlO	D,L-endopeptidase	Cell wall synthesis, cell elongation, cell wall turnover	Outer lateral sidewall of the cell	Exponential growth	(Yamaguchi *et al.* 2004, Hashimoto *et al.* 2012)
CwlS	D,L-endopeptidase	Cell separation	Cell separation sites and cell poles	Vegetative growth	(Fukushima *et al.* 2006)

Protein	Activity	Function	Location	Expression	Reference
CwlT	*N*-acetylmuramidase (N-terminus) and D,L-endopeptidase (C-terminus)	Conjugative transfer of the integrative and conjugative element (ICEBs1)	Conjugation sites	Conjugation	(Fukushima *et al.* 2008, DeWitt and Grossman 2014)
LytE	D,L-endopeptidase	Cell elongation, cell separation, cell lysis	Cell separation sites and cell poles	Vegetative growth (late stationary phase)	(Margot *et al.* 1998, Yamamoto *et al.* 2003)
LytF	D,L-endopeptidase	Cell separation	Cell separation sites and cell poles	Vegetative growth (mid-exponential phase)	(Margot *et al.* 1999, Yamamoto *et al.* 2003, Hashimoto *et al.* 2012, Fukushima *et al.* 2018)
PgdS	γ- D,L-glutamyl hydrolase	Polyglutamic acid degradation			(Suzuki and Tahara 2003)
			Peptidase M15 family		
CwlK	L,D-endopeptidase	Cell wall turnover	Cell membrane	Vegetative growth	(Fukushima *et al.* 2007)
			Peptidase M23B family		
LytH	L,D-endopeptidase	Maturation of the spore cortex	Spore cortex	Late during sporulation in the mother cell	(Horsburgh *et al.* 2003a)
			Peptidase S12 family		
AmiE	*N*-acetylmuramoyl-L-alanine amidase	Cleavage of the amide bond of turnover products	Cell wall	Late exponential and early stationary phase	(Litzinger *et al.* 2010)
			SleB family		
SleB	Cell wall hydrolase	Cleavage of spore peptidoglycan during germination	Spore cortex	Late during sporulation in the forespore	(Moriyama *et al.* 1996, Boland *et al.* 2000, Zheng *et al.* 2016)

Protein	Activity	Function	Location	Expression	Reference
			Transglycosylase Slt family		
CwlP	*N*-acetylmuramidase (SLT domain) and D,D-endopeptidase (M23 domain)	Cell wall turnover, functions as a tail protein?	Cell membrane	SP-β prophage protein	(Sudiarta *et al.* 2010a)
CwlQ	Lytic transglycosylase and muramidase	Cell wall turnover, swarming motility	Secreted by the flagellar type III secretion system	Vegetative growth	(Sudiarta *et al.* 2010b, Sanchez *et al.* 2021)
			Unknown protein family		
SpoIIP	*N*-acetylmuramoyl-L-alanine amidase and D,D-endopeptidase	Required for proper localization of SpoIIQ	Cell membrane	Early during sporulation in the forespore	(Morlot *et al.* 2010, Rodrigues *et al.* 2013)
SpoIID	Lytic transglycosylase	Cleavage of asymmetric septum during sporulation		Early during sporulation in the forespore	(Driks and Losick 1991, Gutierrez *et al.* 2010, Morlot *et al.* 2010)
YkvT	Putative cell wall hydrolase	Similar to spore cortex-lytic enzymes		Member of the WalRK regulon	(Howell *et al.* 2003, Salzberg *et al.* 2013)
YocH	Cell wall hydrolase	Cell wall turnover, similar to cell wall-binding proteins (LysM domain)		Member of the WalRK regulon	(Molle *et al.* 2003, Dobihal *et al.* 2019)
YpbE	contains a *N*-acetyl-glucosamine-polymer-binding LysM domain	Likely involved in sidewall synthesis during cell growth			(Cleverley *et al.* 2019)

The process of autolysis in *B.* subtilis is linked to the collapse of the proton motive force (PMF). The WTA and the electronegative peptidoglycan layers create a negatively charged cell wall leading to the accumulation of protons around the cell membrane. These accumulated protons and the transmembrane gradient of protons give rise to the PMF (McGivney *et al.* 2017). The PMF is essential for the synthesis of ATP and for the transport of various solutes. It consists on the one hand of the difference between the intracellular pH and the extracellular pH (ΔpH) and on the other hand of the transmembrane difference in electrical potential (ΔΨ). In most bacteria the inner leaflet is negatively charged compared to the more positive charged outer leaflet, which leads to an H^+ ion gradient (Krulwich *et al.* 2011). As already mentioned, LTA and WTA can be modified by the addition of a D-alanyl ester at the glycerol phosphate units, which creates a positive charge. This causes a buffer zone on the outer side of the negatively charged cell envelope. Activity of autolysins is repressed in this buffer zone due to the protonated WTA. The effect of D-alanylation is in turn controlled by the PMF and its pH gradient (Koch 1986, Kemper *et al.* 1993, Calamita and Doyle 2002, Rice and Bayles 2008). With increasing distance from the cell membrane, the pH would increase relative to the pH of the environment. This change of pH from low to approximately neutral leads to destabilization of D-alanylation as well as its de-protonation resulting in de-regulation of autolysins near the outer peptidoglycan layers and causing PGN hydrolysis (Jolliffe *et al.* 1981, Neuhaus and Baddiley 2003, Rice and Bayles 2008). Due to the loss of the PGN integrity the cell membranes burst by the increasing pressure of the turgor, thereby releasing the contents of the cell and cell fragments which can be used by other cells as nutrients (Figure 8) (McGivney *et al.* 2017).

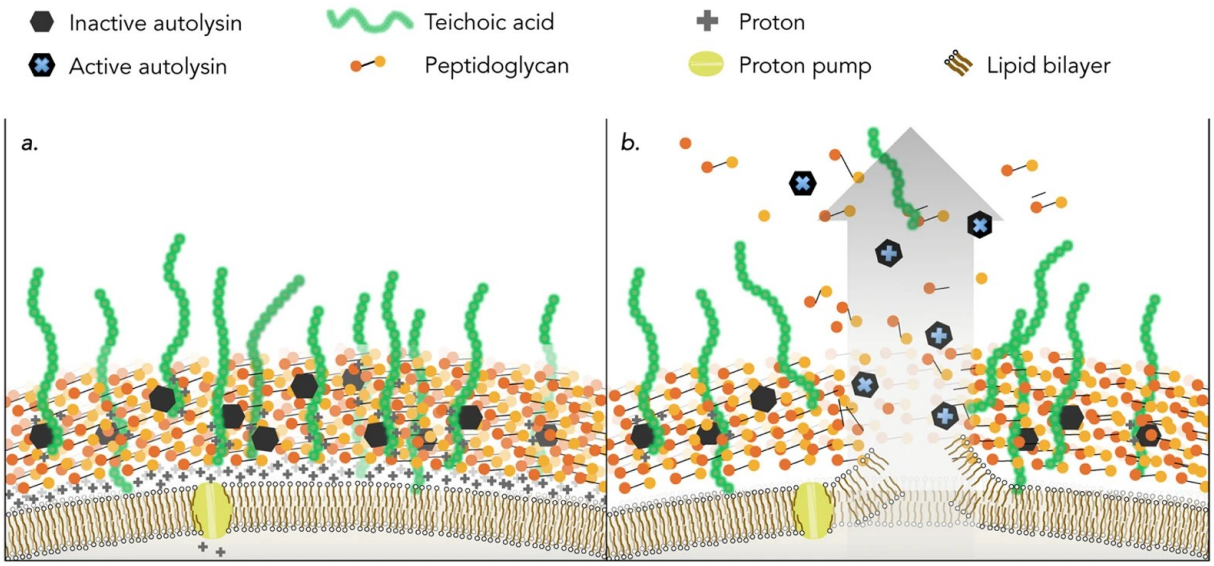

Figure 8 | Scheme of the autolytic mechanism in *B. subtilis*. (a) Under non-starving conditions the cell controls the autolysins present around the surface due to the D-alanylated WTA and the PMF. **(b)** Under starvation conditions the cell cannot maintain the PMF, leading to the loss of D-alanylation of the WTA and therefore activation of the autolysins. The peptidoglycan hydrolysis leads to an increase of the turgor pressure and the cell membrane bursts, releasing nutrients into the surrounding. The figure was taken from (McGivney *et al.* 2017).

Hydrolases responsible for the autolytic process are the major *N*-acetylmuramoyl-L-alanine amidase LytC and the *N*-acetylglucosaminidase LytD, cleaving in between the amino sugar backbone of the peptidoglycan and the peptide stem bound to it (Smith *et al.* 1996, Blackman *et al.* 1998, Atrih *et al.* 1999). Further autolysins involved are the D,L-endopeptidases CwlO, CwlS, LytE, and LytF, which cleave the bond between D-Glu and *m*-DAP of the peptides (Atrih *et al.* 1999, Smith *et al.* 2000, Do *et al.* 2020). Autolysis takes place when nutrients are limited or while cell growth reaches stationary phase (Jolliffe *et al.* 1981, Lewis 2000, Vollmer *et al.* 2008b).

Restriction of carbon sources leads to a collapse of the PMF and, as a second consequence, to the activation of autolysins due to the destabilization of the cell wall caused by the removal of the D-alanylations of the WTA. Subsequently, cells lyse and release nutrients of the cytoplasm into the environment (McGivney *et al.* 2017).

1.4 Regulation of sporulation

During nutrient limiting conditions, the global regulator Spo0A is activated by phosphorylation via a phosphorelay (see Figure 1 and Figure 2) (Piggot and Hilbert 2004, Claverys and Havarstein 2007). Thereby, the phosphorylation cascade is determined by three positive feedback loops and one negative feedback loop, which guarantee a just-in-time supply of the needed kinases and their products, responsible for Spo0A. First, the relay protein Spo0F gets phosphorylated by the action of five different kinases (KinABCDE). Spo0F-P transfers the phosphate to Spo0B, whereas the phosphate of Spo0B-P gets transferred to Spo0A (López *et al.* 2009, Chastanet *et al.* 2010). This phosphorylation cascade is regulated by the mentioned feedback loops. Spo0A-P triggers the transcription of its own gene *spo0A* as well as the expression of *spo0F*. Additionally, Spo0A-P represses AbrB, which represses, among others, the RNA polymerase sigma factor *sigH*. The role of SigH is to regulate the transcription of early stationary phase genes, responsible for sporulation and competence. Therefore, SigH is accountable for the expression of *kinA*, *spo0A* and *spo0F*. Furthermore, Spo0A-P represses *spo0E* by inhibition of AbrB (Figure 9) (Chastanet *et al.* 2010).

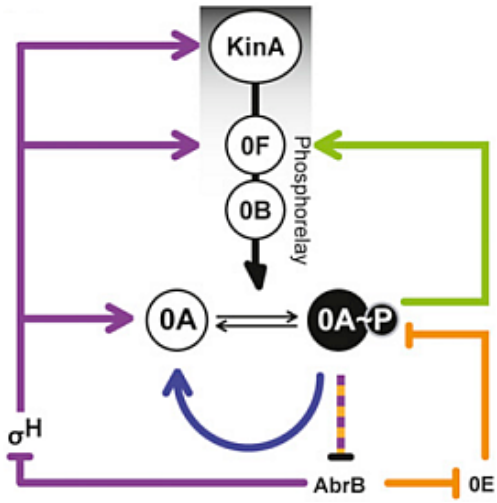

Figure 9 | Scheme of the feedback loop network. Purple lines show the control of AbrB and SigH (σH), respectively, on the transcription of the genes for KinA, Spo0F (0F) and Spo0A (0A). The orange lines show the control of AbrB and Spo0E (0E), respectively, for the dephosphorylation of Spo0A phosphate (0A-P). The blue and green lines show the positive feedback that stimulates the expression of the genes *spo0A* (0A) and *spo0F* (0F) by accumulation of Spo0A-P. The figure was modified after (Chastanet *et al.* 2010).

To trigger the sporulation process, Spo0A-P needs to be present in high amounts in the cells due to its weak binding to regulatory sites of sporulation genes. The level of Spo0A-P controlled via the kinases involved in the phosphorelay responsible for the activation of Spo0A (Fujita *et al.* 2005, López *et al.* 2009, Chastanet *et al.* 2010).

Spo0A-P controls the replication of the chromosome, thereby initiating an asymmetric cell division in the onset of sporulation. The chromosome gets condensed and stretches from one pole to another where it is anchored to the cell poles by RacA through interaction with DivIVA (Edwards and Errington 1997, Schumacher *et al.* 2016). After chromosome replication the cell forms an asymmetric septum, which is a stage in sporulating *B. subtilis* cells known as “the point of no return”, meaning that they are no longer able to resume vegetative growth if nutrients get available again. The septum divides the cell into a smaller compartment, the forespore, and a larger one, the mother cell (Dworkin and Losick 2005, Gutierrez *et al.* 2010).

In the mother cell, proteins are produced which get incorporated in the developing spore from the outside, whereas the forespore expresses enzymes responsible for the completion of the spore from the inside. The next stage in spore formation is the engulfment of the forespore by the asymmetric septum (Figure 10), which involves the hydrolysis of the peptidoglycan within the septum to a thin layer (Gutierrez *et al.* 2010).

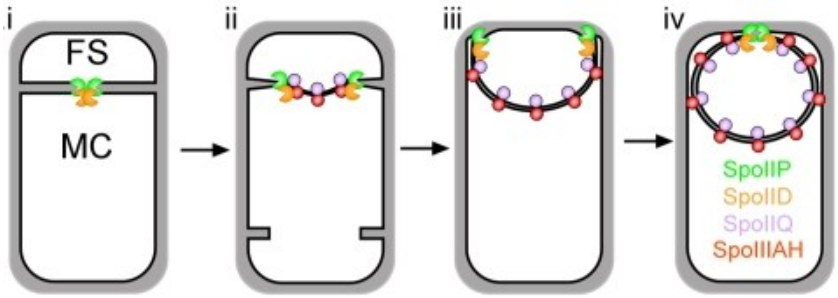

Figure 10 | Forespore engulfment in *B. subtilis*. (i) First, the asymmetric septum is formed which divides the cell into the mother cell (MC) and the forespore (FS). SpoIIP (green) and SpoIID (orange) localize at the septum. (ii) SpoIIP and SpoIID hydrolyse the peptidoglycan within the septum to a thin layer from the inside of the cell to the outside. SpoIIQ (purple), produced by the FS, and SpoIIIAH (red), produced in the MC, assemble at the septum, and form a protein-protein-zipper. (iii) During membrane migration, peptidoglycan hydrolases localize to the leading edges. Additional SpoIIQ-SpoIIAH complexes form around the forespore. (iv) Membrane cleavage occurs at the tip of the forespore, through which the forespore is released into the cytoplasm of the mother cell. The figure was modified after (Gutierrez *et al.* 2010).

Afterwards, the coat and the cortex of the forespore matures, consisting of an inimitable, highly preserved structure, helping to maintain dormancy and resistance against heat. The coat is the outer shell of the forespore, is composed of roughly 70 proteins and consists of four different layers: a basement layer, an inner coat, an outer coat and a crust. The inner shell of the forespore, is spatially separated from the coat by the outer forespore membrane and consists of two different peptidoglycan layers, one that serves as the base for the new vegetative cell wall (germ wall) and the other

with a special peptidoglycan (cortex) (Figure 11) (Piggot and Hilbert 2004, Paredes-Sabja *et al.* 2011).

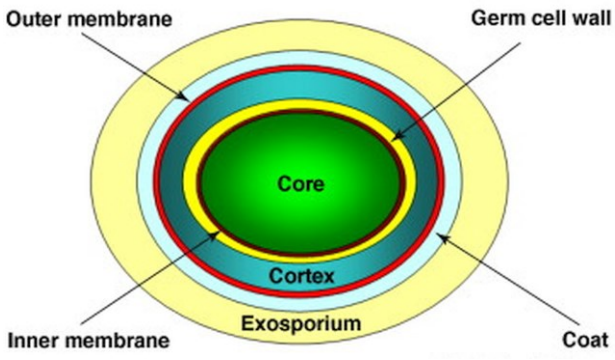

Figure 11 | Scheme of a mature *B. subtilis* spore. The spore is built by various layers. In the center is the core containing the condensed spore DNA, which is surrounded by the inner membrane, composed of lipids, and functioning as a permeability barrier to protect the DNA from damage. On top of the inner membrane, there is the germ cell wall, built up of the peptidoglycan of vegetative cells, serving as the new peptidoglycan after germination. Next, there is the cortex, composed of the specialized spore peptidoglycan with less transpeptidation and which possesses a muramic acid δ-lactam structure. The cortex is surrounded by an outer membrane followed by the coat, composed of proteins and functioning as a barrier to protect the spore from lytic enzymes and chemicals. The figure was taken from (Paredes-Sabja et al. 2011)

This peptidoglycan differs from the ones of vegetative growing cells by less transpeptidation due to D,D-carboxypeptidase activity of CwlD and PdaA (cross-linked at only 2.9% muramic acid residues) and by possessing a muramic acid δ-lactam structure. This muramic lactam is only found in bacterial endospores and appears at 50% of the disaccharide subunits (Smith *et al.* 1996, Atrih *et al.* 1999, Vollmer *et al.* 2008b, Tan and Ramamurthi 2014). The forespore obtains heat resistance by decreasing its water content, condensing the chromosome, and taking up dipicolinic acid (DPA) synthesized from the mother cell, to further reduce the water content by mineralizing (Tan and Ramamurthi 2014). Subsequently, the mother cell lyses and releases the mature, dormant spore. Thereby, the cell wall of the mother cell is hydrolyzed by autolysins. Two of them are the *N*-acetylmuramoyl-L-alanine amidases LytC and, more importantly, CwlC (Smith *et al.* 1996, Dworkin and Losick 2005, Vollmer *et al.* 2008b, Do *et al.* 2020). The process of sporulation is a very time and energy consuming process and takes seven hours at 37°C from the onset of sporulation to the release of the mature spore, which is structured with a core in the center of the spore, surrounded by an inner membrane, consisting out of lipids with a low permeability to protect the DNA in the core from damage. On top of the inner membrane is a germ cell wall built up of a typical vegetative PGN, which is enclosed

by the cortex with its specialized spore PGN, followed by an outer membrane. On the outside of the spore is the coat, which is composed of proteins and protects the spore from lytic enzymes and chemicals.

After the mature spore is released, it can survive in a dormant state until the environmental conditions get more favorable. Therefore, the spores monitor their surrounding area constantly via germinant receptors (Smith *et al.* 1996, Vollmer *et al.* 2008b, Paredes-Sabja *et al.* 2011). L-alanine serves as the main trigger for germination in *B. subtilis*, whereas L-asparagine, fructose, glucose, and potassium chloride as well as high hydrostatic pressures are also sensed by the receptors. Once the receptors recognize these triggers, they initiate a signal cascade by which monovalent cations and DPA are released from the spore core. The release of DPA leads to the activation of the cell wall hydrolase CwlJ, specialized for the unique spore peptidoglycan. Additionally, changes in cortex due to for example partial core hydration induce the expression of the spore cortex-lytic transglycosylase SleB. These two enzymes degrade the cortex peptidoglycan, subsequently leading to the uptake of water, core expansion, and outgrowth as a vegetatively growing cell (Smith *et al.* 1996, Vollmer *et al.* 2008b, Paredes-Sabja *et al.* 2011).

1.5 Biofilm growth

Another strategy of *B. subtilis* to protect cells from stress, high concentrations of bactericidal antimicrobials and harsh environmental conditions is the formation of biofilms (Lewis 2000, Hamon and Lazazzera 2001). The formation of biofilms depends on a high cell density and is initiated via quorum sensing. Biofilms consist of cell communities attached to surfaces that produce an extracellular polymeric matrix, which coheres them together and has a structural and a protective role for the biofilm community. The extracellular polymeric matrix is composed of exopolysaccharides, encoded by *epsA-O* operon, amyloid fibers synthesized by TapA, DNA, and proteins. Within a biofilm, multiple cell types are observed, like motile cells, spores, matrix-producers, or dead cells (Branda *et al.* 2005, Kraigsley and Finkel 2009, Shank *et al.* 2011, Cairns *et al.* 2014). Biofilm formation is initiated by the activation of the global regulator Spo0A via phosphorylation (Branda *et al.* 2001). Threshold-levels of Spo0A-P lead via anti-repression to the transcription of operons responsible for biofilm formation. Thereby, AbrB a regulator responsible for repressing biofilm gene expression gets inhibited by Spo0A-P and additionally, the AbrB anti-repressor AbbA

is expressed due to Spo0A-P, leading to activation of the biofilm operons (Hamon and Lazazzera 2001). Secondly, SinR, a repressor responsible for inhibition of biofilm gene expression, gets eased by the activation of its counterpart SinI due to threshold-levels of Spo0A-P, also leading to the expression of the biofilm operons (Cairns *et al.* 2014). Furthermore, the repression of AbrB results in the transcription of the *eps*-operon and *tapA*, which are needed to produce the extracellular polymeric matrix. Those cells, which are responsible for generating the extracellular matrix in the biofilm community are able to produce and secrete toxins in order to kill futile cells inside the biofilm. By killing these cells, they provide the community with nutrients and delay sporulation, which eventually is initiated when nutrients get limited and thereby the levels of Spo0A-P in the cells further increase (Shank *et al.* 2011).

1.6 Cannibalism

Under nutrient limitation, *B. subtilis* has several approaches to survive, enhancing motility, production of biofilms, development of competence and salvage of alternative nutrients. The ultimate process is the formation of endospores, which can exist for a long time in a dormant state until the environmental conditions become more favorable again. But as already mentioned, sporulation is a very time and energy consuming process. For this reason, *B. subtilis* tries to delay sporulation until it is necessary by all the mentioned approaches and by a strategy called cannibalism. If *B. subtilis* lacks alternatives, it cannibalizes sibling cells under starvation conditions to feed on them to overcome nutrient limitation for a short time period (González-Pastor *et al.* 2003, Vollmer *et al.* 2008b, López *et al.* 2009). When nutrients are limited, a subpopulation of a heterogeneous cell population notices this earlier than others. A signal for the cells for nutrient limitation is the cell density of the community. In populations with high number of cells, kinases, responsible for the activation of the global regulator Spo0A by phosphorylation, get activated. Spo0A-P leads to the expression of the secreted quorum-sensing lipopeptide surfactin (Nakano *et al.* 1988), as well as the cannibalism loci, which are the *skf* (sporulation killing factor) and the *spd* (sporulation delay protein) operon (González-Pastor *et al.* 2003, Engelberg-Kulka *et al.* 2006, López *et al.* 2009, Chastanet *et al.* 2010).

Thereby, Spo0A-P is present at low levels in the cells which is regulated by the different kinases involved in the phosphorelay and the period from start of the Spo0A activation. Low concentrations of Spo0A-P are sufficient for activating the operons because of

their strong binding sites for Spo0A-P. Activated Spo0A-P leads directly to the expression of the *skf* operon and indirectly to the expression of the *sdp* operon by inhibition of the repressor AbrB (Figure 2) (Fujita *et al.* 2005, Claverys and Havarstein 2007, López *et al.* 2009, Chastanet *et al.* 2010).

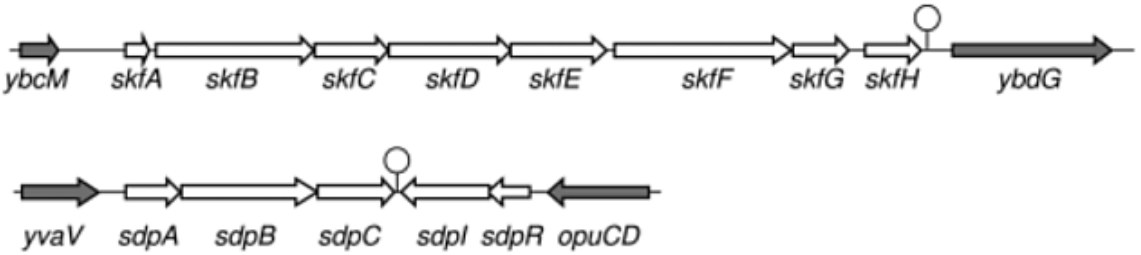

Figure 12 | Scheme of the cannibalism operons of *B. subtilis*. The upper operon is the *skfABCDEFGH* operon, encoding for the toxin SKF, its secretion and resistance against it. The lower cluster is composed of two operons *sdpABC* and *sdpRI*, whereas the first encodes for the toxin SDP and the second is responsible for the secretion and the immunity. The two hairpins represent the transcriptional terminators. The figure was taken from (González-Pastor 2011).

The operons (Figure 12) encode for cannibalism toxins, their secretion, and the resistance against them to protect the producing cells. The *skf* operon is built up of eight genes *skfABCDEFGH*. The first gene in this operon is *skfA* and encodes for the toxin SKF, which is a bacteriocin-like antibiotic. *skfB* and *skfD* might be involved in the post-translational modification and maturation of SkfA generating the functional toxin SKF. Secretion of and immunity against the produced toxin is mediated by *skfE* and *skfF*, which are encoding for two components of an ABC-transporter. The role of the other genes encoded in the operon has not been identified yet (González-Pastor *et al.* 2003, Ellermeier *et al.* 2006, Claverys and Havarstein 2007, González-Pastor 2011, Pérez Morales *et al.* 2013). The *spd* cluster consists of two operons, one with three genes *sdpABC* and, contiguously, the second operon with two genes *sdpRI*. In the first operon *sdpC* encodes for the toxin SDP, which is derived from the C-terminus of SdpC and refers to an antimicrobial peptide structure. *sdpA*, which might be acting as a chaperone, and *sdpB* are responsible for the maturation and secretion of the toxin, but their exact functions are still unknown. The second operon *sdpRI* is responsible for the immunity against SDP. Thereby, *sdpR* encodes for an autorepressor, blocking the expression of the operon. *sdpI* encodes for an integrated membrane protein, which binds SDP and acts as a signal-transducer responding to SDP. SdpI undergoes a conformational change and sequesters SdpR leading to activation of the *sdpRI* operon and synthesis of the immunity protein (Figure 13) (Ellermeier *et al.* 2006, Claverys and Havarstein 2007, González-Pastor 2011, Pérez Morales *et al.* 2013).

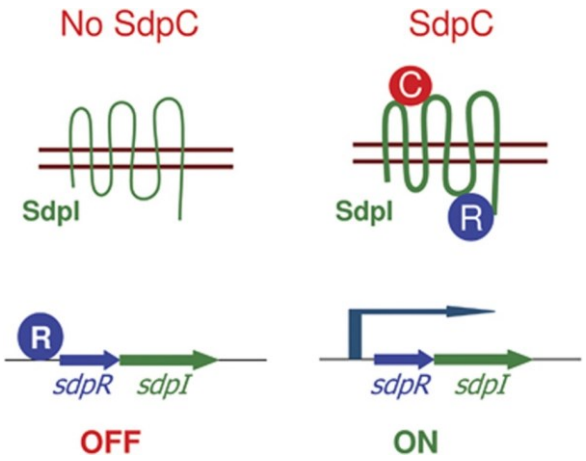

Figure 13 | Mechanism of the self-induced immunity against SDP. On the left, the model shows non-cannibalistic conditions. The operons for the toxin are not expressed, merely SdpI is present in the membrane in threshold amounts and SdpR (R) represses the resistance operon expression. On the right, the model shows cannibalistic conditions, where SDP (SdpC) is present. This is sensed by SdpI, bound to it from the outside and leading to a conformational change of the membrane protein. SdpR gets sequestered at the membrane which leads to the expression of the immunity operon *sdpRI* and therefore synthesis of SdpI. The figure was taken from (González-Pastor 2011).

The toxins produced by cannibalistic cells attack prey cells, who have not sensed nutrient limitation and therefore have not activated Spo0A by phosphorylation. Due to the lack of Spo0A-P, the cannibalism operons are repressed by AbrB and the cells cannot protect themselves against the toxins (Ellermeier *et al.* 2006, Engelberg-Kulka *et al.* 2006). Prey cells exposed to SKF and SDP show a collapse of the PMF and autolysis as a second consequence since autolysins always present around the cell envelope get deregulated (Figure 14) (Lamsa *et al.* 2012).

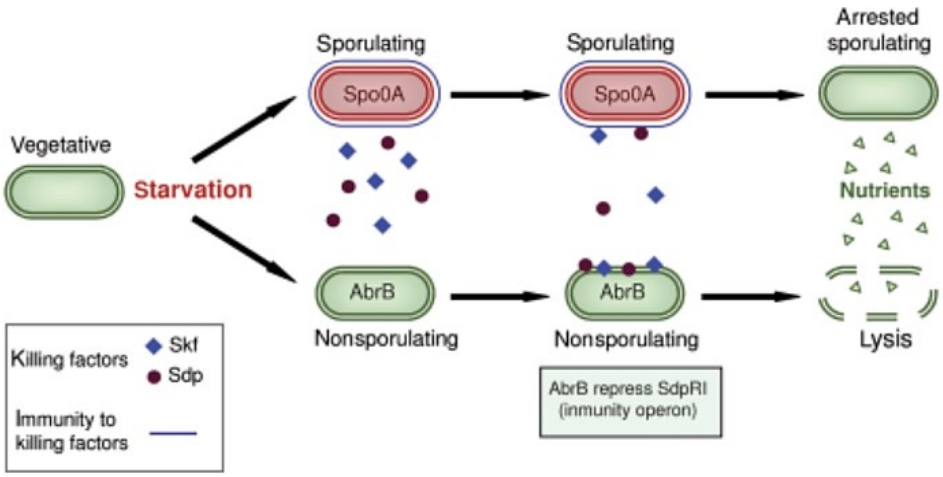

Figure 14 | Scheme of cannibalism in *B. subtilis*. A cell population of vegetative growing cells undergoes nutrient limitation. A part of the community senses starvation earlier than others and initiate the sporulation process by activating Spo0A. These Spo0A-active (0A-P) cells express under low levels of 0A-P the toxins SKF and SDP and likewise the resistance against them. The cells, which have not sensed the nutrient limitation and are Spo0A-inactive are sensitive against the toxins. The non-cannibalistic cells are killed by toxin activity and lyse, releasing nutrients in the medium. Cannibalistic cells can feed on the new nutrients, resume growth and delay sporulation. The figure was taken from (González-Pastor 2011).

The collapse of the PMF is due to the translocation of protons across the membrane, which is probably by the action of SDP. Although the exact mechanism is unknown, it might be possible that SDP forms pores in the membrane which serve as channels for the protons. Furthermore, the PMF, or more precisely ΔΨ, directs the insertion of membrane proteins and is required for the correct positioning of division proteins. A collapse of the PMF might therefore be responsible for the dislocation of autolysins to non-target sites of the peptidoglycan and hence, uncontrolled hydrolysis (Lamsa *et al.* 2012). By cell lysis, nutrients like peptidoglycan fragments are set free into the surrounding environment and serve as new carbon sources for cannibalistic cells. Based on the availability of nutrients, *B. subtilis* can overcome starvation and delay the sporulation (Lamsa *et al.* 2012). Responsible for the hydrolysis of the peptidoglycan of prey cells are endo-acting as well as exo-acting hydrolases, like LytC, LytD, LytE, LytF, NagZ and AmiE (Smith *et al.* 2000, Litzinger *et al.* 2010). An autolysin-defective strain, missing *lytC*, *lytD*, *lytE* and *lytF* is not lysed but nonetheless gets killed by the action of the toxins.

A second reason for cannibalism except nutrient limitation might be the elimination of cells, that are useless for the cell population, because they are not contributing to biofilm formation or are no longer beneficial for the community. Besides, the elimination allows the rest of the population to grow further and to produce new useful cells (Lamsa *et al.* 2012). *B. subtilis* biofilms, which are also regulated indirectly by the global regulator Spo0A, get promoted due to cannibalistic activity. The killing of sibling cells provides nutrients to help the matrix-producing cannibalistic cells retain growth, further formation of biofilm and delaying sporulation (González-Pastor 2011).

Additionally, the toxin SDP is not only active against sibling cells, but also against a variety of microorganisms in the phylum of Firmicutes, *E. coli*, *Xanthomonas oryzae*, *Listeria monocytogenes*, and *Staphylococcus aureus*. This gives a hint that cannibalism is not only be a strategy to survive nutrient limitation, however it might be important to protect the population versus encroaching species (Nandy *et al.* 2007, Lamsa *et al.* 2012, Pérez Morales *et al.* 2013).

1.7 Research objective

The aim of this study was to investigate the role of autolysins and peptidoglycan recycling in bacterial survival and during the process of cannibalism in the onset of sporulation. I focused on solving the mechanisms of PGN cleavage in the cannibalism process and how cannibalistic cells can feed on PGN fragments of siblings. Therefore, the autolysins LytC, LytD, LytE, and LytF were investigated as they were shown to be somehow involved in cell lysis (Lamsa *et al.* 2012). At the moment, nothing is known about the flow of nutrients and whether cell wall fragments released from prey cells can be utilized by the cannibals. Therefore, I aimed to explore the flow of nutrients, particularly the released PGN fragments, from prey to cannibalistic cells using a cell wall labeling strain, generated during this study. Cannibalistic cells should be able to incorporate released peptidoglycan fragments of prey cells because *B. subtilis* has the capability to recycle its own peptidoglycan. The recycling of *B. subtilis* was proven by measurement of MurNAc-6P accumulation in the cytoplasm (Borisova *et al.* 2016, Mayer *et al.* 2019). Furthermore, it was shown, that recycling takes place during transition and stationary phase, and that the so-called MurNAc recycling operon, consisting of *murQ*, *murR*, *murP*, *amiE*, *nagZ*, and *ybbC*, is involved (Litzinger *et al.* 2010, Borisova *et al.* 2016). In the MurNAc recycling operon, the genes *nagZ* and *amiE* encode for the exo-*N*-acetylglucosaminidase NagZ and the *N*-acetylmuramyl-L-alanine amidase AmiE, which have been shown to possess this exo-cleaving specificity as they chip off GlcNAc (NagZ) and the peptide stem (AmiE) from the non-reducing end of a peptidoglycan chain, thereby generating single cell wall sugars (GlcNAc) and peptides. Additionally, it was shown, that both are expressed in stationary phase, which is the same period of nutrient limitation and cannibalism, respectively (Litzinger *et al.* 2010). However, these both enzymes are not able to degrade fragments bigger than GlcNAc-MurNAc-peptides into single cell wall sugars and as this would require the help of an exo-*N*-acetylmuramidase as it was described by Del Rio and colleagues (Del Rio *et al.* 1973, Del Rio and Berkeley 1976). I aimed to explore the role of the MurNAc recycling operon in *B. subtilis* survival under nutrient limitation and to characterize the gene of unknown function *ybbC* in the MurNAc recycling operon, which might be the missing link for the formation of single cell wall sugars that may serve as carbon sources during nutrient limitation.

2 Methods and material

2.1 Chemicals and devices

Solutions and chemicals were acquired from AppliChem, Bachem Holding AG, Carbosynth, Carl Roth GmbH + Co. KG, Difco Laboratories, Merck KGaA, Sigma-Aldrich GmbH, SERVA Electrophoresis GmbH, Thermo Fisher Scientific Inc. and VWR GmbH. Restriction enzymes, polymerases and other enzymes were purchased from Genaxxon bioscience GmbH, New England Biolabs GmbH, Pharmacia Fine Chemicals AB, Sigma Aldrich GmbH and Thermo Fisher Scientific Inc. Filters, reaction tubes and other devices were acquired from Bio-Rad Laboratories, Carl Roth GmbH + Co. KG, Eppendorf AG, Merck KGaA, Greiner Bio-One, Sarstedt AG, Thermo Fisher Scientific Inc., Sartorius AG, VWR GmbH. Devices were from Bio-Rad Laboratories, Brand GmbH + Co. KG, Bruker Corporation, Dionex Corporation, Eppendorf AG, GE Healthcare GmbH, Heidolph Instruments GmbH + Co. KG, Hitachi Chemical Company, Martin Christ Gefriertrocknungsanlagen GmbH, Mettler-Toledo GmbH, Molecular Devices LLC., Peqlab Biotechnologie GmbH, Thermo Fisher Scientific Inc., VWR GmbH.

2.2 Strains and plasmids

Escherichia coli strains

Table 2 | *E. coli* strains used in this study

Strain **# strain collection**	**Genotype**	**Reference**
DH5α #1201	*fhuA2 Δ(argF-lacZYA)U169 phoA glnV44 Φ80' Δ(lacZ)M15 gyrA96 recA1 relA1 endA1 thi-1 hsdR17*	New England Biolabs GmbH, Frankfurt, Germany
BL21(DE3) #1205	*fhuA2 [lon] ompT gal (λ DE3) [dcm] ΔhsdS λ DE3 = λ sBamHIo ΔEcoRI-B int::(lacI::PlacUV5::T7 gene1) i21 Δnin5*	New England Biolabs GmbH, Frankfurt, Germany

Escherichia coli plasmids

Table 3 | *E. coli* plasmids used in this study

Plasmid # plasmid collection	Genotype	Reference
pET16b-*BsnagZ* #11319 (# strain collection)	expression vector, P_{T7}, $Term_{T7}$, ori_{pBR322}, ori_{f1}, N-terminal His_{10}-Tag, Factor Xa site, *lacI*, ap^r, *nagZ* of *B. subtilis 168*, *Nde*I, *Xho*I	(Litzinger *et al.* 2010)
pET22b-*amiE* #117	expression vector, P_{T7}, $Term_{T7}$, ori_{pBR322}, ori_{f1}, N-terminal *pelB* signal sequence, C-terminal His_6-Tag, *lacI*, ap^r, *amiE* of *B. subtilis 168* in pET22b, *Nco*I, *Xho*I	(Engelbrecht 2016)
pET28a-atl^{Glc} #2124	expression vector, P_{T7}, $Term_{T7}$, ori_{pBR322}, ori_{f1}, N-terminal His_6-Tag/thrombin/T7-Tag, C-terminal His_6-Tag, *lacI*, km^r, atl^{Glc} of *S. aureus* JE2 in pET22b, *Nco*I, *Xho*I	cloned by M. Borisova-Mayer
pET28a-*cwlC* #3185	expression vector, P_{T7}, $Term_{T7}$, ori_{pBR322}, ori_{f1}, N-terminal His_6-Tag/thrombin/T7-Tag, C-terminal His_6-Tag, *lacI*, km^r, *cwlC* of *B. subtilis 168* in pET22b, *Nco*I, *Xho*I	(Teufel 2019)
pET29b-*ybbC* #21868 (# strain collection)	expression vector, P_{T7}, $Term_{T7}$, ori_{pBR322}, ori_{f1}, N-terminal S-Tag/thrombin, C-terminal His_6-Tag, *lacI*, km^r, *ybbC* of *B. subtilis 168* in pET29b, *Nde*I, *Xho*I	(Duckworth 2016)

Bacillus subtilis strains

Table 4 | *B. subtilis* strains used in this study

Strain # strain collection	Genotype	Reference
168 #22025	*trpC2*	Bacillus Genetic Stock Center (BGSC), Columbus, USA
168-Δ*spo0A::erm* #11444	*trpC2* Δ*spo0A::erm*	BGSC
168-Δ*spo0A* #11436	*trpC2* Δ*spo0A*	this study
168-Δ*lytC::erm* #11542	*trpC2* Δ*lytC::erm*	BGSC
168-Δ*lytC* #11601	*trpC2* Δ*lytC*	(Mühleck 2016)
168-Δ*lytD::erm* #11567	*trpC2* Δ*lytD::erm*	BGSC
168-Δ*lytD* #11602	*trpC2* Δ*lytD*	(Mühleck 2016)
168-Δ*lytE::erm* #11543	*trpC2* Δ*lytE::erm*	BGSC
168-Δ*lytE* #11603	*trpC2* Δ*lytE*	(Mühleck 2016)
168-Δ*lytF::erm* #11521	*trpC2* Δ*lytF::erm*	BGSC
168-Δ*lytF* #11604	*trpC2* Δ*lytF*	(Mühleck 2016)
168-Δ*lytC*Δ*spo0A::erm* #21769	*trpC2* Δ*lytC* Δ*spo0A::erm*	(Mühleck 2016)
168-Δ*lytD*Δ*spo0A::erm* #21770	*trpC2* Δ*lytD* Δ*spo0A::erm*	(Mühleck 2016)

Strain **# strain collection**	**Genotype**	**Reference**
168-Δ*lytE*Δ*spo0A::erm* #21771	*trpC2* Δ*lytE* Δ*spo0A::erm*	(Mühleck 2016)
168-Δ*lytF*Δ*spo0A::erm* #21772	*trpC2* Δ*lytF* Δ*spo0A::erm*	(Mühleck 2016)
168-*amyE::cfp* #21901	*trpC2 amyE::*(P_{gudB}-*cfp cm*)	(Gunka *et al.* 2013)
168-*amyE::yfp* #21881	*trpC2 amyE::*(P_{gudB}-*iyfp cm*)	(Gunka *et al.* 2013)
168-*amyE::yfp*Δ*spo0A::erm* #21908	*trpC2* Δ*spo0A::erm amyE::*(P_{gudB}-*iyfp cm*)	this study
168-*amyE::yfp*Δ*lytC::erm* #21909	*trpC2* Δ*lytC::erm amyE::*(P_{gudB}-*iyfp cm*)	this study
168-*amyE::yfp*Δ*lytD::erm* #21910	*trpC2* Δ*lytD::erm amyE::*(P_{gudB}-*iyfp cm*)	this study
168-Δ*murQ* #21766	*trpC2* Δ*murQ*	(Dalügge 2015)
168-Δ*nagA::erm* #11518	*trpC2* Δ*nagA::erm*	BGSC
168-Δ*murQ*Δ*nagA::erm* #21773	*trpC2* Δ*murQ* Δ*nagA::erm*	(Mühleck 2016)
168-Δ*murQ*Δ*nagA* #21902	*trpC2* Δ*murQ* Δ*nagA*	this study
168-Δ*murQ*Δ*nagA*_pGP888-PAM #21916	*trpC2* Δ*murQ* Δ*nagA ganA::*(pGP888-*mupPamgKmurU*)	this study
168_pGP888 #21926	*trpC2 ganA::*(pGP888)	this study
168-Δ*murQ*Δ*nagA*_pGP888 #21927	*trpC2* Δ*murQ* Δ*nagA ganA::*(pGP888)	this study

Strain **# strain collection**	**Genotype**	**Reference**
168-Δ*murQ*Δ*murR*Δ*murP* #21856	*trpC2* Δ*murQ* Δ*murR* Δ*murP*	(Borisova *et al.* 2016)
168-Δ*namZ::erm* #11462	*trpC2* Δ*namZ::erm*	BGSC
168-Δ*namZ* #22075	*trpC2* Δ*namZ*	this study
168-Δ*nagZ::erm* #11459	*trpC2* Δ*nagZ::erm*	BGSC
168-Δ*nagZ* #22074	*trpC2* Δ*nagZ*	this study
168-Δ*amiE::erm* #22026	*trpC2* Δ*amiE::erm*	BGSC
168-Δ*amiE* #22073	*trpC2* Δ*amiE*	this study
168-Δ*amiE*Δ*nagZ*Δ*namZ* #22048	*trpC2* Δ*amiE* Δ*nagZ* Δ*namZ*	this study
168-Δ*sdpC::erm* #11419	*trpC2* Δ*sdpC::erm*	BGSC
168-Δ*sdpC* #21956	*trpC2* Δ*sdpC*	this study
168-Δ*skfA::erm* #11442	*trpC2* Δ*skfA::erm*	BGSC
168-Δ*skfA* #21905	*trpC2* Δ*skfA*	this study
168-Δ*sdpC*Δ*skfA::erm* #22050	*trpC2* Δ*sdpC* Δ*skfA::erm*	this study
168-Δ*skfA*Δ*sdpC::erm* #22051	*trpC2* Δ*skfA* Δ*sdpC::erm*	this study
B. subtilis 168-Δ*lytABC::neo* Δ*lytD::tet*Δ*lytE::cm*Δ*lytF::spec*	*trpC2* Δ*lytABC::neo* Δ*lytD::tet* Δ*lytE::cm* Δ*lytF::spec*	BGSC

Bacillus subtilis plasmids

Table 5 | *B. subtilis* plasmids used in this study

Plasmid # plasmid collection	Genotype	Reference
pBP26 #2145	pAC5 derivative, P_{gudB}, i*yfp*, integration in *amyE* site, ap^r (*E. coli*), cm^r (*B. subtilis*)	(Gunka *et al.* 2013)
pBP27 #2146	pAC5 derivative, P_{gudB}, *cfp,* integration in *amyE* site, ap^r (*E. coli*), cm^r (*B. subtilis*)	(Gunka *et al.* 2013)
pJM103-I-SceI #296	suicide integration vector (Perego 1993),with I-SceI restriction site, ap^r (*E. coli*), cm^r (*B. subtilis*)	(Perego, unpublished)
pJM103-I-SceI_Δ*murQRP* #2103	pJM103-I-SceI carrying *murQ murR murP* flanking regions for chromosomal integration in *B. subtilis*, *Xma*I, *Bam*HI, *Hind*III	(Borisova *et al.* 2016)
pJM103-I-SceI_Δ*amiE* Δ*nagZ*Δ*namZ* #3193	pJM103-I-SceI carrying *amiE nagZ namZ* flanking regions for chromosomal integration in *B. subtilis*, *Eco*RI, *Xma*I, *Bam*HI	this study
pBKJ223 #295	I-SceI expression vector, ap^r (*E. coli*), tc^r (*B. subtilis*)	(Janes and Stibitz 2006)
pDR244 #290	loop-out plasmid, ori_{pACYC}, *cre*, *cop*, *repF*, ap^r (*E. coli*), $spec^r$ (*B. subtilis*)	BGSC
pGP888 #291	pUC19 derivative, P_{xylA}, *xylR*, C-YFP, integration in *ganA* site, ap^r (*E. coli*), kan^r (*B. subtilis*)	(Diethmaier *et al.* 2011)
pGP888-PAM #2147	pGP888 carrying *mupP*, *amgK*, *murU* (from *Pseudomonas putida*), *Xba*I, *Bam*HI	this study
pX #297	P_{xylA}, *xylR*, integration in *amyE* site, ap^r (*E. coli*), cm^r (*B. subtilis*)	(Kim *et al.* 1996)

Plasmid # plasmid collection	Genotype	Reference
pX-PAM #21924 (# strain collection)	pX carrying *mupP*, *amgK*, *murU* (from *Pseudomonas putida*)	cloned by S. Unsleber

2.3 Oligonucleotides

Table 6 | Oligonucleotides used in this study[1)]

Application	Name	Sequence* (5' → 3')[2]
amplification of *spo0A* flanking regions	spo0A_500fw	GCA CAA CGC CGC AAA AAT TCC
	spo0A_500r	GCA ATT GTG AAC ACA CAA GGC T
amplification of *lytC* flanking regions	lytC-f	ACG AAA TCT TTG GAC TTA ACG AAG
	lytC-r	CCA GAC TTC TCG GCA TCT ATT TTC A
amplification of *lytD* flanking regions	lytD-f	AGC AAA ATT CAG ATG CCA CAT ACC G
	lytD-r	CCA TTC TTA TGA AAA CTT CAT GAA TCA T
amplification of *lytE* flanking regions	lytE-f	CTC CTT TAA TGT ATT CCG TTT ATC ATG
	lytE-r	GCA GAT ATC GGA CTA AGC TGT TTA A
amplification of *lytF* flanking regions	lytF-f	CCG GAG AAC TTT CAA ATA TAA AAC AGA
	lytF-r	AGT TTA TGC CGC ATC CTC TGT TAT TGA
amplification of *nagA* flanking regions	nagA-ko_for	CGG GCT TGA ACC TAA AAC AGA TTT TAT AA
	nagA-ko_nagB_r	CAT AAT CTG ATA GTA AAT CGG AAT AGG CG
cloning of *mupP*, *amgK*, *murU* in pGP888	PAM-BamHI-for	AGC TTG GAT CCA TGC GTT TGC GAG CAG TA
	PAM-XbaI-rev	AAG CTT TCT AGA TCA GGC GCG CTC GCC AAT CAG

[1] All oligonucleotides used in this study were ordered at and synthesized by Eurofins Genomics Germany GmbH, Ebersberg, Germany.
[2] restriction sites are underlined

Application	Name	Sequence* (5' → 3')[2]
cloning of *nagA* in pGP888	nagA-XbaI-for	AGC TTT CTA GAG GCA GAG AGT CTT CTT ATC AAA GAC ATT GCG
	nagA-BamHI-rev	ATA GAG GAT CCT CAT TCA TAT CTG GTC AGC CTC CTT GG
amplification of flanking region of *murP* Δ*murQRP*	pJMOp-XmaI-fw	AGC TGC CCG GGT TCC GGC GTG TAA AAG TAA A
	pJMOp-BamHIrev	CAG CTG GAT CCG TGA AAA CAA AGA CAC TGT T
amplification of flanking region of *murQ* for generating of Δ*murQRP*	pJMOp-BamHI-fw	AGC TTG GAT CCG AGG ATG CCC CCT GTT TTA A
	pJMOp-Hind3rev	CAG CTA AGC TTT CCA ATC ATT CAC GCT CAC C
amplification of *amiE* flanking regions	amiE_500_fw	GCTCTTTTCCGATGATGCTGCCGG
	amiE_500_rev	CGTAACCGGACTGCATCAAGGC
amplification of *nagZ* flanking regions	nagZ_500_fw	GCGGCTTCCATTGCGTATGCC
	nagZ_500_rev	GCGTTATTCAATTCCCTAACATCCGC
amplification of *namZ* flanking regions	namZ_500_fw	GCTTCAGTTTGGCTAATTCCG
	namZ_500_rev	CAAACCCGTATCCCTCAGC
amplification of flanking region of *namZ* for generating of Δ*amiE* Δ*nagZ* Δ*namZ*	pJMybbCDE-EcoRI-fw	AGC TGG AAT TCG CCG GAC TGC AAG ATT TTC GAT ATG
	pJMybbCDE-XmaI-rev	CAG CTC CCG GGA ACA TAA GCA TCG TAT GTT ACA CGT G
amplification of flanking region of *amiE* for generating of Δ*amiE* Δ*nagZ* Δ*namZ*	pJMybbCDE-XmaI-fw	AGC TTC CCG GGA GGC TAG CCC CTT TCT GTG CTT CTA TCC C
	pJMybbCDE-BamHI-rev	CAG CTG GAT CCC GGG CTT TAT TCT GGG CGC AAC CTT CCT TC

[2] restriction sites are underlined

Application	Name	Sequence* (5' → 3')[2]
amplification of *sdpC* flanking regions	sdpC::erm-500fw	ATT TAA ACG CAG CTT TAG AGC G
	sdpC::erm-500rv	TGG TCA GGAAAT AAA CCG GCT GC
amplification of *skfA* flanking regions	SkfA_500fw	GCG TAA TGA AGA GTG TTA CTG TGG
	SkfA_500rev	CCC GGT CAG CGT AAT ATC AGC AAC
control of insertion of vectors pBP27, pBP26 and pX into *amyE* site	amyE_FW	ATG TTT GCA AAA CGA TTC AA
	amyE_RV	TCA ATG GGG AAG AGA ACC GCT
control of chromosomal integration of pJM103-I-SceI	cat_FW	TGA ACT TTA ATA AAA TTG ATT
	cat_RV	AAA AGC CAG TCA TTA GGC CTA TCT
control of chromosomal integration of erm^r cassette	erm-f	ATG AAC GAG AAA AAT ATA AAA CAC AGT CAA
	erm-rev	TTA CTT ATT AAA TAA TTT ATA GCT ATT GAA AAG AG
control of insertion of vector pGP888 into *ganA* site	ganA-FW	GTG ATG TCA AAG CTT GAA AAA ACG C
	ganA-RV	CTA ATG TGT GTT TAC GAC AAT TCT CAC

[2] restriction sites are underlined

2.4 Media and buffers

Table 7 | Media and buffers used in this study

Rich medium

LB broth (Lennox)	20 g	powdered medium
	fill up to 1 L dH_2O	
	For agar plates:	
	15 g	bacto-agar
	Medium and agar were autoclaved.	

Starch agar	8 g	nutrient broth
	10 g	soluble starch
	16 g	bacto-agar
	Suspend in 1 L dH_2O, mix thoroughly and heat with frequent agitation. Boil carefully, excessive heating may hydrolyze starch.	
	Agar was autoclaved.	

Minimal medium for *B. subtilis*

10x MM	440 mM	potassium dihydrogen phosphate
	600 mM	dipotassium phosphate
	29 mM	trisodium citrate
	150 mM	ammonium sulfate
	Medium was autoclaved.	
MGE medium	2 ml	10x MM
	800 µl	glucose (50%)
	144 µl	L-glutamate (40%)
	100 µl	ammonium iron(III) citrate (2 mg ml^{-1})
	100 µl	yeast extract (5%)
	200 µl	tryptophan (5 mg ml-1)
	100 µl	casamino acids (10%)
	40 µl	magnesium sulfate (1 M)
	40 µl	calcium chloride (0.5 M)
	fill up to 20 ml with dH2O	
	Ingredients were sterile filtered using a 0.2 µM filter, except for magnesium sulfate and calcium chloride. These were autoclaved.	

Buffers for HPLC analysis

Buffer A	0.1%	formic acid
	0.05%	ammonium formate
Buffer B	100%	acetonitrile

Buffers for enzyme assays

Stock solutions for phosphate buffers	Stock solution A:	
	0.4 M	sodium dihydrogen phosphate monohydrate
	Stock solution B:	
	0.4 M	disodium hydrogen phosphate
Phosphate buffer (pH 6.0, 0.2 M)	87.7 ml	stock solution A (0.4 M)
	12.3 ml	stock solution B (0.4 M)
	100 ml	dH_2O
Phosphate buffer (pH 7.0, 0.2 M)	39 ml	stock solution A (0.4 M)
	61 ml	stock solution B (0.4 M)
	100 ml	dH_2O
Phosphate buffer (pH 7.5, 0.02 M)	20 mM	disodium hydrogen phosphate
	0.5 M	sodium chloride
Phosphate buffer (pH 8.0, 0.2 M)	3.3 ml	stock solution A (0.4 M)
	96.7 ml	stock solution B (0.4 M)
	100 ml	dH_2O
Phosphate buffer (pH 8.0, 0.02 M)	10 ml	phosphate buffer (0.2 M, pH 8.0)
	90 ml	dH_2O
Borate buffer	0.5 M	boric acid
	10 mg ml^{-1}	sodium borohydride
	adjust to pH 11.0	
Stopping buffer (pH 3.2)	1%	formic acid
	0.5%	ammonium formate
Clark & Lubs buffer (pH 2.0)	8 ml	potassium chloride (0.2 M)
	2.5 ml	hydrochloric acid (0.2 M)
Citric acid sodium phosphate buffer (pH 3.0 – 7.0)	pH 3.0:	
	46.1 ml	citric acid (0.1 M)
	3.9 ml	disodium hydrogen phosphate (0.2 M)
	pH 4.0:	
	21.36 ml	citric acid (0.1 M)
	9.64 ml	disodium hydrogen phosphate (0.2 M)

Citric acid sodium phosphate buffer (pH 3.0 – 7.0)	pH 5.0:	
	8.35 ml	citric acid (0.1 M)
	6.3 ml	disodium hydrogen phosphate (0.2 M)
	pH 6.0:	
	11.61 ml	citric acid (0.1 M)
	15.79 ml	disodium hydrogen phosphate (0.2 M)
	pH 7.0:	
	2.77 ml	citric acid (0.1 M)
	8.24 ml	disodium hydrogen phosphate (0.2 M)
Hydrochloric acid tris buffer (pH 8.0)	2.92 ml	hydrochloric acid (0.1 M)
	11.85 ml	tris (0.1 M)
	2.08 ml	dH_2O
Glycine sodium hydroxide buffer (pH 9.0)	pH 9.0:	
	2.85 ml	glycine (0.1 M)
	3.44 ml	sodium hydroxide (0.2 M)
	7.06 ml	dH_2O
Glycine sodium hydroxide buffer (pH 10.0)	pH 10.0:	
	2.8 ml	glycine (0.1 M)
	5.62 ml	sodium hydroxide (0.2 M)
	5.9 ml	dH_2O

2.5 Antibiotics

The listed antibiotics were sterile-filtered using a 0.2 µM filter and stored at -20°C.

Antibiotics for *E. coli*

	Final concentration in media	Solved in
Ampicillin	100 µg ml^{-1}	dH_2O
Kanamycin	50 µg ml^{-1}	dH_2O

Antibiotics for *B. subtilis*

	Final concentration in media	Solved in
Chloramphenicol	5 µg ml^{-1}	50% ethanol
Erythromycin	10 µg ml^{-1}	50% ethanol
Kanamycin	50 µg ml^{-1}	dH_2O
Spectinomycin	100 µg ml^{-1}	dH_2O
Tetracycline	7.5 µg ml^{-1}	50% ethanol

2.6 Molecular biological and genetic methods

2.6.1 Polymerase chain reaction (PCR)

Amplification of specific DNA fragments was accomplished by polymerase chain reaction (PCR) using a peqSTAR thermocycler (PEQLAB, VWR GmbH, Radnor, Pennsylvania, USA). A standard reaction mixture (total volume 50 µl) contained 0.5 µl Q5 High-Fidelty DNA polymerase, 1 µl template DNA, 0.2 mM dNTPs, 0.2 µM primers and 5x Q5 reaction buffer. As typical protocol for DNA amplification was used the followed:

Table 8 | PCR program for amplification of DNA

Step	Temperature [°C]	Time [sec]
Initial denaturation	98	300
30 to 35 cycles	98	30
	50 to 72[3]	30
	72	30 sec/kb (Q5 DNA polymerase) or 60 sec/kb (Taq DNA polymerase)
Final elongation	72	300
Hold	4	∞

[3] depending on the primer melting temperature

As a variety of standard PCR, the colony-PCR was applied to verify the successful ligation of DNA fragments into a plasmid after transformation of *E. coli* DH5α cells and to screen for introduced mutations in the genome of *B. subtilis*. For the colony-PCR of *E. coli* cells, single colonies were picked from plates. A reaction mixture (total volume 15 µl) contained 7.5 µl 2x RedMastermix and 0.2 µM primers. The protocol was carried out as described above. For the colony-PCR of *B. subtilis* cells, single colonies were picked and transferred into 10 µl milliQ. The tubes were incubated for 5 min on ice and, subsequently, heated for 1 min in the microwave on full power. Afterwards the cells were kept in ice again for 30 sec. These steps were performed three times in total. Finally, the samples were incubated for 5 min on ice and 1 µl was transferred into the reaction mixture for the colony-PCR (total volume 20 µl). The mixture contained 0.2 µl Q5 High-Fidelity DNA polymerase, 1 µl template, 0.2 mM dNTPs, 0.2 µM primers and 5x Q5 reaction buffer. The protocol for PCR reaction was the same as described above.

Successful DNA fragment amplification was verified by agarose gel electrophoresis. To determine DNA fragment size a DNA standard (GeneRuler 1 kb DNA ladder, Thermo Fisher Scientific Inc.) was used (Figure 15).

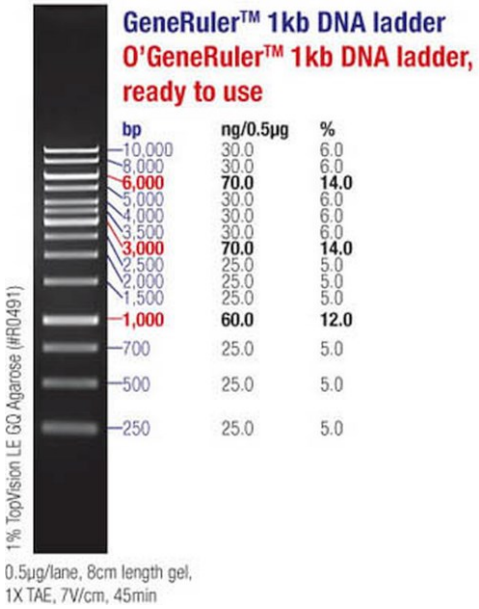

Figure 15 | DNA size marker. GeneRuler 1 kb DNA ladder (Thermo Fisher Scientific Inc.).

50x TAE	242 g	tris (2 M)
	18.6 g	EDTA (50 mM)
	57.1 ml	acetic acid
	Fill up to 1 L with dH_2O	
1% agarose gel	1% (w/v) agarose in 1x TAE	

2.6.2 Isolation of genomic DNA and plasmids

Isolation of genomic DNA was performed using the GeneJET Genomic DNA Purification Kit (Thermo Fisher Scientific Inc., Waltham, Massachusetts, USA). Isolation of plasmids was accomplished using a protocol published by Birnboim and Doly (Birnboim and Doly 1979) or achieved with the GeneJET Plasmid Miniprep Kit (Thermo Fisher Scientific Inc., Waltham, Massachusetts, USA).

2.6.3 Restriction of DNA

Isolated DNA was digested using restriction enzymes under buffer conditions recommended by the manufacturer. Reaction mixture (total volume for PCR products 20 µl, total volume for plasmids 40 µl) contained 20 to 100 ng plasmid or genomic DNA, 10 U restriction enzymes, 10x reaction buffer. Reaction mixture was incubated for 30 min up to 2 h at the recommended temperature for the respective restriction enzyme (37°C mostly). Successful restriction digest was verified via agarose gel electrophoresis. Linearized plasmid DNA was purified by gel extraction using GeneJET Gel Extraction Kit (Thermo Fisher Scientific Inc., Waltham, Massachusetts, USA). Digested PCR products were purified by GeneJET PCR Purification Kit (Thermo Fisher Scientific Inc., Waltham, Massachusetts, USA).

2.6.4 Ligation of DNA fragments

DNA fragments originated by restriction digest were ligated using T4 DNA ligase. Reaction mixture (total volume 20 µl) contained x µl linearized plasmid DNA, x µl digested DNA fragments, 1 µl T4 DNA ligase, 10x T4 DNA ligase reaction buffer. The amount of applied DNA (plasmid and insert) was calculated individually, after measurement of DNA concentration, with the formula followed:

$$\frac{ng\ plasmid\ DNA\ x\ bp\ insert}{bp\ plasmid}\ x\ molar\ ratio\ insert : plasmid = ng\ insert$$

Reaction mixture was incubated overnight at room temperature. Afterwards, ligation reaction was stopped at 65°C for 10 min.

2.6.5 Cloning of overexpression plasmids

Plasmids pET16b, pET22b, pET28a and pET29b were used to overexpress recombinant proteins heterologously in *E. coli* BL21(DE3). Via PCR the genes were amplified using primers that attached specific restriction sites. Restriction sites for cloning in pET22b and pET28a were *Nco*I and *Xho*I, for cloning in pET16b and

pET29b, they were *Nde*I and *Xho*I. By cloning of genes in the used pET vectors, they were fused with a His_6-tag on the C-terminus or a His_{10}-tag on the N-terminus for pET16b. After ligation, *E. coli* DH5α was transformed with the ligation mixture and selected by ampicillin or kanamycin resistance. Resistant colonies were tested for the final plasmid by colony-PCR and restriction digest. Plasmids with expected results were verified by sequencing (Eurofins Genomics Germany GmbH, Ebersberg, Germany).

2.6.6 Cloning of suicide integration plasmids

Markerless *B. subtilis* deletion mutants were generated by introducing a suicide integration plasmid called pJM103-I-SceI, according to a modified protocol of Janes and Stibitz (Janes and Stibitz 2006). Therefore, genomic DNA of *B. subtilis* 168 was purified. Via PCR the up- and downstream regions of the gene of interest were amplified. Each region was around 500 bp, including the start codon of the gene of interest in the upstream amplicon and the stop codon of the gene in the downstream region. Used primers attached specific restriction sites, by which the up- and the downstream fragment could be ligated into the vector pJM103-I-SceI. *E. coli* DH5α was transformed with the ligation mixture and selected by ampicillin resistance. Ampicillin resistant colonies were checked for the final plasmid by colony-PCR and restriction digest. Plasmids with expected results were verified by sequencing (Eurofins Genomics Germany GmbH, Ebersberg, Germany).

2.6.7 Cloning of complementation plasmids

Complementation of *B. subtilis* mutants was achieved by introducing knocked-out genes into the chromosomal DNA. Therefore, plasmids pX and pGP888 were used which integrate into specific regions of the genome, like the *amyE* or the *ganA* site. Genes to be complemented were amplified via PCR using primers that attached specific restriction sites by which the genes could be ligated into the vector pX or pGP888. *E. coli* DH5α was transformed with the ligation mixture and selected by ampicillin resistance. Ampicillin resistant colonies were checked for the final plasmid by colony-PCR and restriction digest. Plasmids with expected results were verified by sequencing (Eurofins Genomics Germany GmbH, Ebersberg, Germany).

2.7 Microbiological methods

2.7.1 Cultivation and storage conditions

Strains were grown at 37°C in indicated liquid media in test tubes, conical flasks, with and without chicane, under continuous shaking at 130 to 150 rpm. The media were inoculated with single colonies or from overnight cultures. Strains on LB agar plates were grown at 37°C. If necessary, antibiotics were added to liquid cultures and agar plates. The concentration depended on the strain and the respective antibiotic (see chapter 2.5). For long-term storage, bacterial cultures were mixed with 15% glycerol and stored at -80°C.

2.7.2 Preparation of chemically competent *E. coli* cells

To 100 ml LB medium 2 ml of Mg_2 solution were added and inoculated with 2 ml of an overnight culture. Cells were grown at 37°C with steadily shaking until they reached an OD_{600} of 0.5 to 0.7. The culture was harvested at 5000 g for 10 min at 4°C. The pellet was resuspended in 25 ml TMF buffer, and the cell suspension was incubated for 1 h on ice before centrifuging again at 5000 g for 10 min at 4°C. The pellet was resuspended in 5 ml TMF buffer, with 87% glycerin added, and aliquots with 200 µl cell suspension were stored at -80°C.

Mg_2 solution	0.5 M	magnesium chloride
	0.5 M	magnesium sulfate
	fill up to 1 L with milliQ	
TMF buffer	0.1 M	calcium chloride
	40 mM	manganese (II) chloride
	50 mM	rubidium chloride
	fill up to 1 L with milliQ	

2.7.3 Transformation of *E. coli*

200 µl aliquots of competent cells were thawed in ice. 1 µl of plasmid or 10 µl of ligation mixture were added, carefully mixed, and incubated for 30 min on ice. Afterwards, the cell suspension was heat shocked for 45 sec at 42°C and immediately stored back on ice for 5 min. For phenotypic expression, 900 µl LB medium were added and cells were incubated at 37°C with constant shaking for 30 min. Following, cells were streaked out on LB agar plates with antibiotic selection.

2.7.4 Preparation of naturally competent *B. subtilis* cells

20 ml MGE medium were inoculated with 250 µl of an overnight culture and incubated at 37°C with continuously shaking. Growth was monitored by measuring the optical density at 600 nm to determine the beginning of transition phase. 90 to 150 min after entering transition phase, when growth was beginning to remain static, the cells were harvested at 5000 x g for 4 min at 4°C and resuspended in 1/10 volume of supernatant with 17% (v/v) glycerin. Aliquots with 300 µl cell suspension were stored at -80°C (Schönert 2004).

2.7.5 Transformation of *B. subtilis*

300 µl aliquots of competent cells were thawed by adding a thawing solution and vortexing. 0.1 to 1 µg DNA was added to 300 µl thawed cells and the mixture was incubated for 30 min at 37°C under constant shaking. Afterwards, 100 µl of a phenotypic expression solution were added and the culture was further incubated at the same conditions for 90 min. Following, cells were streaked out on LB agar plates with antibiotic selection (Schönert 2004).

Thawing solution	170 µl	10 x MM
	17 µl	glucose (50%)
	34 µl	magnesium sulfate (1 M)
	1.7 ml	milliQ
Phenotypic expression solution	300 µl	yeast extract (5%)
	150 µl	casamino acids (10%)
	15 µl	tryptophan (5 mg ml^{-1})
	150 µl	milliQ

2.7.6 Generation of *B. subtilis* mutants

A knock-out of genes can be achieved in different ways. Two possibilities are either to exchange the gene of interest with an antibiotic resistance cassette or to generate a markerless deletion of the gene of interest.

For the strategy of substituting the gene with an antibiotic resistance cassette, the genomic DNA of a BGSC strain with an erythromycin resistance cassette at the targeted position was used as a template in PCR. The used primers bound 500 bp up- and downstream apart of the erm^r cassette. The strain could then be transformed with the amplified DNA fragment. By homologous recombination via the overlapping up-

and downstream regions, the gene of interest was exchanged by the erythromycin resistance cassette. Successful mutant generation was proved by PCR with specific erythromycin resistance cassette primers and by sequencing of the amplified PCR product (Eurofins Genomics Germany GmbH, Ebersberg, Germany). This method was used to generate second knock outs in mutant strains.

For markerless deletions of genes of interest a modified protocol of Janes and Stibitz (Janes and Stibitz 2006) was followed. The genomic DNA of *B. subtilis* wild type served as a template in PCR. Fragments with 500 bp length from the up- and downstream region of the gene of interest were amplified using primers that attached specific restriction sites. By restriction digest and ligation, both fragments were integrated into the plasmid pJM103-I-SceI (see chapter 2.6.6). Competent *B. subtilis* cells were transformed with pJM103-I-SceI containing the up- and downstream regions of the gene of interest. By a single crossover event the entire plasmid integrated into the genome. Integration of the plasmid into the genome was verified by PCR. The resulting *B. subtilis* strain was transformed with pBKJ223, the plasmid encoding for I-SceI endonuclease. Cleavage by the endonuclease lead to a double-stranded break in the genome at the I-SceI restriction site of the integrated plasmid, which was repaired by a homologous recombination event, leading either to the generation of the markerless mutant or to the excision of the plasmid and therefore to degeneration to wild type. Successful I-SceI endonuclease activity and generation of markerless mutants was verified by chloramphenicol sensitivity, PCR, and sequencing of the PCR product (Eurofins Genomics Germany GmbH, Ebersberg, Germany). To lose the second plasmid pBKJ223, the mutant colonies were streaked out on LB-plates without antibiotics as long as necessary. Loss of pBKJ223 was verified by tetracycline sensitivity.

2.7.7 Excision of the erythromycin resistance cassette of *B. subtilis* mutants

The mutants with a gene exchanged with an erythromycin resistance cassette could be made markerless by using the *cre/lox*-mediated loop-out plasmid pR244. This plasmid encodes for a *cre* recombinase which catalyzes the cleavage and reconnection of DNA between specific *loxP* recognition sites. The introduced erm^r cassettes were flanked by such *loxP* sites. Mutant strains were transformed with pDR244, selected for spectinomycin, and incubated at 30°C. Transformant colonies were transferred to LB plates without antibiotic and incubated overnight at 42°C. Grown colonies were screened for the loss of pDR244 by spectinomycin sensitivity and the

loss of the erythromycin resistance cassette by erythromycin sensitivity and sequencing (Eurofins Genomics Germany GmbH, Ebersberg, Germany).

2.7.8 Agar diffusion spot assay

B. subtilis autolysin-*spo0A* double-mutants were studied for their impact in cannibalism. Therefore, agar diffusion spot assays were conducted. 10 ml LB medium were inoculated with 100 µl of an overnight culture of different strains (*B. subtilis* 168, *B. subtilis* 168-Δ*spo0A::erm*, *B. subtilis* 168-Δ*lytC*-Δ*spo0A::erm*, *B. subtilis* 168-Δ*lytD*-Δ*spo0A::erm*, *B. subtilis* 168-Δ*lytE*-Δ*spo0A::erm*, and *B. subtilis* 168-Δ*lytF*-Δ*spo0A::erm*) and incubated at 37°C with continuously shaking. Cultures were grown until an optical density at 600 nm of 1.8 was reached. 50 µl of each culture were transferred into 2.5 ml water agar (0.75%) and put on top of a 17.5 ml LB plate. After drying, wild type was spotted on top of the soft lawn containing the mutant cells. Plates were incubated overnight at 37°C. Resulting halos were measured.

2.7.9 Co-cultivation of cannibalistic mutants

20 ml LB medium were inoculated to an OD_{600} of 0.05 with overnight cultures of *B. subtilis* 168-*amyE::cfp* and *B. subtilis* 168-*amyE::yfp*Δ*spo0A::erm*. The cultures were incubated at 37°C with continuously shaking until OD_{600} of 2.0 was reached. The cultures were transferred to a black 96-well plate in different ratios: single cultures of 168-*amyE::cfp* and 168-*amyE::yfp*Δ*spo0A::erm*, as well as ratios 1:1, 2:1, 1:2, 3:1 and 1:3. For a negative control, LB medium was used. Cultures were further grown in a spectrophotometer (Spark 10 M microplate reader, Tecan) at 37°C under continuous shaking. Fluorescence was measured from the top every 20 min for 3 h using the excitation and emission wavelengths of 480 nm of 520 nm for CFP and 485 nm and 535 nm for YFP.

2.7.10 Growth of cannibalistic mutants

100 ml LB medium were inoculated to an OD_{600} of 0.05 with overnight cultures of *B. subtilis* wild type 168, *B. subtilis* 168-Δ*skfA::erm*, *B. subtilis* 168-Δ*sdpC::erm*, *B. subtilis* 168-Δ*sdpC*Δ*skfA::erm*, *B. subtilis* 168-Δ*spo0A::erm* and *B. subtilis* 168-Δ*lytABC::neo*Δ*lytD::tet*Δ*lytE::cm*Δ*lytF::spec*. The cultures were incubated at 37°C with continuously shaking for 48 h. The OD_{600} was measured hourly for the first 9 h, and after 24 h of incubation every 2 hours and once after 48 h.

2.7.11 Expression of cell wall recycling enzymes

Expression of cell wall recycling enzymes was performed slightly modified as described by Litzinger and colleagues (Litzinger *et al.* 2010). 1 L LB medium were inoculated with *B. subtilis* wild type 168, *B. subtilis* 168-Δ*nagZ::erm* and *B. subtilis* 168-Δ*murQ*Δ*murR*Δ*murP* overnight cultures to an OD_{600} of 0.05. The cultures were incubated at 37°C under constant shaking. Cells were harvested with an OD_{600} of 10 ml^{-1} after 4 h, 6 h, 8 h and 24 h at 1500 x g for 10 min. Supernatants were transferred into a fresh tube and centrifuged at 10500 x g for 30 min. Pellets were resuspended in 1 ml phosphate buffer (0.2 M, pH 5.8). For measuring the expression of cell wall recycling enzymes, 45 µl cell suspension were incubated with 0.86 mM pNP-GlcNAc at 37°C for 16 h. The reactions were started by adding 45 µl cell suspension to 0.86 mM pNP-GlcNAc and incubated at 37°C. After 16 h the reactions were ended by addition of borate buffer (0.5 M, pH 11.0). Samples were analyzed by measurement of optical density at 405 nm using a spectrophotometer (SpectraMax M2, Molecular Devices).

2.7.12 Preparation of cytosolic fractions for HPLC-MS analysis

100 ml LB medium were inoculated with 1 ml of an overnight culture. Thereby, LB was supplemented with 0.1% cell wall sugars or 0.3% xylose, if necessary. Culture was incubated at 37°C with continuously shaking. For samples of cells in exponential growth phase, cultures with an OD_{600} of 0.8 were harvested at 1600 x g for 15 min at 4°C. For samples of cells in stationary growth phase, cultures were harvested at an OD_{600} of 2.0 at 1600 x g for 15 min at 4°C. For samples of cells grown for 24 h, cultures were harvested after 24 h at 1600 x g for 15 min at 4°C. Cell pellets were resuspended in 200 µl milliQ and boiled for 45 min at 100°C to break the cells. Afterwards, the suspension was centrifuged at 12100 x g for 15 min and 100 µl of the supernatant was transferred into a fresh tube. Proteins were precipitated with 400 µl ice-cold acetone, followed by another centrifugation step at 12100 x g for 10 min to separate proteins from cytosol. The supernatant was dried using a SpeedVac at 45°C, subsequently. For HPLC-MS analysis, the pellets were resuspended in 30 µl milliQ and transferred into vials.

2.7.13 Preparation of culture supernatants for HPLC-MS analysis

100 ml LB medium were inoculated with 1 ml of an overnight culture and incubated at 37°C under constant shaking. Cells were harvested after 24 h at 4000 x g for 15 min. 200 µl of supernatant was transferred into a fresh tube. Proteins were precipitated with 800 µl ice-cold acetone, followed by incubation at -20°C for 1 h and a centrifugation step at 12100 x g for 10 min. The supernatant was dried using a SpeedVac at 45°C, subsequently. For HPLC-MS analysis, the pellets were resuspended in 30 µl milliQ and transferred into vials.

2.7.14 Isolation of peptidoglycan and purification of MurNAc-GlcNAc using HPLC (Teufel 2019)

Isolation of *B. subtilis* peptidoglycan was performed slightly modified as described by Schaub and Dillard (Schaub and Dillard 2017). 2 L LB medium were inoculated with an overnight culture of *B. subtilis* cells to an OD_{600} of 0.1 and incubated at 37°C under constant shaking. Once, the culture reached an OD_{600} of 1.8, cells were harvested at 5000 g for 15 min at 4°C. Pellet was washed with 25 ml PBS buffer at 5000 g for 15 min at 4°C and the resulting pellet was stored at -20°C. Frozen pellet was resuspended in 20 ml phosphate buffer, added drop by drop into boiling phosphate buffer (20 ml) with 8% SDS and boiled for 30 min. After the sample cooled down to room temperature, it was centrifuged at 50000 g for 30 min at 40°C. Pellet was washed with phosphate buffer until the SDS was completely sequestered, which was proven by a methylene blue assay (Hayashi 1975). After removal of SDS, the pellet was resuspended in 10 ml phosphate buffer and incubated with 100 µg ml^{-1} α-amylase for 1 h at 37°C. Following, 200 µg ml^{-1} pronase from *Streptomyces griseus* were added and the sample was incubated overnight at 37°C. Subsequently, the sample was centrifuged at 16500 g for 10 min at room temperature. The resulting pellet was incubated with 5 ml of 1 M hydrochloric acid for 4 h at 37°C to get rid of the wall teichoic acids. After incubation, washing of the pellet with milliQ (16500 g, 10 min, room temperature) followed until a pH of 5 to 6 was obtained. The pellet was resuspended in 20 ml phosphate buffer, added dropwise into boiling phosphate buffer (20 ml) with 4% SDS and boiled for 30 min. Removal of SDS was performed as previously described. Purified peptidoglycan was dried using a SpeedVac and stored at 4°C.

900 mg of purified peptidoglycan were incubated with purified 1 µM CwlC and 1 µM Atl^{Glc} in 90 ml phosphate buffer overnight at 37°C with constant shaking. The next

day, the enzymes in the sample were heat-inactivated at 95°C for 25 min. To separate the peptidoglycan fragments, 90 µl of the sample were applied on a semi-preparative Gemini C18 column and separated by reversed-phase HPLC at 20°C with a flow rate of 1.5 ml min^{-1} referring to a previously described program (Gisin *et al.* 2013) with slight modifications. First, the column was washed for 10 min with 100% buffer A (see chapter 2.4), then the sample was injected followed by a second step with 100% buffer A for 5 min. After that, a linear gradient to 40% buffer B (see chapter 2.4) over 30 min was applied, with a hold for 5 min of 40% buffer B. Finally, re-equilibration with a one-minute step to 100% buffer A ends the program. Sample fractions were collected for each minute of flow and those containing MurNAc-GlcNAc were lyophilized, resuspended in 3 ml milliQ, dried using a SpeedVac at 40°C and stored at 4°C.

PBS buffer	137 mM	sodium chloride
	2.7 mM	potassium chloride
	10 mM	disodium hydrogen phosphate
	1.8 mM	potassium dihydrogen phosphate
Phosphate buffer pH 6.0	21.55 mM	sodium dihydrogen phosphate monohydrate
	3.45 mM	disodium hydrogen phosphate
Phosphate buffer pH 8.0	3.3 ml	sodium dihydrogen phosphate monohydrate (0.2 M)
	96.7 ml	disodium hydrogen phosphate (0.2 M)
	100 ml	dH_2O

2.7.15 Isolation of peptidoglycan for enzymatically sequential digest

1 L LB medium was inoculated to an OD_{600} of 0.1 with an overnight culture of *B. subtilis* cells and incubated at 37°C with continuous shaking. Once the culture reached an OD_{600} of 1.0, cells were harvested at 5000 g for 15 min at room temperature. Pellet was resuspended in 15 ml tris-HCl buffer with 0.4 mg proteinase K, added drop by drop to boiling tris-HCl buffer (15 ml) and boiled for 60 min. After the sample cooled down to room temperature, it was centrifuged at 2900 g for 15 min and the resulting pellet was stored at -20°C. Frozen pellet was resuspended in 6 ml tris-HCl buffer containing magnesium sulfate and incubated with 0.1 mg RNase A and 50 U DNase I for 2 h at 37°C with constant shaking. Following, 0.4 mg proteinase K were added to the sample, the solution was added drop by drop to a boiling SDS solution (end-concentration of SDS was 2%) and boiled for 60 min. After the sample cooled down to room

temperature, it was transferred into ultracentrifugation bottles and centrifuged at 104500 g for 30 min at 40°C. Pellet was washed with pre-warmed milliQ until the SDS was completely sequestered, which was proven by a methylene blue assay (Hayashi 1975). After removal of SDS, the pellet was resuspended in 2 ml hydrofluoric acid and incubated for 48 h at 4°C under continuous shaking to get rid of the wall teichoic acids. After incubation, the pellet was washed with phosphate buffer for several times at 20000 g for 5 min, followed by neutralizing with milliQ until a pH above 6.5 was reached. Purified peptidoglycan was dried using a SpeedVac and stored at 4°C.

Tris-HCl buffer pH 7.5	50 mM	TRIS base
Tris-HCl buffer with $MgSO_4$ pH 7.5	50 mM 10 mM	TRIS base magnesium sulfate
Phosphate buffer pH 7.0	39 ml 61 ml 100 ml	sodium dihydrogen phosphate monohydrate (0.2 M) disodium hydrogen phosphate (0.2 M) dH_2O

2.8 Biochemical methods

2.8.1 SDS PAGE

Sodium dodecyl sulfate polyacrylamide gel electrophoresis (SDS PAGE) was used to segregate and determine denatured protein samples. The SDS PAGE gel consisted of a 12% resolving and a 5% stacking gel (Laemmli 1970). Proteins and cell pellets were incubated with 6x Laemmli buffer for 10 min at 95°C to denature proteins, followed by a short centrifugation step. Proteins were separated at 50 mA in SDS running buffer. Staining was accomplished by incubating gels in a coomassie brilliant blue solution (CBB staining solution). To determine protein size a prestained protein ladder (Color prestained protein standard, broad range (11-245 kDa), NEB) was used (Figure 16).

Laemmli buffer	60 mM	Tris-HCl (pH 6.8)
	2% (v/v)	SDS (20%)
	10%	Glycerol
	5%	β-mercaptoethanol
	0.01%	Bromophenol blue
SDS solution B	1.5 M	Tris-HCl
	0.4% (v/v)	SDS (20%)
	adjust to pH 8.8	
SDS solution C	0.5 M	Tris-HCl
	0.4% (v/v)	SDS (20%)
	adjust to pH 6.8	
Resolving gel (12%)	2.5 ml	SDS solution B
	4 ml	Acrylamide
	3.45 ml	milliQ
	80 µl	APS
	8 µl	TEMED
Stacking gel (5%)	1.25 ml	SDS solution C
	0.65 ml	Acrylamide
	3.07 ml	milliQ
	25 µl	APS
	5 µl	TEMED
Running buffer	15 g	Tris
	72 g	Glycine
	25 ml	SDS (20%)
	fill up to 5 L with dH_2O and adjust to pH 8.5	
CBB staining solution	60 - 80 mg	Coomassie brilliant blue G-250
	fill up to 1 L of dH_2O and stir for 2 to 4 h.	
	3 ml	Hydrochloric acid (37%)

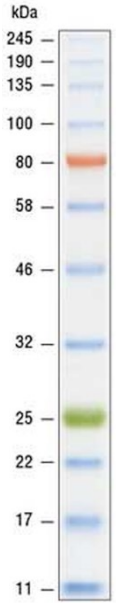

Figure 16 | Protein size marker. Color Prestained Protein Standard, Broad Range (11-245 kDa) (New England Biolabs).

2.8.2 Heterologous protein expression and purification

Heterologous protein expression was accomplished by transforming *E. coli* BL21(DE3) cells with cloned overexpression plasmids (see chapter 2.6.5). For the expression both 1 L and 2 L LB medium containing antibiotic were inoculated with 1% (v/v) of the respective overnight culture and incubated at 37°C under constant shaking. Cultures were grown until an OD_{600} of around 0.7 was reached, then protein expression was induced by adding 1 mM IPTG to the culture. Afterwards, cultures were grown further either at 37°C for 3 h or at 18°C overnight with continuous shaking. Cells were harvested at 4000 x g for 30 min at 4°C and pellets were resuspended in 20 ml of ÄKTA buffer A. Cells were broken using French Press (Sim Aminco Spectronic Instruments, Inc. Rochester, NY, United States) three times at 1000 psi. To remove cell debris and whole cells, the suspension was centrifuged at 38000 x g for 60 min at 4°C. The supernatant was filtered using a 0.2 µm filter. Purification of proteins was performed by Ni^{2+} affinity chromatography via a His_x-tag at the N- and the C-terminus, depending on the expression plasmid used. Therefore, a 1 ml His-Trap column was pre-equilibrated with ten column volumes, firstly with milliQ and secondly with ÄKTA buffer A, using a ÄKTApurifier system. Afterwards, the filtered supernatant was loaded on the column with a flow rate of 1 ml min^{-1}. Elution of the bound protein was achieved by a linear gradient from 4% to 100% of ÄKTA buffer B. Successful expression and purification was verified by SDS PAGE (see chapter 2.8.1). Fractions containing proteins were further purified using a ÄKTApurifier system by size exclusion

chromatography using a HiLoad 16/60 Superdex 200 column. Therefore, the column was pre-equilibrated with both milliQ and ÄKTA buffer A before the protein sample was loaded on the column using sodium phosphate buffer A as an eluent with a flow rate of 1 ml min^{-1}. Successful purification of proteins was verified by SDS PAGE (see chapter 2.8.1), protein containing fractions were pooled and stored at 4°C and -20°C without as well as with added glycerol (10%) and DTT (1 mM).

ÄKTA buffer A	20 mM	disodium hydrogen phosphate
	0.5 M	sodium chloride
	adjust to pH 7.5	
ÄKTA buffer B	20 mM	disodium hydrogen phosphate
	0.5 mM	sodium chloride
	0.5 mM	imidazole
	adjust to pH 7.5	

2.8.3 Determination of protein concentration

Protein concentrations were determined using the extinction coefficient at 280 nm, which was ascertained by Expasy ProtParam tool (https://web.expasy.org/protparam/). Protein samples were measured in a 1 ml quartz cuvette using a SpectraMax M2 spectrophotometer (Molecular Devices).

Table 9 | Extinction coefficients of purified proteins to determine protein concentration

Protein	Extinction coefficient
NamZ	36330 M^{-1} cm^{-1}
NagZ	36300 M^{-1} cm^{-1}
AmiE	50770 M^{-1} cm^{-1}
CwlC	15930 M^{-1} cm^{-1}
Atl^{Glc}	97180 M^{-1} cm^{-1}

2.8.4 Methods for characterization of NamZ

As NamZ belongs to an entirely novel glycosidase family, we wanted to characterize the enzyme in a detailed manner. Therefore, different enzyme characteristics were determined.

2.8.4.1 Substrate specificity

The specificity of NamZ was determined using different chromogenic and natural substrates. Firstly, pNP-MurNAc was chemically synthesized as described in Müller *et al.* 2021, and it was applied along with pNP-GlcNAc and oNP-Galactose (oNP-Gal) in an assay together with the purified enzymes NamZ, NagZ and LacZ. Each 100 µl reaction mixture contained purified enzyme (0.7 µM NamZ, 0.48 µM NagZ, 1500 U LacZ) and chromogenic substrate (100 µM each) in phosphate buffer (0.2 M, pH 8.0, see chapter 2.4). The reactions were started by adding the enzymes and incubated at 37°C. After 30 min the reactions were ended by addition of borate buffer (100 mM, pH 10.0) and release of nitrophenol groups by specific action of enzymes could be seen by a yellow color.

Additionally, purified MurNAc-GlcNAc and GlcNAc-MurNAc were applied in an assay with the purified enzymes NamZ and NagZ. Each 25 µl reaction mixture contained purified enzyme (420 nM NamZ and 280 nM NagZ) and substrate (100 µM each) in phosphate buffer (0.2 M, pH 7.0, see chapter 2.4). Additionally, controls without enzyme were prepared for each substrate. The reactions were started by adding the enzymes and incubated at 37°C. After 30 min the reactions were ended by addition of stopping buffer (see chapter 2.4) and the reaction mixtures were transferred into vials and analyzed by using HPLC-MS.

2.8.4.2 **Reaction and stability optima** (Engelbrecht 2016)

The optimal temperature conditions for NamZ were determined prior to kinetic studies using the chromogenic substrate pNP-MurNAc. For temperature stability, the enzyme was pre-incubated for 30 min at different temperatures, like 4°C, 20°C, 37°C, 45°C, 55°C and 60°C. Meanwhile, a 100 µl reaction mixture was prepared, containing 200 µM pNP-MurNAc in phosphate buffer (0.02 M, pH 7.5, see chapter 2.4). 105 nM of pre-incubated NamZ were added to this reaction mixture and incubated for 1 h at 37°C. For temperature optimum, a 100 µl reaction mixture was prepared, containing 200 µM pNP-MurNAc and 105 nM NamZ in phosphate buffer (0.02 M, pH 7.5, see chapter 2.4). Following, the reaction mixture was incubated for 1 h at different

temperatures, like 4°C, 20°C, 37°C, 45°C, 55°C and 60°C. Samples of both experiments were analyzed by measurement of optical density at 405 nm using a spectrophotometer (SpectraMax M2, Molecular Devices).

The optimal pH conditions for NamZ were determined prior to kinetic studies using the chromogenic substrate pNP-MurNAc and buffers in the pH range of 2.0 to 10.0 (i.e., Clark and Lubs buffer (pH 2.0), citric acid-sodium phosphate buffer (pH 3.0 to 7.0), hydrochloric acid-tris buffer (pH 8.0) and glycine-sodium hydroxide buffer (pH 9.0 to 10.0), see chapter 2.4). For pH stability, the enzyme was diluted to a final concentration of 50 ng μl^{-1} in buffers from pH 2.0 to 10.0 and pre-incubated for 30 min at room temperature. Afterwards, the samples were washed with 50 µl phosphate buffer (0.02 M, pH 7.5, see chapter 2.4) using centrifugal filter units for three times. Next, the volume was adjusted to 50 µl with phosphate buffer (0.02 M, pH 7.5, see chapter 2.4) to preserve the concentration of NamZ of 50 ng μl^{-1}. A 100 µl reaction mixture was prepared, containing 200 µM pNP-MurNAc and 105 nM pre-incubated NamZ in phosphate buffer (0.02 M, pH 7.5, see chapter 2.4). Following, the reaction mixture was incubated for 1 h at 37°C. For pH optimum, a 100 µl reaction mixture was prepared, containing 200 µM pNP-MurNAc in buffers from a pH range from 2.0 to 10.0 (see chapter 2.4) and 105 nM NamZ. Following, the reaction mixture was incubated for 1 h at 37°C. Afterwards, the reaction was ended by the addition of borate buffer (250 mM disodiumtetraborate, 1 M NaOH, pH 10.8). Samples of both experiments were analyzed by measurement of optical density at 405 nm using a spectrophotometer (SpectraMax M2, Molecular Devices).

2.8.4.3 Kinetic parameters

The kinetic parameters of NamZ were ascertained for the chromogenic substrate pNP-MurNAc and the minimal natural substrate MurNAc-GlcNAc. Prior to the kinetic experiments, the purity of pNP-MurNAc was analyzed using HPLC-MS. Therefore, 100 µl reaction mixtures containing 100 µM substrate in phosphate buffer (0.2 M, pH 7.0, see chapter 2.4) with and without the addition of 105 nM NamZ were incubated for 30 min at 37°C and immediately analyzed by HPLC-MS. To de-methylate the pNP-MurNAc stock, we incubated 1 mM substrate under basic conditions in phosphate buffer (0.02 M, pH 8.0, see chapter 2.4) for 30 min at 37°C. Following, 100 µl reaction mixtures containing 100 µM pre-incubated pNP-MurNAc in phosphate buffer (0.2 M, pH 7.0, see chapter 2.4) with and without the addition of 105 nM NamZ were incubated for 30 min at 37°C and immediately analyzed by HPLC-MS.

To determine kinetic parameters of NamZ for pNP-MurNAc was pre-incubated under basic conditions before usage as described above. Afterwards, a 100 µl reaction mixture was prepared, containing substrate in different concentrations from 13 µM to 860 µM in phosphate buffer (0.2 M, pH 8.0, see chapter 2.4) in a 96-well plate. The reaction was initiated by the addition of 105 nM NamZ. The samples were incubated for 30 min at 37°C and thereby measured continuously at OD_{405} in a spectrophotometer (Spark 10 M microplate reader, Tecan). The activity of NamZ was measured by the amount of released 4-nitrophenol. To know the exact quantity of product, a 4-nitrophenol standard in phosphate buffer (0.2 M, pH 8.0, see chapter 2.4), in a concentration range from 13 µM to 430 µM, was measured at OD_{405}.

Additionally, kinetic parameters of NamZ for MurNAc-GlcNAc as substrate were determined. A 20 µl reaction mixture was prepared, containing substrate in different concentrations from 0.025 mM to 6 mM in phosphate buffer (0.2 M, pH 7.0, see chapter 2.4) in an eppendorf tube. The reaction was initiated by the addition of 10.5 nM NamZ. The samples were incubated for 5 min at 37°C and then stopped with stopping buffer (pH 3.2, see chapter 2.4). For analysis, the samples were transferred into vials and analyzed using HPLC-MS. The activity of NamZ was measured by the amount of released MurNAc. To know the exact quantity of product, a MurNAc standard in a concentration range of 0.019 nmol 3 $µl^{-1}$ to 2.4 nmol 3 $µl^{-1}$ was analyzed by HPLC-MS. The MurNAc standard was dissolved in an equal ratio of phosphate buffer (0.2 M, pH 7.0, see chapter 2.4) and stopping buffer (pH 3.2, see chapter 2.4) to ascertain the same ionization conditions during HPLC-MS measurement.

Data of kinetic experiments were analyzed by nonlinear regression of the reaction curve using Prism 6 (GraphPad Software, San Diego, California, USA).

2.8.5 Digestion of peptidoglycan

Peptidoglycan of *B. subtilis* was purified (see chapter 2.7.15) to serve as substrate in digestion using different enzymes. Hence, various approaches have been implemented. One approach was performed with NagZ, AmiE and NamZ. Therefore, a 150 µl reaction mixture was prepared, containing 2.5 mg peptidoglycan dissolved in phosphate buffer (0.2 M, pH 7.0, see chapter 2.4) and 2.5 µM NagZ, 2.5 µM AmiE and 2.5 µM NamZ. The solution was incubated overnight at 37°C and thereby continuously shaken. Afterwards, the reaction was stopped by heating at 95°C for 30 min. To separate products of the digestion from undigested peptidoglycan, the sample was

centrifuged at 12100 x g for 15 min and the supernatant was dried at 37°C using a SpeedVac. Finally, the pellets were dissolved in 50 µl milliQ, transferred into vials and analyzed using HPLC-MS.

A second approach was performed using peptidoglycan that was pre-digested with mutanolysin before adding NagZ, AmiE and NamZ. Therefore, a 300 µl reaction mixture was prepared, containing 5 mg peptidoglycan dissolved in phosphate buffer (0.2 M, pH 6.0, see chapter 2.4) and 5 µM mutanolysin. The solution was incubated overnight at 37°C and thereby continuously shaken. Afterwards, the reaction was stopped by heating at 95°C for 30 min. To separate products of the digestion from undigested peptidoglycan, the sample was centrifuged at 12100 x g for 15 min. 150 µl of the supernatant were dried at 37°C using a SpeedVac. The pellet was dissolved in a total of 150 µl of phosphate buffer (0.2 M, pH 7.0, see chapter 2.4) and 2.5 µM NagZ, 2.5 µM AmiE and 2.5 µM NamZ. The solution was incubated overnight at 37°C and thereby continuously shaken. Afterwards, the reaction was stopped by heating at 95°C for 30 min. To separate products of the digestion from undigested peptidoglycan, the sample was centrifuged at 12100 x g for 15 min and the supernatant was dried at 37°C using a SpeedVac. Finally, the pellets were dissolved in 50 µl milliQ, transferred into vials and analyzed using HPLC-MS.

A third approach was performed with with Alt^{Glc}, AmiE and NamZ. Therefore, a 150 µl reaction mixture was prepared, containing 2.5 mg peptidoglycan dissolved in phosphate buffer (0.2 M, pH 7.0, see chapter 2.4) and 2.5 µM Atl^{Glc}, 2.5 µM AmiE and 2.5 µM NamZ. The solution was incubated overnight at 37°C and thereby continuously shaken. Afterwards, the reaction was stopped by heating at 95°C for 30 min. To separate products of the digestion from undigested peptidoglycan, the sample was centrifuged at 12100 x g for 15 min and the supernatant was dried at 37°C using a SpeedVac. Finally, the pellets were dissolved in 50 µl milliQ, transferred into vials and analyzed using HPLC-MS.

The last approach was performed with with Alt^{Glc} and NamZ. Therefore, a 150 µl reaction mixture was prepared, containing 2.5 mg peptidoglycan dissolved in phosphate buffer (0.2 M, pH 7.0, see chapter 2.4), 2.5 µM Atl^{Glc} and 2.5 µM NamZ. The solution was incubated overnight at 37°C and thereby continuously shaken. Afterwards, the reaction was stopped by heating at 95°C for 30 min. To separate products of the digestion from undigested peptidoglycan, the sample was centrifuged at 12100 x g for 15 min and the supernatant was dried at 37°C using a SpeedVac.

Finally, the pellets were dissolved in 50 µl milliQ, transferred into vials and analyzed using HPLC-MS.

2.8.6 Size exclusion chromatography using HPLC analysis

Purified NamZ had a calculated theoretical molecular mass of 44.7 kDa, including the added His_6-tag. To ascertain the molecular weight of native NamZ size exclusion chromatography via HPLC was performed using a BioSep SEC-S3000 column (300 x 7.8 mm, 5 µm, 290 Å). The molecular weight of NamZ was determined by comparison of the retention times of defined standard enzymes. Therefore, a standard curve with the proteins albumin (66 kDa), ovalbumin (44.2 kDa), chymotrypsinogen (25.6 kDa) and ribonuclease A (13.7 kDa) was created. The protein standards were dissolved with a concentration of 3 mg ml^{-1} on ÄKTA buffer A and injected on the size exclusion column. The separation on the column was performed with a flow rate of 1 ml min^{-1} of ÄKTA buffer A for 15 min at 20°C. 10 µl of protein were injected on the BioSep SEC-S3000 column and analyzed by HPLC with an absorption at 280 nm. The retention times of the standard enzymes were used to calculate a standard curve using Prism 6 (GraphPad Software, San Diego, USA). Likewise, 10 µl NamZ (2.8 mg ml^{-1}, in ÄKTA buffer A) were injected, separated on the column and analyzed by HPLC with an absorption at 280 nm. Measured retention time of NamZ was fitted into the standard curve to determine the molecular weight using Prism 6.

ÄKTA buffer A	20 mM	disodium hydrogen phosphate
	0.5 M	sodium chloride
	adjust to pH 7.5	

2.9 HPLC-MS analysis

Cytosolic samples, supernatants and probes of enzyme assays were analyzed using HPLC-MS. After separation of the sample substances by HPLC (Ultimate 3000 HPLC System, Dionex), they got ionized by electrospray ionization (ESI). The ions got accelerated by an electric field of known strength and analyzed by their time of flight (TOF) depending on their mass to charge ratio (m/z). Ions respectively secondary electrons were detected by a semi-conductive layer (MicrOTOF II, Bruker). The samples were measured in positive and negative ion mode, depending on the ionization abilities of the samples. HPLC was performed using a Gemini C18 column (150 x 4.6 mm, 5 µm, 110 Å). 3 µl of samples were injected on the column and separated with a flow rate of 0.2 ml min^{-1}. First, the column was equilibrated for 10 min with 100% buffer A (see chapter 2.4), then the sample was injected followed by a second step with 100% buffer A for 5 min. After that, a linear gradient to 40% buffer B (see chapter 2.4) over 30 min was applied, with a hold for 5 min of 40% buffer B. Finally, re-equilibration with a one-minute step to 100% buffer A ended the program (Gisin *et al.* 2013). HPLC-MS analysis was evaluated by creating base peak chromatograms (BPC) and extracted ion chromatograms (EIC) using Data Analysis (Bruker), creating differential spectra using Metabolite Detect (Bruker) and searching for compounds using Target Analysis (Bruker).

An overview of the masses measured for the functional analysis of YbbC (NamZ) within the peptidoglycan recycling metabolism in *B. subtilis* can be found in Table 10.

Table 10 | Overview of peptidoglycan fragments and their calculated theoretical masses as well as their obtained masses using HPLC-MS analysis

Compound	Theoretical mass	Obtained mass(es)	Found in	Reference
anhMurNAc	$(M+H)^+$ 276.108 m/z	$(M+H)^+$ 276.105 m/z	Culture supernatant of *B. subtilis* 168	Chapter 3.1.1
		$(M+H)^+$ 276.106 m/z	Culture supernatant of *B. subtilis* 168-Δ*namZ*	Chapter 3.1.1
	$(M-H)^-$ 274.093 m/z	$(M-H)^-$ 274.094 m/z	Peptidoglycan of *B. subtilis* sequentially digested with NagZ, AmiE and NamZ of *B. subtilis*	Chapter 3.1.6
GlcNAc	$(M+H)^+$ 222.097 m/z	$(M+H)^+$ 222.097 m/z	Purified MurNAc-GlcNAc after digest with NamZ of *B. subtilis*	Chapter 3.1.3
		$(M+H)^+$ 222.097 m/z	Purchased GlcNAc-MurNAc after digest with NagZ of *B. subtilis*	Chapter 3.1.3
		$(M+H)^+$ 222.098 m/z	Peptidoglycan of *B. subtilis* sequentially digested with NagZ, AmiE and NamZ of *B. subtilis*	Chapter 3.1.6
MurNAc	$(M+H)^+$ 294.118 m/z	$(M+H)^+$ 294.118 m/z	Purified MurNAc-GlcNAc after digest with NamZ of *B. subtilis*	Chapter 3.1.3
		$(M+H)^+$ 294.118 m/z	Purchased GlcNAc-MurNAc after digest with NagZ of *B. subtilis*	Chapter 3.1.3
	$(M-H)^-$ 292.104 m/z	$(M-H)^-$ 292.113 m/z	Purified MurNAc-GlcNAc after digest with NamZ of *B. subtilis*	Chapter 3.1.5
		$(M-H)^-$ 292.104 m/z	Peptidoglycan of *B. subtilis* sequentially digested with NagZ, AmiE and NamZ of *B. subtilis*	Chapter 3.1.6
GlcNAc-anhMurNAc	$(M+H)^+$ 479.187m/z	(M+H)+ 479.185 m/z	Culture supernatant of *B. subtilis* 168-Δ*nagZ*	Chapter 3.1.1

Compound	Theoretical mass	Obtained mass(es)	Found in	Reference
GlcNAc-MurNAc	$(M+H)^+$ 497.198 m/z	$(M+H)^+$ 497.196 m/z	Culture supernatant of *B. subtilis* 168-Δ*nagZ*	Chapter 3.1.1
		$(M+H)^+$ 497.198 m/z	Purchased GlcNAc-MurNAc before digest with NagZ of *B. subtilis*	Chapter 3.1.3
		$(M+H)^+$ 497.198 m/z	Purchased GlcNAc-MurNAc after digest with NamZ of *B. subtilis*	Chapter 3.1.3
MurNAc-GlcNAc	$(M+H)^+$ 497.198 m/z	$(M+H)^+$ 497.207 m/z	Culture supernatant of *B. subtilis* 168	Chapter 3.1.1
		$(M+H)^+$ 497.204 m/z	Culture supernatant of *B. subtilis* 168-Δ*namZ*	Chapter 3.1.1
		$(M+H)^+$ 497.196 m/z	Peptidoglycan of *B. subtilis* after digest with CwlC of *B. subtilis* and Atl^{Glc} of *S. aureus*	Chapter 3.1.2
		$(M+H)^+$ 497.196 m/z	Purified MurNAc-GlcNAc before digest with NamZ of *B. subtilis*	Chapter 3.1.3
MurNAc-GlcNAc-anhMurNAc	$(M+H)^+$ 754.288 m/z	$(M+H)^+$ 754.283 m/z	Culture supernatant of *B. subtilis* 168	Chapter 3.1.1
		$(M+H)^+$ 754.284 m/z	Culture supernatant of *B. subtilis* 168-Δ*namZ*	Chapter 3.1.1
		$(M+H)^+$ 754.288 m/z	Culture supernatant of *B. subtilis* 168-Δ*nagZ*	Chapter 3.1.1
Tripeptide with one amidation (L-Ala-γ-D-Glu-*m*-DAP)	$(M-H)^-$ 388.184 m/z	$(M-H)^-$ 388.187 m/z	Peptidoglycan of *B. subtilis* sequentially digested with NagZ, AmiE and NamZ of *B. subtilis*	Chapter 3.1.6
Tri-tetrapeptide with two amidations (L-Ala-γ-D-Glu-*m*-DAP / L-Ala-γ-D-Glu-*m*-DAP-D-Ala)	$(M-H)^-$ 830.401 m/z	$(M-H)^-$ 830.406 m/z	Peptidoglycan of *B. subtilis* sequentially digested with NagZ, AmiE and NamZ of *B. subtilis*	Chapter 3.1.6

Compound	Theoretical mass	Obtained mass(es)	Found in	Reference
Tri-tetrapeptide with one amidation (L-Ala-γ-D-Glu-*m*-DAP / L-Ala-γ-D-Glu-*m*-DAP-D-Ala)	$(M-H)^-$ 831.390 m/z	$(M-H)^-$ 831.388 m/z	Peptidoglycan of *B. subtilis* sequentially digested with NagZ, AmiE and NamZ of *B. subtilis*	Chapter 3.1.6

3 Results

3.1 Functional analysis of YbbC (NamZ) within the peptidoglycan recycling metabolism in *B. subtilis*

In this study, I elucidated the role of *ybbC,* the last unknown gene of the MurNAc recycling operon in *B. subtilis*, which will henceforth be named *namZ* (see Figure 7). First, an HPLC-MS analysis of *B. subtilis* cell wall recycling mutants was performed to asses changes in metabolite levels due to impaired recycling. Next, MurNAc-GlcNAc, the proposed natural minimal substrate of NamZ, was purified from digested peptidoglycan. Then, the substrate specificity of NamZ was investigated using natural and artifical, chromogenic substrates. Furthermore, the temperature and pH dependence and kinetic parameters were determined. Lastly, the recycling enzymes were heterologously expressed and purified to perform peptidoglycan digestion.

3.1.1 Metabolite analysis of *B. subtilis* cell wall recycling mutants

To gain insight into the role of recycling operon gene *namZ* in *B. subtilis*, culture supernatants were analyzed by HPLC-MS. For this purpose, the mutants 168-Δ*nagZ::erm* and 168-Δ*namZ::erm* from the BGSC strain were used to generate markerless mutants. The erythromycin resistance cassette of these mutant strains was excised using the plasmid pDR244 as described in chapter 2.7.7, resulting in the strains 168-Δ*nagZ* and 168-Δ*namZ*, which were verified by sequencing.

To investigate the influence of *namZ*, the supernatants of the *B. subtilis* 168 wild type and mutant 168-Δ*nagZ* and 168-Δ*namZ* cultures were analyzed using HPLC-MS ((Müller *et al.* 2021); Figure 17).

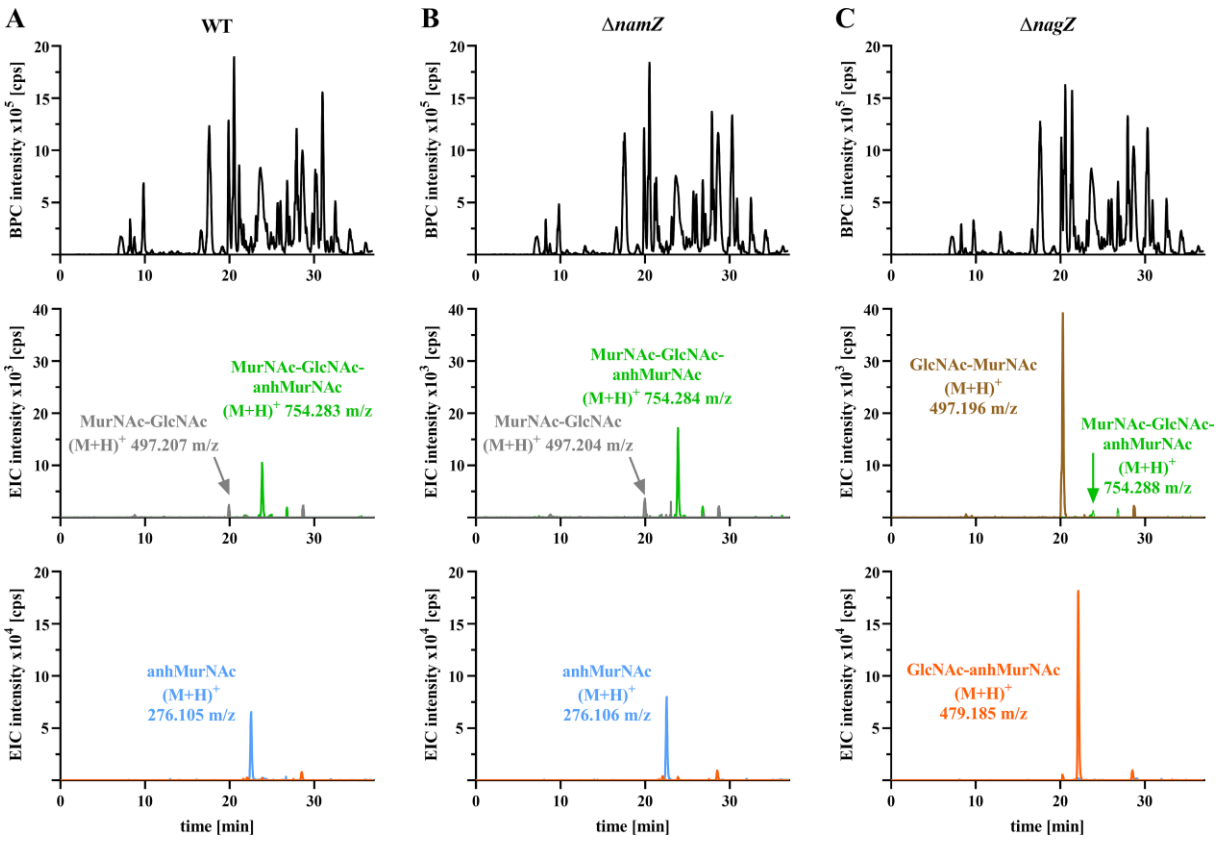

Figure 17 | HPLC-MS analysis of culture supernatants of *B. subtilis* 168 wild type, 168-Δ*namZ* and 168-Δ*nagZ*. Presented are base peak chromatograms (BPC; black) and extracted ion chromatograms (EIC). For **(A)** wild type, the disaccharide MurNAc-GlcNAc ($(M+H)^+$ 497.207 m/z; grey), the trisaccharide MurNAc-GlcNAc-anhMurNAc ($(M+H)^+$ 754.283 m/z; green), and anhMurNAc ($(M+H)^+$ 276.105 m/z; blue) are shown. For **(B)** Δ*namZ*, the disaccharide MurNAc-GlcNAc ($(M+H)^+$ 497.204 m/z; grey), the trisaccharide MurNAc-GlcNAc-anhMurNAc ($(M+H)^+$ 754.284 m/z; green), and anhMurNAc ($(M+H)^+$ 276.106 m/z; blue) are shown. For **(C)** Δ*nagZ*, the disaccharide GlcNAc-MurNAc ($(M+H)^+$ 497.196 m/z; brown), the trisaccharide MurNAc-GlcNAc-anhMurNAc ($(M+H)^+$ 754.288 m/z; green), and GlcNAc-anhMurNAc ($(M+H)^+$ 479.185 m/z; orange) are shown (Müller *et al.* 2021).

HPLC-MS analysis of culture supernatants showed some minor differences between *B. subtilis* 168 wild type, Δ*namZ*, and Δ*nagZ* (Figure 17). The analyses showed the accumulation of the disaccharide MurNAc-GlcNAc (theoretical mass $(M+H)^+$ 497.198 m/z) with a measured mass in positive ion mode of $(M+H)^+$ 497.207 m/z for wild type and $(M+H)^+$ 497.204 m/z for Δ*namZ*, whereas the amount was twice as high in the Δ*namZ* mutant compared to the wild type. For Δ*nagZ*, the disaccharide GlcNAc-MurNAc (theoretical mass $(M+H)^+$ 497.198 m/z) could be identified with a measured mass in positive ion mode of $(M+H)^+$ 497.196 m/z. Furthermore, the trisaccharide MurNAc-GlcNAc-anhMurNAc (theoretical mass $(M+H)^+$ 754.288 m/z) with a measured mass in positive ion mode of $(M+H)^+$ 754.283 m/z for wild type, $(M+H)^+$ 754.284 m/z for Δ*namZ*, and $(M+H)^+$ 754.288 m/z for Δ*nagZ* could be identified. In the Δ*nagZ* mutant, the amount was remarkably lower compared to wild type and Δ*namZ*. Instead,

the disaccharide GlcNAc-anhMurNAc (theoretical mass $(M+H)^+$ 479.187m/z) with a measured mass in positive ion mode of (M+H)+ 479.185 m/z could be shown for Δ*nagZ* but not for wild type or Δ*namZ*. Additionally, anhMurNAc (theoretical mass $(M+H)^+$ 276.108 m/z) could be identified with a measured mass in positive ion mode of $(M+H)^+$ 276.105 m/z for wild type and $(M+H)^+$ 276.106 m/z for Δ*namZ* but was missing in Δ*nagZ* (Müller *et al.* 2021).

3.1.2 Isolation of peptidoglycan and purification of MurNAc-GlcNAc

For the biochemical characterization of NamZ, the potential minimal natural substrate MurNAc-GlcNAc was prepared. Therefore, peptidoglycan of *B. subtilis* was isolated according to the protocol as described in chapter 2.7.14. To generate the disaccharide MurNAc-GlcNAc, the isolated PGN was digested with CwlC of *B. subtilis*, and Atl^{Glc} of *S. aureus* as described in chapter 2.7.14. The fragments generated by the enzymatic digest were separated by HPLC as described in chapter 2.7.14. Large amounts of MurNAc-GlcNAc could be detected that elutes at a retention time of 21 min (peak 5, Figure 18), besides crosslinked and non-crosslinked peptides (peaks 1 to 4). In peak 1, amidated tripeptide (L-Ala-γ-D-Glu-*m*-DAP) that elutes at a retention time of 8.9 min could be detected (Figure 18). Peak 2 showed amidated tetrapeptide (L-Ala-γ-D-Glu-*m*-DAP-D-Ala) that elutes at a retention time of 9.9 min (Figure 18). In peak 3, tri-tetrapeptide with two amidations (L-Ala-γ-D-Glu-*m*-DAP / L-Ala-γ-D-Glu-*m*-DAP-D-Ala) that elutes at a retention time of 11.6 min could be detected (Figure 18). Peak 4 showed tri-tetrapeptide with one amidation (L-Ala-γ-D-Glu-*m*-DAP / L-Ala-γ-D-Glu-*m*-DAP-D-Ala) that elutes at a retention time of 14.3 min (Figure 18). Additionally, further peaks were detected in small amounts by HPLC, for which no retention times could be assigned, and which presumably belong to other saccharides release during enzymatic digest of peptidoglycan.

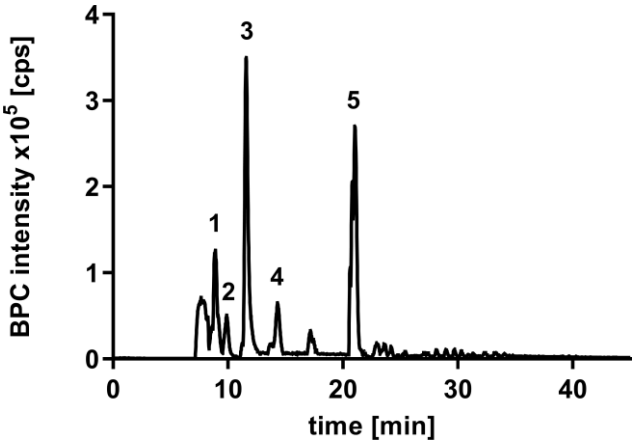

Figure 18 | Enzymatic digest of peptidoglycan and analysis by HPLC-MS before purification by HPLC. Peaks 1 to 4 show different peptides derived from peptidoglycan. Peak 1 showed amidated tripeptide at a retention time of 8.9 min. Peak 2 showed amidated tetrapeptide at a retention time of 9.9 min. Peak 3 showed tri-tetrapeptide with two amidations at a retention time of 11.6 min. Peak 4 showed tri-tetrapeptide with one amidation at a retention time of 14.3 min. Peak 5 showed MurNAc-GlcNAc at a retention time of 21 min. Results are presented as base peak chromatograms (BPC) (modified after Müller *et al.* 2021).

MurNAc-GlcNAc from peak 5 was purified by semi-preparative HPLC, as described in chapter 2.7.14. After purification, the disaccharide was almost free of crosslinked and non-crosslinked peptides which was verified by HPLC-MS analysis as described in chapter 2.9 (Figure 19).

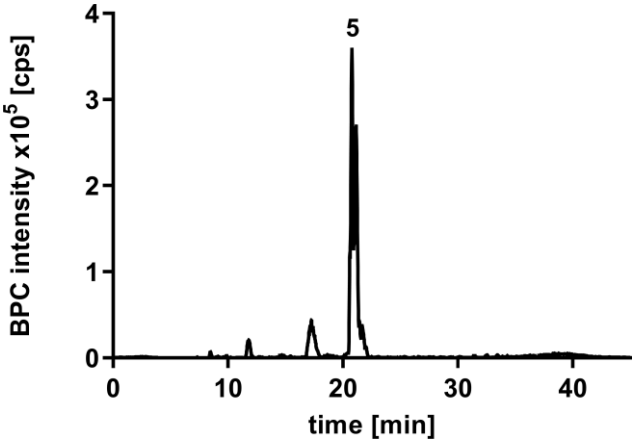

Figure 19 | Enzymatic digest of peptidoglycan and analysis by HPLC-MS after purification by HPLC. Peak 5 showed MurNAc-GlcNAc at a retention time of 21 min. Purity of MurNAc-GlcNAc after semi-preparative HPLC was verified by HPLC-MS analysis. Results are presented as base peak chromatograms (BPC) (modified after Müller *et al.* 2021).

The mass spectrum of peak 5 after purification (Figure 19) revealed a main molecule mass of $(M+H)^+$ 497.196 m/z (Figure 20) which corresponds to the disaccharide MurNAc-GlcNAc with a theoretical mass of $(M+H)^+$ 497.198 m/z.

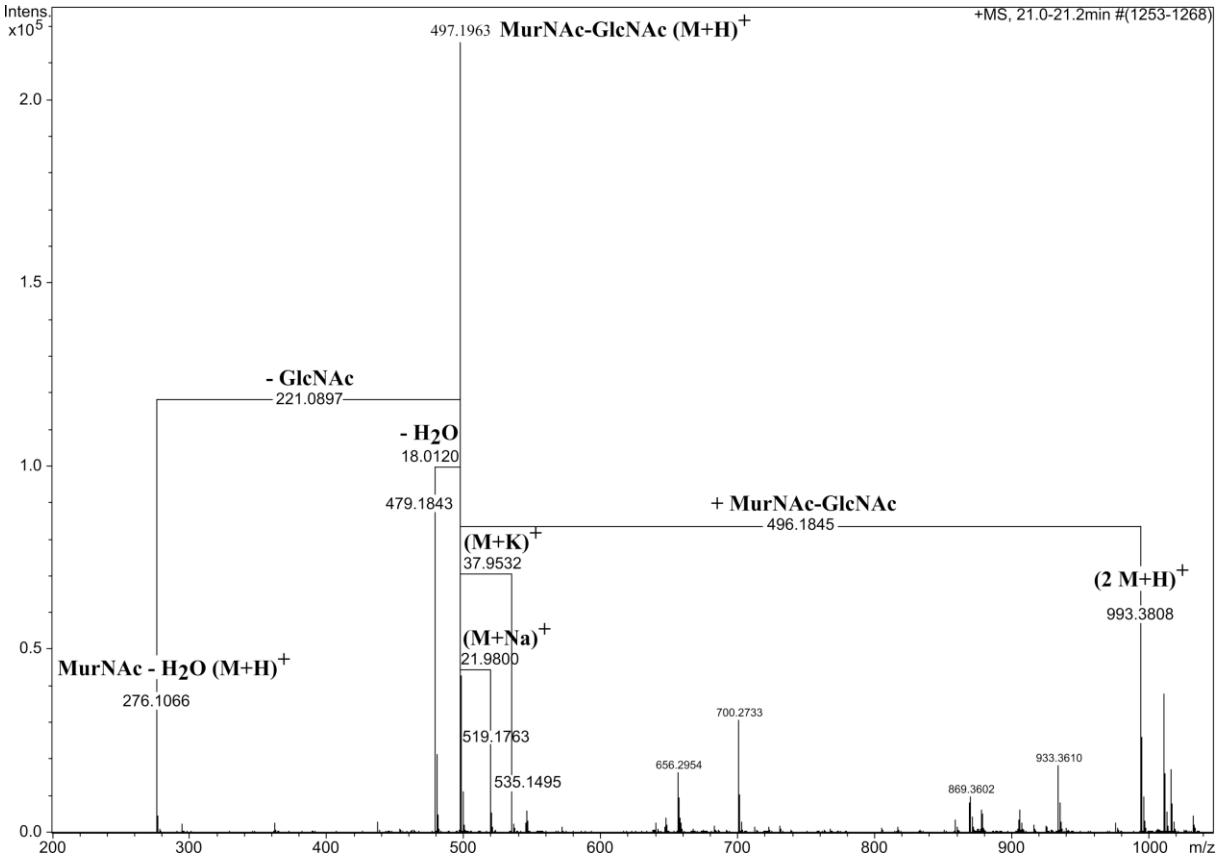

Figure 20 | Mass spectrum of MurNAc-GlcNAc peak after purification by HPLC. Main molecule mass was $(M+H)^+$ 497.196 m/z which corresponds to MurNAc-GlcNAc with the theoretical mass of $(M+H)^+$ 497.198 m/z. The other masses measured could be associated with MurNAc-GlcNAc, as well: MurNAc-GlcNAc as a dimer $(2M+H)^+$ 993.381 m/z, sodium and potassium ion adducts, as well as water and GlcNAc elimination products (modified after Müller *et al.* 2021).

In addition to the mass of MurNAc-GlcNAc, the mass spectrum showed the mass of the MurNAc-GlcNAc dimer $(2M+H)^+$ 993.381 m/z, the mass of a sodium ion adduct $(M+H)^+$ 519.176 m/z, the mass of a potassium ion adduct $(M+H)^+$ 535.150 m/z as well as a water elimination product $(M+H)^+$ 479.184 m/z and a GlcNAc and water elimination product $(M+H)^+$ 276.107 m/z (Figure 20).

A total of 3.94 mg of purified MurNAc-GlcNAc was obtained from peptidoglycan isolation and enzymatic digest.

3.1.3 NamZ substrate specificity

To characterize NamZ as a potential glycosidase, substrate specificity was determined using different substrates as described in chapter 2.8.4.1.

Therefore, NamZ and NagZ were heterologously expressed and purified as described in chapter 2.8.2.

Firstly, various chromogenic substrates like pNP-MurNAc, pNP-GlcNAc and oNP-Gal were used in an assay together with recombinant NamZ and NagZ from *B. subtilis*, and commercially available LacZ from *E. coli*.

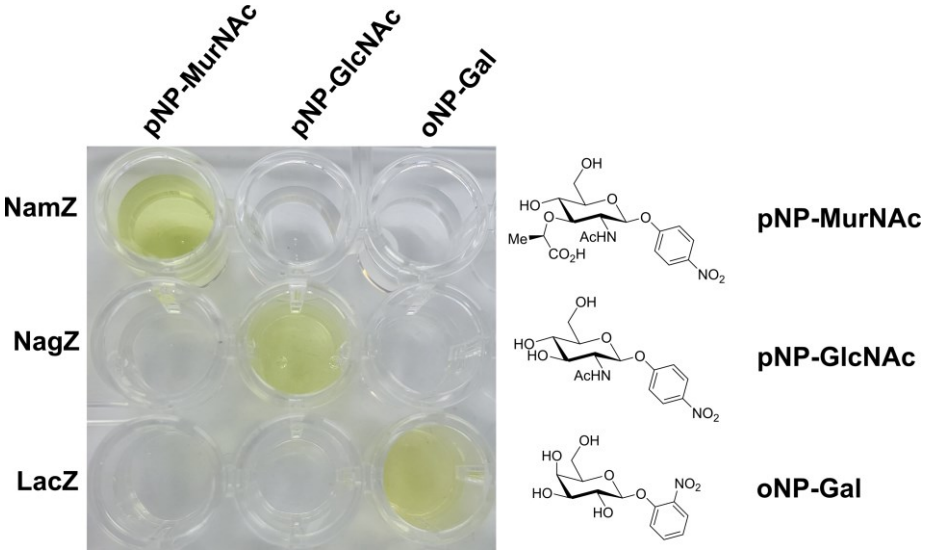

Figure 21 | NamZ of *B. subtilis* uses specifically pNP-MurNAc as substrate. NamZ was shown to only use pNP-MurNAc as a substrate. Other chromogenic substrates (pNP-GlcNAc and oNP-Gal) used in this assay, were no substrates for NamZ and were not cleaved. The controls, NagZ and LacZ cleaved specifically pNP-GlcNAc and oNP-Gal (Müller *et al.* 2021).

Using this assay, it could be shown that the chromogenic substrate pNP-MurNAc serves as a specific substrate for NamZ (Figure 21). NamZ cleaved off the nitrophenolate from the MurNAc residue leading to the characteristic yellow coloration after increasing the pH value using borate puffer. As controls, the exo-β-*N*-acetyl-glycosidase NagZ and the β-galactosidase LacZ were used to specifically cleave the other tested chromogenic substrates pNP-GlcNAc and oNP-Gal. NagZ used pNP-GlcNAc as a substrate while LacZ cleaved oNP-Gal each of them setting free the nitrophenolate during the cleavage, leading to a yellow color at high pH (Figure 21). Thereby, NamZ could be identified as an exo-β-*N*-acetylmuramidase, as it specifically used pNP-MurNAc as substrate in this assay.

Secondly, purified MurNAc-GlcNAc and GlcNAc-MurNAc were used in an assay together with recombinant NamZ and NagZ from *B. subtilis*. The success of substrate cleavage was monitored by HPLC-MS as described in chapter 2.9.

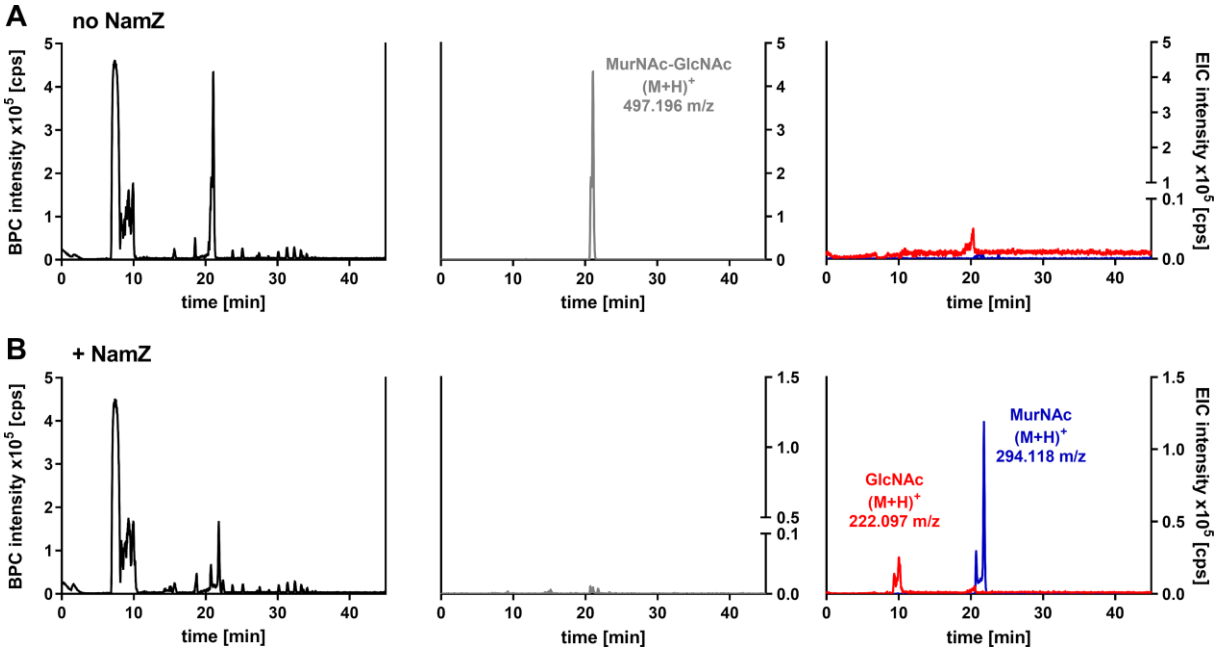

Figure 22 | NamZ of *B. subtilis* uses MurNAc-GlcNAc as a substrate revealed by HPLC-MS analysis. (A) For MurNAc-GlcNAc without addition of the enzyme, a peak at a retention time of 21.1 min with a mass of $(M+H)^+$ 497.196 m/z could be detected corresponding to MurNAc-GlcNAc (grey). **(B)** For MurNAc-GlcNAc with addition of NamZ, two peaks could be detected; one at a retention time of 10.0 min with a mass of $(M+H)^+$ 222.097 m/z corresponding to GlcNAc (red) and one at a retention time of 21.8 min with a mass of $(M+H)^+$ 294.118 m/z corresponding to MurNAc (blue). Results are presented as base peak chromatograms (BPC; black, left y-axis) and extracted ion chromatograms (EIC; red and blue, right y-axis) (Müller *et al.* 2021).

For the sample with MurNAc-GlcNAc as substrate without addition of NamZ, large amounts of MurNAc-GlcNAc could be detected at a retention time of 21.1 min with an observed mass of $(M+H)^+$ 497.196 m/z (theoretical mass of MurNAc-GlcNAc is $(M+H)^+$ 497.198 m/z) (Figure 22A). For the sample with MurNAc-GlcNAc as substrate and addition of NamZ, the peak for MurNAc-GlcNAc could not be detected. Instead, two other peaks appeared, revealing GlcNAc and MurNAc. GlcNAc was shown at a retention time of 10.0 min with an observed mass of $(M+H)^+$ 222.097 m/z (theoretical mass of GlcNAc is $(M+H)^+$ 222.097 m/z) and MurNAc was shown at a retention time of 21.8 min with an observed mass of $(M+H)^+$ 294.118 m/z (theoretical mass of MurNAc is $(M+H)^+$ 294.118 m/z) (Figure 22B).

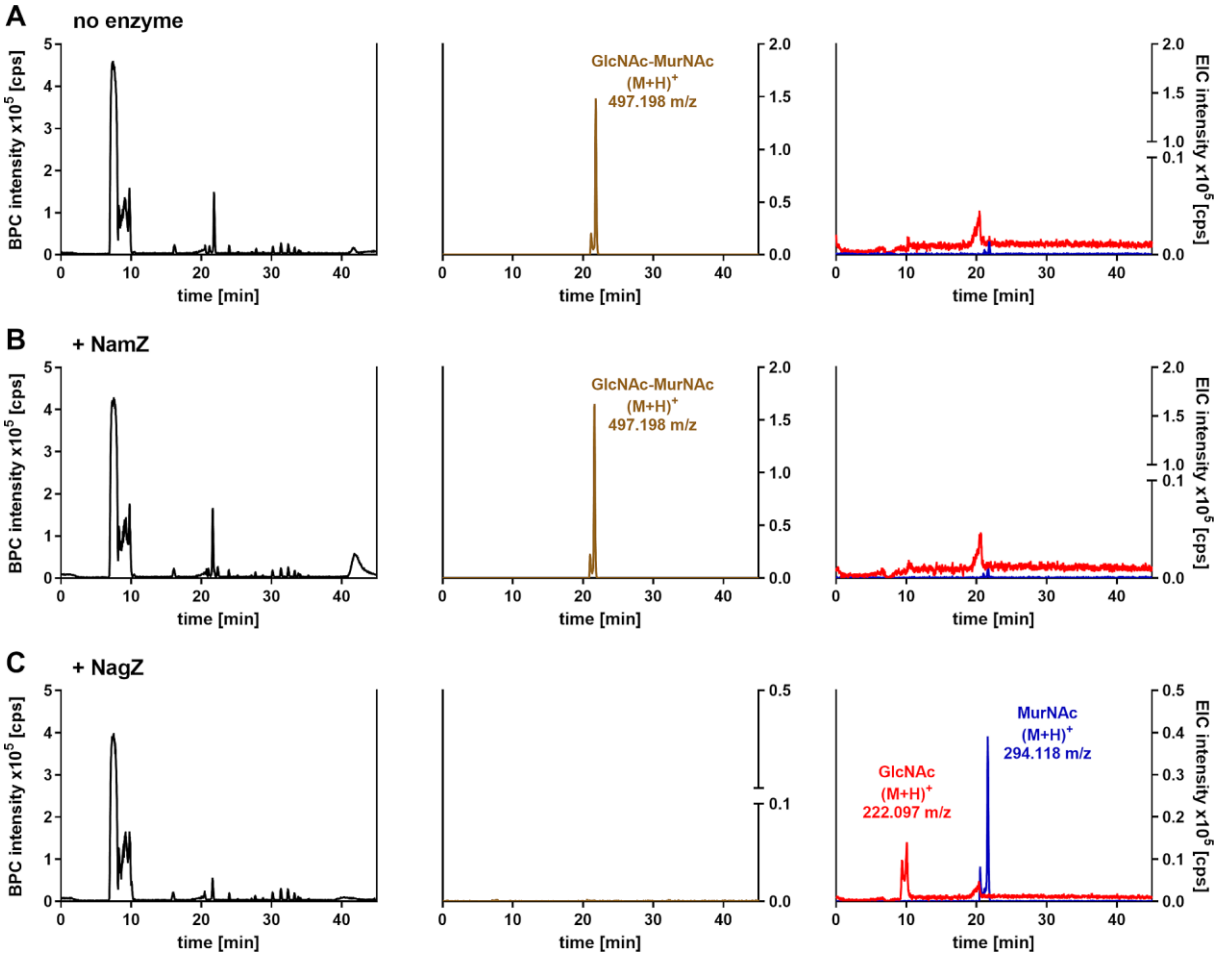

Figure 23 | NamZ of *B. subtilis* does not use GlcNAc-MurNAc as a substrate, whereas NagZ does revealed by HPLC-MS analysis. (A) For GlcNAc-MurNAc without addition of enzymes, a peak at a retention time of 21.8 min with a mass of $(M+H)^+$ 497.198 m/z could be detected corresponding to GlcNAc-MurNAc (brown). **(B)** For GlcNAc-MurNAc with addition of NamZ, a peak at a retention time of 21.6 min with a mass of $(M+H)^+$ 497.198 m/z could be detected corresponding to GlcNAc-MurNAc (brown). **(C)** For GlcNAc-MurNAc with addition of NagZ, two peaks could be detected; one at a retention time of 10.1 min with a mass of $(M+H)^+$ 222.097 m/z corresponding to GlcNAc (red) and one at a retention time of 21.6 min with a mass of $(M+H)^+$ 294.118 m/z corresponding to MurNAc (blue). Results are presented as base peak chromatograms (BPC; black, left y-axis) and extracted ion chromatograms (EIC; brown, red and blue, right y-axis) (Müller *et al.* 2021).

Additionally, for the sample with GlcNAc-MurNAc as substrate without the addition of NamZ or NagZ, large amounts of GlcNAc-MurNAc could be detected at a retention time of 21.8 min with an observed mass of $(M+H)^+$ 497.198 m/z (theoretical mass of GlcNAc-MurNAc is $(M+H)^+$ 497.198 m/z) (Figure 23A). Also, for the sample with GlcNAc-MurNAc as substrate and addition of NamZ, large amounts of GlcNAc-MurNAc could be detected at a retention time of 21.6 min with an observed mass of $(M+H)^+$ 497.198 m/z (theoretical mass of GlcNAc-MurNAc is $(M+H)^+$ 497.198 m/z) (Figure 23B). In contrast, for the sample with GlcNAc-MurNAc as substrate and addition of NagZ, the peak for GlcNAc-MurNAc could not be detected. Instead, two

other peaks appeared, revealing GlcNAc and MurNAc. GlcNAc was shown at a retention time of 10.1 min with an observed mass of $(M+H)^+$ 222.097 m/z (theoretical mass of GlcNAc is $(M+H)^+$ 222.097 m/z) and MurNAc was shown at a retention time of 21.6 min with an observed mass of $(M+H)^+$ 294.118 m/z (theoretical mass of MurNAc is $(M+H)^+$ 294.118 m/z) (Figure 23C).

These results confirmed the assumption from the chromogenic substrate specificity assay that NamZ acts as an exo-β-*N*-acetylmuramidase, which requires the MurNAc entity at the non-reducing end.

3.1.4 NamZ reaction and stability optima

For further biochemical characterization of NamZ, the reaction and stability optima were determined in an assay using the chromogenic substrate pNP-MurNAc as described in chapter 2.8.4.2. The temperature optimum was identified between 4°C and 60°C and the pH optimum was identified at values between 2.0 and 10.0. Measuring was carried out using a spectrophotometer.

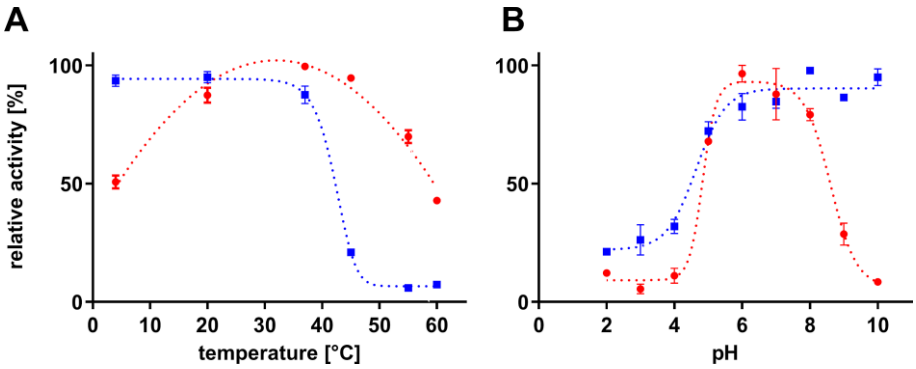

Figure 24 | Reaction and stability optima of NamZ from *B. subtilis*. (A) Temperature optimum (red circles) of NamZ was shown to be at 37°C, whereas temperature stability (blue squares) of NamZ was shown to be between 4°C and 37°C. **(B)** pH optimum (red circles) of NamZ was shown to be between 6.0 and 10.0, whereas pH stability (blue squares) of NamZ was shown to be between 6.0 and 8.0. Standard errors (SEM) were calculated out of three biological replicates (Müller *et al.* 2021).

NamZ was found to be stable at a temperature range between 4°C and 37°C and had an activity optimum at 37°C (Figure 24A). Furthermore, NamZ also proved to be largely stable in a pH range of 6.0 to 10.0, with an activity optimum between pH 6.0 and 8.0 (Figure 24B). For long-term storage at 4°C or -20°C, NamZ remained active for several months after purification.

3.1.5 Kinetic parameters

Kinetic parameters were determined to complete the biochemical characterization of NamZ. Therefore, both substrates pNP-MurNAc and MurNAc-GlcNAc were used in two different assays as described in chapter 2.8.4.3. Determination of kinetic parameters was carried out at 37°C for both assays, as it was shown to be the optimal temperature for NamZ. The colorimetric assay using pNP-MurNAc was performed at a pH of 8.0 because nitrophenolate requires alkaline conditions to show the characteristic yellow coloring. The assay using MurNAc-GlcNAc was performed at a pH of 7.0. Both pH values represent optimal conditions for NamZ as shown before.

Kinetic parameters for pNP-MurNAc were measured at 405 nm using a spectrophotometer. To calculate the maximal velocity and the Michaelis-Menten constant, a standard curve was prepared for para-nitrophenol.

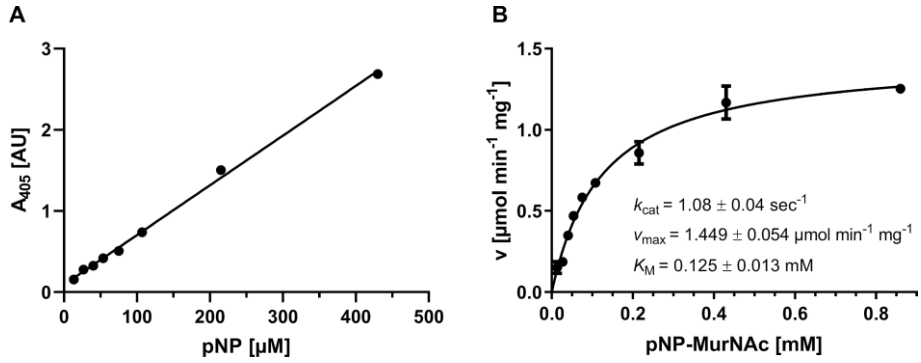

Figure 25 | Standard curve of para-nitrophenol and kinetic parameters of NamZ using pNP-MurNAc. (A) Standard curve for para-nitrophenol with concentrations from 13 µM to 430 µM. **(B)** Kinetic parameters using pNP-MurNAc as substrate with concentrations from 13 µM to 860 µM. For the maximal velocity a k_{cat} of 1.08 sec^{-1} and v_{max} of 1.449 µmol min^{-1} mg^{-1} was determined, and for Michaelis-Menten constant a K_M of 0.125 mM was calculated. Absorption was measured at 405 nm and standard errors (SEM) were calculated out of three biological replicates (modified after Müller *et al.* 2021).

For NamZ using pNP-MurNAc as substrate at 37°C and pH 8.0, a maximal velocity was determined with a k_{cat} of 1.08 ± 0.04 sec^{-1} and a v_{max} of 1.449 ± 0.054 µmol min^{-1} mg^{-1} and the Michaelis-Menten constant was K_M of 0.125 ± 0.013 mM (Figure 25).

For determination of the kinetic parameters for MurNAc-GlcNAc the release of MurNAc was measured by HPLC-MS analysis. To calculate the maximal velocity and the Michaelis-Menten constant, a standard curve was prepared for MurNAc.

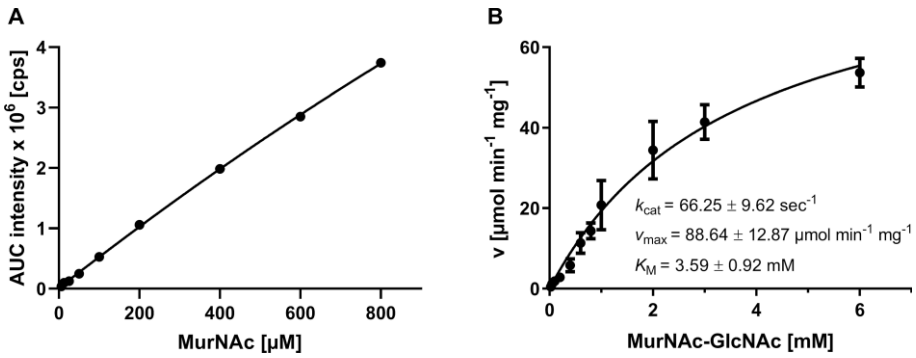

Figure 26 | Standard curve of MurNAc and kinetic parameters of NamZ using MurNAc-GlcNAc. (A) Standard curve for MurNAc with concentrations from 6.25–800 µM. **(B)** Kinetic parameters using MurNAc-GlcNAc as substrate with concentrations from 0.025 mM to 6 mM. For the maximal velocity a k_{cat} of 66.25 sec^{-1} and v_{max} of 88.64 µmol min^{-1} mg^{-1} was determined, and for Michaelis-Menten constant a K_M of 3.59 mM was calculated. Amount of MurNAc was analyzed using the area under curve (AUC) by generating extracted ion chromatograms (EIC) for measured mass of MurNAc $(M-H)^-$ 292.113 m/z. Standard errors (SEM) were calculated out of three biological replicates (modified after Müller *et al.* 2021).

For NamZ using MurNAc-GlcNAc as substrate at 37°C and pH 7.0, a maximal velocity was determined with a k_{cat} of 66.25 ± 9.62 sec^{-1} and a v_{max} of 88.64 ± 12.87 µmol min^{-1} mg^{-1} and the Michaelis-Menten constant was K_M of 3.59 ± 0.92 mM (Figure 26).

Hence, the reaction of NamZ with MurNAc-GlcNAc as substrate was faster than with pNP-MurNAc as substrate (k_{cat} of 66.25 sec^{-1} and 1.08 sec^{-1} as well as v_{max} of 88.64 µmol min^{-1} mg^{-1} and 1.45 µmol min^{-1} mg^{-1}), but the affinity of NamZ for MurNAc-GlcNAc was less than for pNP-MurNAc (K_M of 3.59 mM and 0.125 mM) (Figure 25 and Figure 26). When the kinetic parameters were determined using MurNAc-GlcNAc as substrate, it could be observed that a first saturation was reached at a MurNAc-GlcNAc concentration of 0.2 mM, before the curve reached the second saturation at a concentration of 6 mM. Therefore, the kinetic parameters of the first saturation were calculated as well.

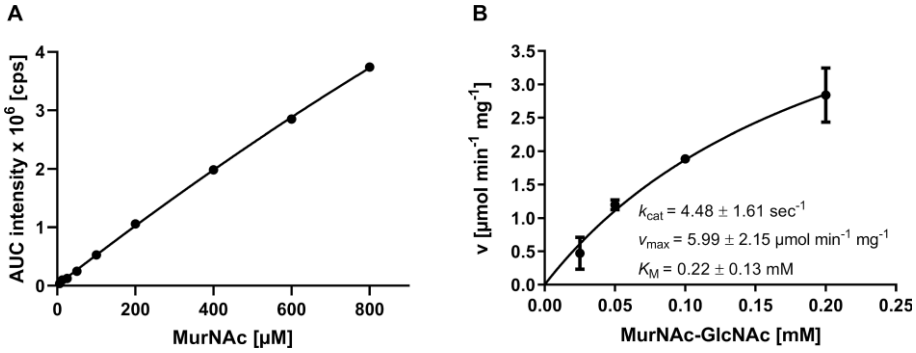

Figure 27 | Standard curve of MurNAc and kinetic parameters of NamZ using MurNAc-GlcNAc. (A) Standard curve for MurNAc with concentrations from 6.25–800 µM. **(B)** Kinetic parameters using MurNAc-GlcNAc as substrate with concentrations from 0.025 mM to 0.2 mM. For the maximal velocity a k_{cat} of 4.48 sec^{-1} and v_{max} of 5.99 µmol min^{-1} mg^{-1} was determined, and for Michaelis-Menten constant a K_M of 0.22 mM was calculated. Amount of MurNAc was analyzed using the area under curve (AUC) by generating extracted ion chromatograms (EIC) for measured mass of MurNAc $(M-H)^-$ 292.113 m/z. Standard errors (SEM) were calculated out of three biological replicates (modified after Müller *et al.* 2021).

For the first saturation of the kinetic reaction of NamZ using MurNAc-GlcNAc as substrate at 37°C and pH 7.0, a maximal velocity was determined with a k_{cat} of 4.48 ± 1.61 sec^{-1} and a v_{max} of 5.99 ± 2.15 µmol min^{-1} mg^{-1} and the Michaelis-Menten constant was K_M of 0.22 ± 0.13 mM (Figure 27).

Hence, the reaction of NamZ with MurNAc-GlcNAc as substrate with concentrations from 0.025 mM to 0.2 mM was, again, faster than with pNP-MurNAc as substrate (k_{cat} of 4.48 sec-1 and 1.08 sec^{-1} as well as v_{max} of 5.99 µmol min^{-1} mg^{-1} and 1.45 µmol min^{-1} mg^{-1}). In contrast to the kinetic parameters calculated for a MurNAc-GlcNAc concentration from 0.025 mM to 6 mM, the affinity of NamZ for MurNAc-GlcNAc was comparable to the affinity for pNP-MurNAc (K_M of 0.22 mM and 0.125 mM) (Figure 25 and Figure 27).

3.1.6 Digestion of peptidoglycan

Finally, the ability of NamZ to digest its natural substrate, peptidoglycan of B. subtilis, was tested. Therefore, PGN was purified as described in chapter 2.7.15. After purification, PGN was applied in an assay together with recombinant enzymes. PGN was digested using the exo-β-*N*-acetylglucosaminidase NagZ, the *N*-acetylmuramyl-L-alanine amidase AmiE and NamZ (all from *B. subtilis*) as described in chapter 2.8.5. Analysis of released products was performed using HPLC-MS.

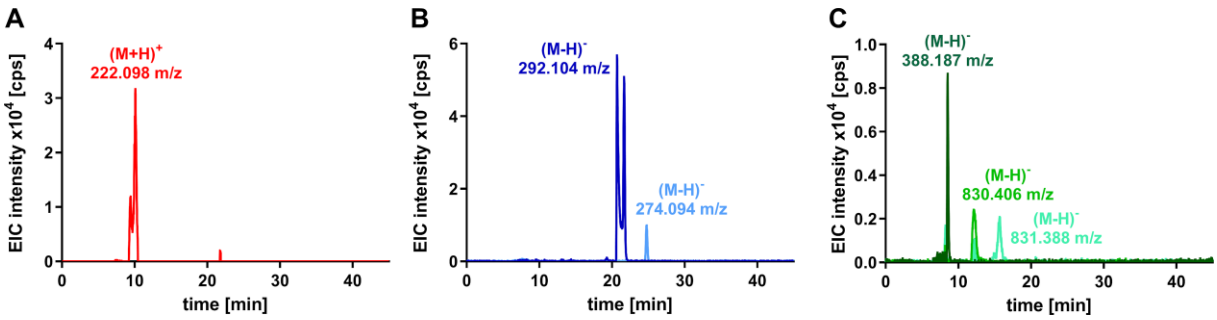

Figure 28 | Peptidoglycan of *B. subtilis* sequentially digested with NagZ, AmiE and NamZ analyzed by HPLC-MS using positive as well as negative ion mode. The following cell wall sugars and peptides could be identified: **(A)** GlcNAc at a retention time of 10.1 min with a measured mass of $(M+H)^+$ 222.098 m/z (red), **(B)** MurNAc at a retention time of 21.1 min with a measured mass of $(M-H)^-$ 292.104 m/z (dark blue) and anhMurNAc at a retention time of 24.8 min with a measured mass of $(M-H)^-$ 274.094 m/z (light blue), and **(C)** amidated tripeptide at a retention time of 8.5 min with a measured mass of $(M-H)^-$ 388.187 m/z (dark green), tri-tetrapeptide with two amidations at a retention time of 12.1 min with a measured mass of $(M-H)^-$ 830.406 m/z (light green), and tri-tetrapeptide with one amidation at a retention time of 15.1 min with a measured mass of $(M-H)^-$ 831.388 m/z (turquoise). All products of sequential digest are shown as extracted ion chromatograms (EIC).

HPLC-MS analysis of digested peptidoglycan showed both, cell wall sugars as well as peptides (Figure 28). For cell wall sugars, GlcNAc could be identified at a retention time of 10.1 min with a measured mass in positive ion mode of $(M+H)^+$ 222.098 m/z (theoretical mass of GlcNAc is $(M+H)^+$ 222.097 m/z), as well as MurNAc at a retention time of 21.1 min with a measured mass in negative ion mode of $(M-H)^-$ 292.104 m/z (theoretical mass of MurNAc is $(M-H)^-$ 292.104 m/z), and anhMurNAC at a retention time of 24.8 min with a measured mass in negative ion mode of $(M-H)^-$ 274.094 m/z (theoretical mass of anhMurNAc is $(M-H)^-$ 274.093 m/z). Additionally, tripeptide with one amidation could be identified at a retention time of 8.5 min with a measured mass in negative ion mode of $(M-H)^-$ 388.187 m/z (theoretical mass of tripeptide with one amidation is $(M-H)^-$ 388.184 m/z), as well as cross-linked tri-tetrapeptide with two amidations at a retention time of 12.1 min with a measured mass in negative ion mode of $(M-H)^-$ 830.406 m/z (theoretical mass of cross-linked tri-tetrapeptide with two amidations is $(M-H)^-$ 830.401 m/z), and cross-linked tri-tetrapeptide with one amidation at a retention time of 12.1 min with a measured mass in negative ion mode of $(M-H)^-$ 831.388 m/z (theoretical mass of cross-linked tri-tetrapeptide with one amidation is $(M-H)^-$ 831.390 m/z). To verify the purity and to confirm the found products the mass spectra of HPLC-MS run were analyzed (see Appendix Figure 40).

Altogether, peptidoglycan of *B. subtilis* could be digested into single cell wall sugars and (cross-linked) peptides by the joint action of NagZ, AmiE and NamZ.

3.1.7 Growth phase-depended expression of cell wall recycling enzymes

In a previous study, NagZ activity was shown to be highest in the late stationary phase (Litzinger *et al.* 2010). In this study, the fluorogenic substrate 4′-methylumbelliferyl *N*-acetyl-β-D-glucosaminide (4MU-GlcNAc) was used. The method used there should be adapted to usage of the chromogenic substrate pNP-GlcNAc (see chapter 2.7.11) and pNP-MurNAc to determine the time point of the highest activity of NagZ and NamZ.

Additionally, to investigate the role of the recycling genes *murQ, murR* and *murP* in the timepoint of the activity, the *B. subtilis* 168-Δ*murQ*Δ*murR*Δ*murP* mutant was used in comparison to *B. subtilis* 168 and *B. subtilis* 168-Δ*nagZ::erm*. The measurement was carried out using a spectrophotometer as depicted in Figure 29. Comparing the growth of the different strains, it was shown that the OD_{600} of the two mutants *B. subtilis* 168-Δ*nagZ::erm* and *B. subtilis* 168-Δ*murQ*Δ*murR*Δ*murP* decreased when reaching late stationary phase in comparison to the wild type (Figure 29A).

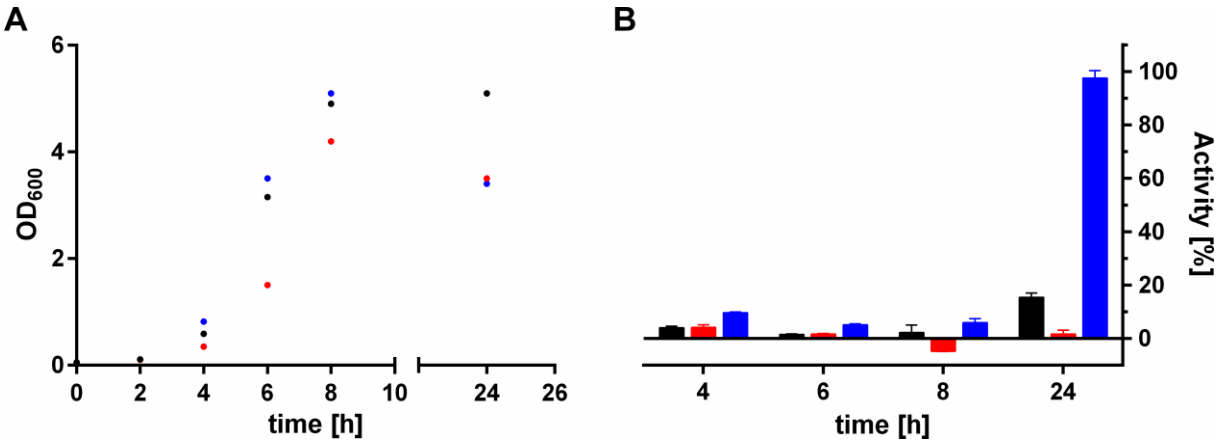

Figure 29 | Monitoring of growth for different *B. subtilis* strains combined with activity of NagZ. (A) 168-Δ*nagZ::erm* (red) and 168-Δ*murQ*Δ*murR*Δ*murP* (blue) showed a drop on OD measurement at 24 h in late stationary phase in comparison to wild type (black). **(B)** In exponential phase, no activity for NagZ could be determined for wild type (black) and 168-Δ*nagZ::erm* (red), whereas for 168-Δ*murQ*Δ*murR*Δ*murP* (blue) slight activity could be monitored, as indicated by an increased absorption at 405 nm. NagZ activity for wild type was highest in late stationary phase as well as for 168-Δ*murQ*Δ*murR*Δ*murP*.

For the adaptation of the published method to the chromogenic substrate pNP-GlcNAc, it could be successfully shown that the wild type and *B. subtilis* 168-Δ*nagZ::erm* performed comparably. For *B. subtilis* 168-Δ*murQ*Δ*murR*Δ*murP* it was evident that a higher activity of NagZ could be measured permanently in comparison the wild type (Figure 29B). The increase in NagZ activity might be since *murR* encodes for the transcriptional MurNAc-6P-sensitive repressor MurR. This that the deletion of MurR affects the activity of NagZ and presumably also on the other two enzymes of the operon, AmiE and NamZ.

3.2 Tools for studying cell wall turnover

Peptidoglycan recycling is well studied in *E. coli* and as mentioned above, it had also been proven to take place in *B. subtilis*. Still, many aspects of this pathway in *B. subtilis* and related Gram-positive bacteria are unclear. For a more in-depth look into the mechanism and as a tool to study PGN recycling in detail, a *B. subtilis* double mutant was generated, along with a plasmid encoding the *Pseudomonas putida* anabolic PGN recycling enzymes. This construct of *B. subtilis* should have the ability to shuttle MurNAc and GlcNAc as precursors directly into peptidoglycan synthesis, since the mutations abolish catabolism via glycolysis and the *P. putida* genes allow conversion to the peptidoglycan precursors UDP-GlcNAc and UDP-MurNAc.

In a first step, the gene *murQ* encoding for the *N*-acetyl-muramic acid-6P etherase was knocked out in *B. subtilis* 168 (Dalügge 2015). Second, competent cells of this 168-Δ*murQ* strain were transformed with the PCR product Δ*nagA::erm* amplificated from the strain 168-Δ*nagA::erm* to generate the double mutant 168-Δ*murQ*Δ*nagA::erm* (Mühleck 2016). To generate a markerless double mutant, the erythromycin resistance cassette was excised using the plasmid pDR244 as described in chapter 2.7.7, resulting in the strain 168-Δ*murQ*Δ*nagA*, which was verified by sequencing.

The generated double mutant should be restricted to use recycled cell wall sugars in glycolysis, as MurNAc-6P cannot be converted into GlcNAc-6P by MurQ and GlcNAc-6P cannot be deacetylated by NagA. Accordingly, MurNAc-6P and GlcNAc-6P should be accumulating in the mutant but not in the wild type. To prove this, accumulation products of cytosolic fractions (prepared as described in chapter 2.7.12) were analyzed using HPLC-MS (Figure 30).

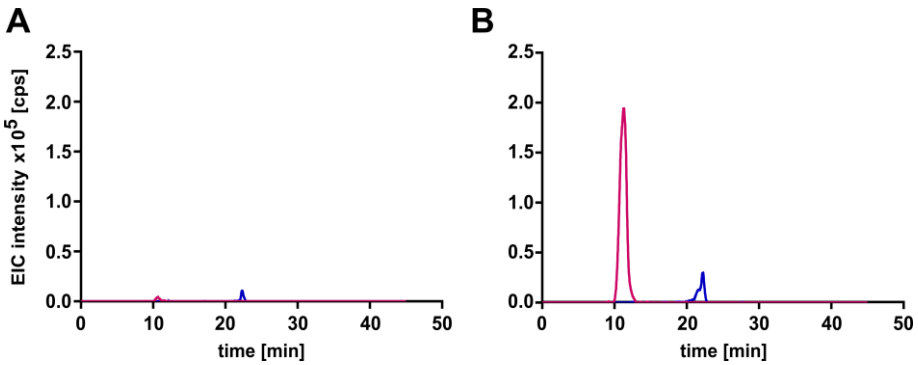

Figure 30 | Accumulation of GlcNAc-6P and MurNAc-6P in the cytosol of *B. subtilis* 168 wild type and 168-Δ*murQ*Δ*nagA* mutant. (A) The wild type and **(B)** the 168-Δ*murQ*Δ*nagA* mutant were cultured for 24 h in LB medium. Cytosolic fractions were analyzed by HPLC-MS using negative ion mode. For wild type no accumulation of GlcNAc-6P and MurNAc-6P could be identified. For 168-Δ*murQ*Δ*nagA* two peaks could be identified: GlcNAc-6P at a retention time of 10.1 min with a theoretical mass of $(M-H)^-$ 300.05 m/z (pink) and MurNAc-6P at a retention time of 21.1 min with a theoretical mass of $(M-H)^-$ 372.07 m/z (blue). Accumulation products are shown as extracted ion chromatograms (EIC).

The EICs of the cytosolic fractions were generated and evaluated by searching for the theoretical masses of MurNAc-6P $(M-H)^-$ 372.07 m/z and GlcNAc-6P $(M-H)^-$ 300.05 m/z. It was shown that neither MurNAc-6P nor GlcNAc-6P accumulate in the wild type. In contrast, the mutant 168-Δ*murQ*Δ*nagA* showed a peak for both MurNAc-6P and GlcNAc-6P, which implements that further use of MurNAc-6P and GlcNAc-6P could be restricted in this strain.

For the targeted re-use of MurNAc-6P and GlcNAc-6P in peptidoglycan synthesis, the recycling genes *mupP*, *amgK* and *murU* of *P. putida* were cloned into the plasmid pGP888 (as described in chapter 2.6.7), which integrates in the β-galactosidase gene *ganA* of the *B. subtilis* genome and possesses a xylose-inducible promotor. The double mutant 168-Δ*murQ*Δ*nagA* was transformed with the vector pGP888-PAM as described in chapter 2.7.5 and successful integration of the plasmid in the *ganA* site was verified by sequencing. By introducing pGP888-PAM into 168-Δ*murQ*Δ*nagA*, the incorporated MurNAc-6P and GlcNAc-6P can be targeted for the synthesis of cell wall precursors. MupP is a phosphatase by which MurNAc-6P and GlcNAc-6P are dephosphorylated. AmgK is an anomeric MurNAc/GlcNAc kinase that phosphorylates the two sugars at their C1 position. The resulting MurNAc α-1P and GlcNAc α-1P can be converted by the uridylyltransferases MurU and GlmU into UDP-MurNAc and UDP-GlcNAc, respectively, which are the precursors of the peptidoglycan. To proof the role of the MupP, AmgK and MurU, *B. subtilis* 168 wild type as well as 168-Δ*murQ*Δ*nagA* mutant were transformed with the empty plasmid pGP888 as described in chapter 2.7.5,

resulting in the strains 168_pGP888 and 168-Δ*murQ*Δ*nagA*_pGP888. For both strains, successful integration of the plasmid in the *ganA* site was verified by sequencing.

The expression of the *P. putida* genes was initiated by adding 0.3% xylose to cultures of 168_pGP888, 168-Δ*murQ*Δ*nagA*_pGP888 and 168-Δ*murQ*Δ*nagA*_pGP888-PAM. Due to introduction of MurP, AmgK and MurU, the previously shown MurNAc-6P and GlcNAc-6P accumulation should vanish. Cytosolic fractions of these strains were analyzed using HPLC-MS (Figure 31).

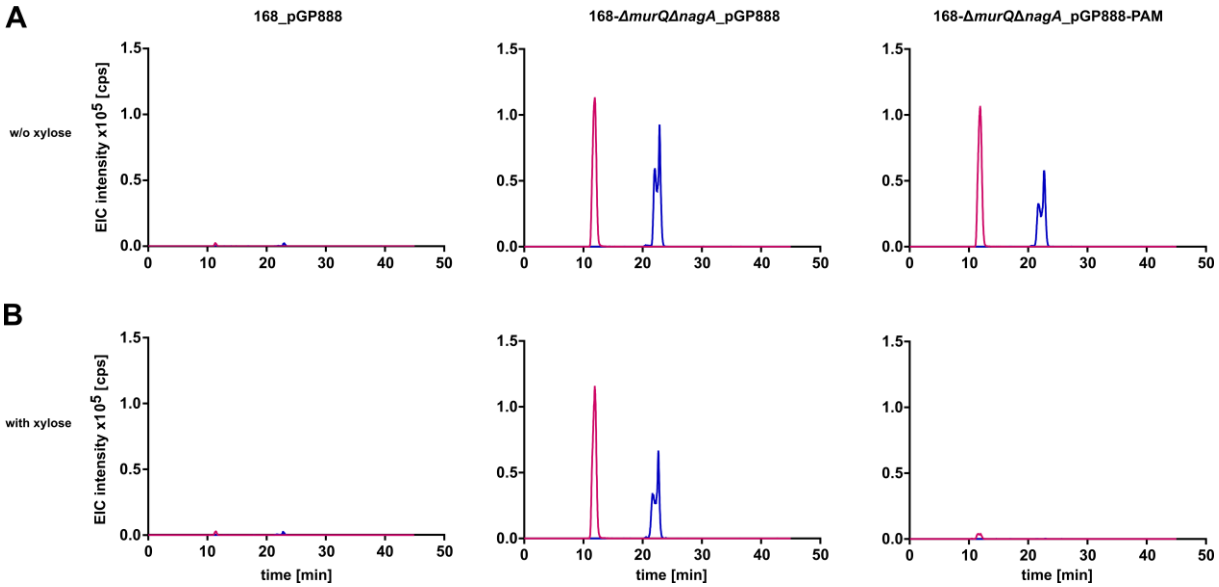

Figure 31 | Accumulation of GlcNAc-6P and MurNAc-6P in the cytosol of *B. subtilis* 168_pGP888, 168-Δ*murQ*Δ*nagA*_pGP888 and 168-Δ*murQ*Δ*nagA*_pGP888-PAM mutants. All strains were cultured for 24 h in LB medium **(A)** without and **(B)** with addition of xylose, respectively. Cytosolic fractions were analyzed by HPLC-MS using negative ion mode. For 168_pGP888, no accumulation could be detected either without or with the addition of xylose. For 168-Δ*murQ*Δ*nagA*_pGP888 either without or with the addition of xylose two peaks could be identified: GlcNAc-6P at a retention time of 10.1 min with a theoretical mass of $(M\text{-}H)^-$ 300.05 m/z (pink) and MurNAc-6P at a retention time of 21.1 min with a theoretical mass of $(M\text{-}H)^-$ 372.07 m/z (blue). For 168-Δ*murQ*Δ*nagA*_pGP888-PAM without the addition of xylose two peaks could be identified: GlcNAc-6P at a retention time of 10.1 min with a theoretical mass of $(M\text{-}H)^-$ 300.05 m/z (pink) and MurNAc-6P at a retention time of 21.1 min with a theoretical mass of $(M\text{-}H)^-$ 372.07 m/z (blue). Both peaks showed comparable intensities to the peaks of 168-Δ*murQ*Δ*nagA*_pGP888. For 168-Δ*murQ*Δ*nagA*_pGP888-PAM with the addition of xylose (0.3%) no accumulation could be detected. Accumulation products are shown as extracted ion chromatograms (EIC).

The EICs of the cytosolic fractions were generated and evaluated by searching for the theoretical masses of MurNAc-6P $(M\text{-}H)^-$ 372.07 m/z and GlcNAc-6P $(M\text{-}H)^-$ 300.05 m/z. It was shown that neither MurNAc-6P nor GlcNAc-6P accumulate in the 168_pGP888 strain whether without or with induction of pGP888 with xylose. In contrast, the mutant 168-Δ*murQ*Δ*nagA*_pGP888 showed again a peak for both MurNAc-6P and GlcNAc-6P without and with addition of xylose, meaning that pGP888

had no impact in the accumulation of the cell wall synthesis intermediates. For 168-Δ*murQ*Δ*nagA*_pGP888-PAM the accumulation of MurNAc-6P and GlcNAc-6P could be measured without xylose-induction of the plasmid. Both accumulation products vanished after inducing the expression of the *P. putida* genes *mupP*, *amgK* and *murU* with xylose (Figure 31), resulting in a strain which can be used for labeling of the cell wall by addition of e.g., radio labeled cell wall precursors.

3.3 Cannibalism

3.3.1 Lytic enzymes involved in cannibalistic behavior of *B. subtilis*

For a better understanding of the autolysins involved in cannibalism, different mutants were generated (see chapters 2.7.6 and 2.7.7) and tested for their lytic phenotype upon exposure to cannibalism toxins or toxin-expressing strains. In these assays Δ*spo0A::erm* cells served as prey cells, since they are not able to confer immunity against the cannibalism toxins. In an earlier study, the double mutants 168-Δ*lytC*Δ*spo0A::erm*, 168-Δ*lytD*Δ*spo0A::erm*, 168-Δ*lytE*Δ*spo0A::erm*, and 168-Δ*lytF*Δ*spo0A::erm* were investigated for the influence of LytC, LytD, LytE and LytF in autolysis in a spot assay (see chapter 2.7.8 and Figure 32) (Mühleck 2016).

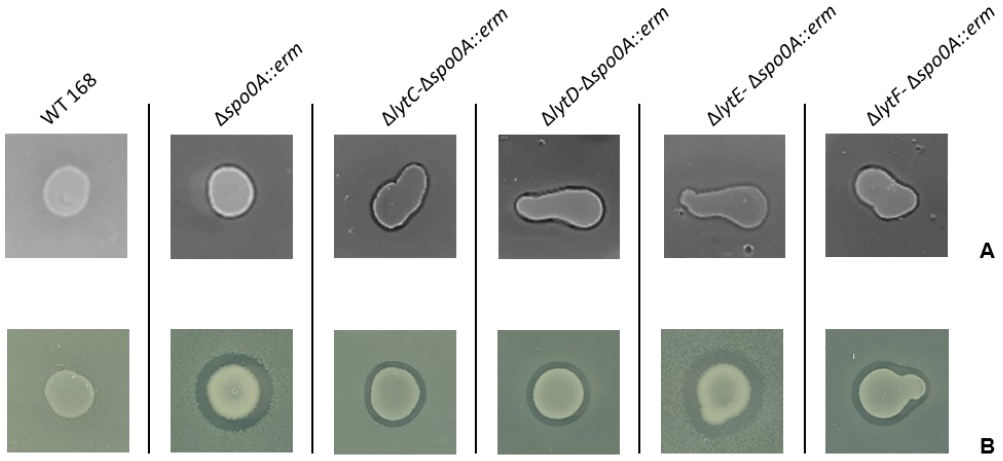

Figure 32 | Spot assay of *B. subtilis* 168-Δ*lytC*-Δ*spo0A::erm*, *B. subtilis* 168-Δ*lytD*-Δ*spo0A::erm*, *B. subtilis* 168-Δ*lytE*-Δ*spo0A::erm*, and *B. subtilis* 168-Δ*lytF*-Δ*spo0A::erm* double mutants. A and B show different independent spot assays. A: No difference in the size of the inhibition zone is seen for the double mutants compared to the positive control *B. subtilis* 168-Δ*spo0A::erm*. *B. subtilis* 168 was used as a negative control. **B:** For the double mutants *B. subtilis* 168-Δ*lytC*-Δ*spo0A::erm*, *B. subtilis* 168-Δ*lytD*-Δ*spo0A::erm*, and *B. subtilis* 168-Δ*lytF*-Δ*spo0A::erm*, a reduction of the inhibition zone size is seen compared to the positive control *B. subtilis* 168-Δ*spo0A::erm*. *B. subtilis* 168-Δ*lytE*-Δ*spo0A::erm* shows no difference of the inhibition zone size compared to the positive control *B. subtilis* 168-Δ*spo0A::erm*. *B. subtilis* 168 was used as a negative control. Spotted was always *B. subtilis* 168. In the lawn (OD_{600} ~1.8) are the growth cultures (*B. subtilis* 168,

B. subtilis 168-Δ*spo0A::erm*, *B. subtilis* 168-Δ*lytC*-Δ*spo0A::erm*, *B. subtilis* 168-Δ*lytD*-Δ*spo0A::erm*, *B. subtilis* 168-Δ*lytE*-Δ*spo0A::erm*, and *B. subtilis* 168-Δ*lytF*-Δ*spo0A::erm*). *B. subtilis* 168 was used as a negative control, and *B. subtilis* 168-Δ*spo0A::erm* was used as a positive control (Mühleck 2016).

In the spot assay, it could be shown that LytC, LytD and LytF do play a role in cannibalism (Figure 32), but due to the lack of reproducibility of the spot assays, the influence of the autolysins LytC, LytD, LytE, and LytF in the cannibalism of *B. subtilis* 168 remained uncertain and were reinvestigated by using fluorescent strains.

The aim was to use different fluorescent dyes to distinguish cannibal and prey cells in fluorescent microscopic experiments visualizing the cannibalistic behavior.

Therefore, the plasmids pBP27 and pBP26 received from (Gunka *et al.* 2013) were used. Plasmid pBP27 encodes the gene for the fluorophore CFP whereas pBP26 encodes the gene for the fluorophore YFP. These plasmids integrate after transformation into the *amyE* site of the *B. subtilis* genomic DNA resulting in the strains 168-*amyE::cfp* and 168-*amyE::yfp* (Gunka *et al.* 2013). Fluorescence was shown using microscopy (Figure 33).

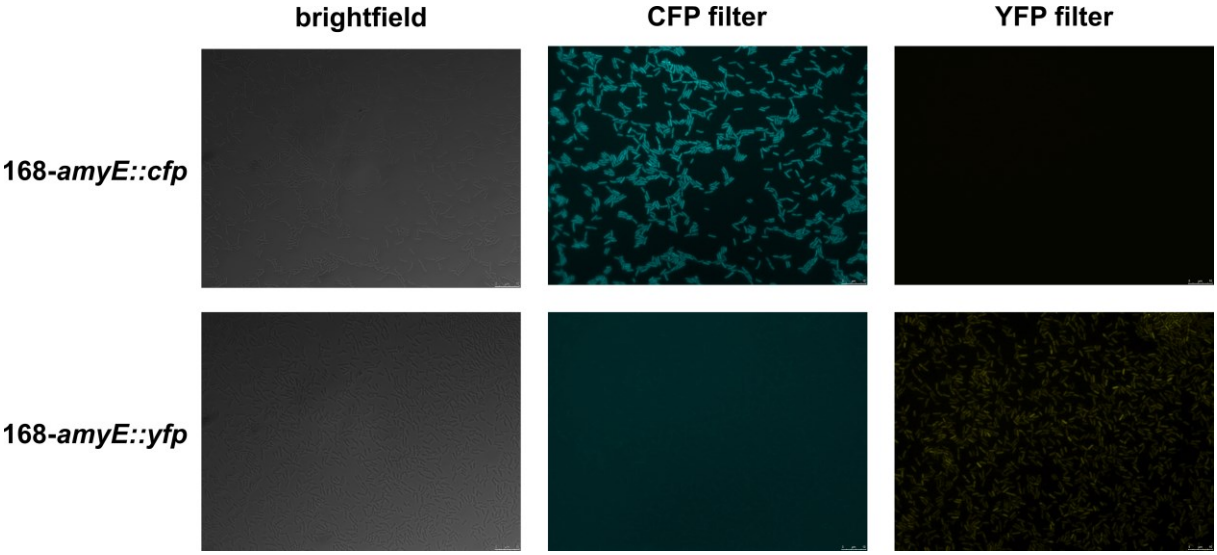

Figure 33 | Microscopy of fluorescence strains 168-*amyE::cfp* and 168-*amyE::yfp*. Shown are microscopic pictures of 168-*amyE::cfp* and 168-*amyE::yfp* with different exposure or filters, respectively. In the brightfield exposure, the cells are visible for both strains. For 168-*amyE::cfp* fluorescence of the cells could be shown using the CFP filter, but not the YFP filter. For 168-*amyE::yfp* fluorescence of the cells could be shown using the YFP filter, but not the CFP filter.

Using brightfield, cells are visible for both strains. Using the CFP filter, fluorescence of the cells could be shown for 168-*amyE::cfp*, but not for 168-*amyE::yfp*. Using the YFP filter, fluorescence of the cells could be shown for 168-*amyE::yfp* but not for 168-*amyE::cfp* (Figure 33).

The strain 168-*amyE::yfp* was used to generate a mutant as described in chapter 2.7.6 lacking *spo0A*. Therefore, the erythromycin resistance cassette from the BGSC strain 168-Δ*spo0A::erm* was amplified using PCR and purified. 168-*amyE::yfp* was transformed as described in chapter 2.7.5 with the purified PCR product. The mutant 168-*amyE::yfp*Δ*spo0A::erm* was successfully generated and verified by sequencing. The strains 168-*amyE::cfp* and 168-*amyE::yfp*Δ*spo0A::erm* were grown in co-culture and fluorescence was measured as described in chapter 2.7.9.

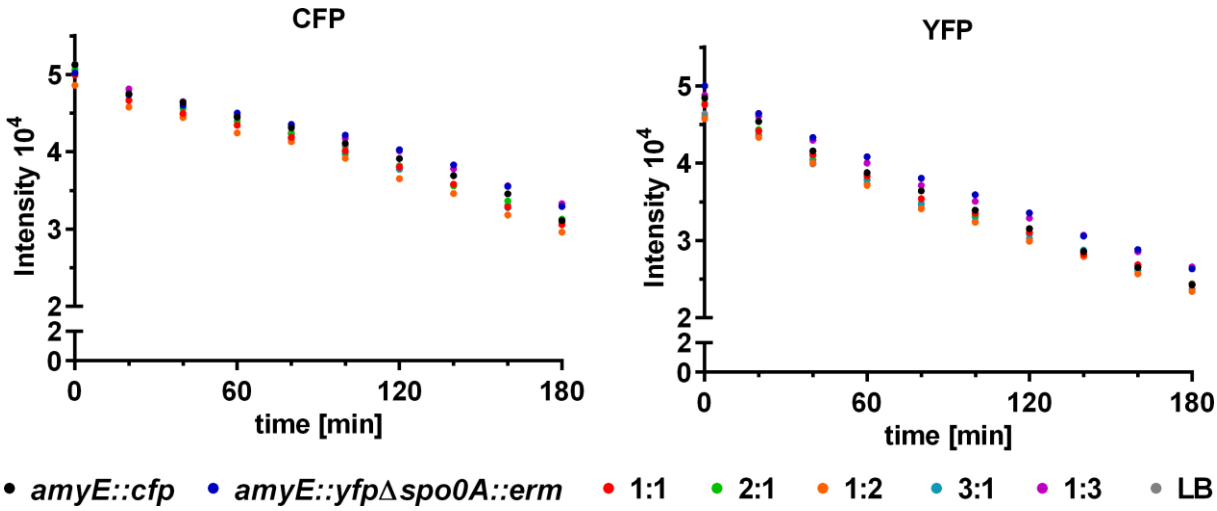

Figure 34 | Measurement of CFP and YFP fluorescence for co-cultivation of 168-*amyE::cfp* and 168-*amyE::yfp*Δ*spo0A::erm*. Single cultures 168-*amyE::cfp* (black) and 168-*amyE::yfp*Δ*spo0A::erm* (blue) were monitored, as well as ratios 1:1 (168-*amyE::cfp* : 168-*amyE::yfp*Δ*spo0A::erm*; red), 2:1 (168-*amyE::cfp* : 168-*amyE::yfp*Δ*spo0A::erm*; green), 1:2 (168-*amyE::cfp* : 168-*amyE::yfp*Δ*spo0A::erm*; orange), 3:1 (168-*amyE::cfp* : 168-*amyE::yfp*Δ*spo0A::erm*; turquoise), 1:3 (168-*amyE::cfp* : 168-*amyE::yfp*Δ*spo0A::erm*; purple). A LB medium control (grey) was also included.

For both CFP and YFP, no difference could be measured between the two single cultures 168-*amyE::cfp* and 168-*amyE::yfp*Δ*spo0A::erm* as well as the co-cultures in various ratios. The blank control with medium also showed the same values (Figure 34).

Additionally, the strain 168-*amyE::yfp* was used to generate mutants as described in chapter 2.7.6 lacking one of the autolysins *lytC*, *lytD*, *lytE* and *lytF*. Therefore, the erythromycin resistance cassette from the BGSC strains 168-Δ*lytC::erm*, 168-Δ*lytD::erm*, 168-Δ*lytE::erm*, and 168-Δ*lytF::erm* was amplified using PCR and purified. 168-*amyE::yfp* was transformed as described in chapter 2.7.5 with the purified PCR product. The mutants 168-*amyE::yfp*Δ*spo0A::erm*, 168-Δ*lytC::erm* and 168-Δ*lytD::erm* were successfully generated and verified by sequencing. The mutants 168-*amyE::yfp*Δ*lytE::erm* and 168-*amyE::yfp*Δ*lytF::erm* could not successfully be generated.

3.3.2 Growth of toxin double mutant

To show the effect of toxins SKF and SPD as well as the influence of autolysins on cannibalistic behavior, growth of different *B. subtilis* strains was monitored as described in chapter 2.7.9. Therefore, a mutant lacking both cannibalism toxins SkfA and SdpC was generated by first excise the erythromycin resistance cassette from BGSC strain 168-Δ*sdpC::erm* as described in chapter 2.7.7. After excision, *skfA* was replaced in the strain 168-Δ*sdpC* by an erythromycin resistance cassette as described in chapter 2.7.6, resulting in the strain 168-Δ*sdpC*Δ*skfA::erm*.

Growth was monitored via OD measurement for *B. subtilis* wild type, 168-Δ*lytABC::neo*Δ*lytD::tet*Δ*lytE::cm*Δ*lytF::spec*, 168-Δ*spo0A::erm*, 168-Δ*skfA::erm*, 168-Δ*sdpC::erm*, and 168-Δ*sdpC*Δ*skfA::erm* (Figure 35 and Appendix Table 11).

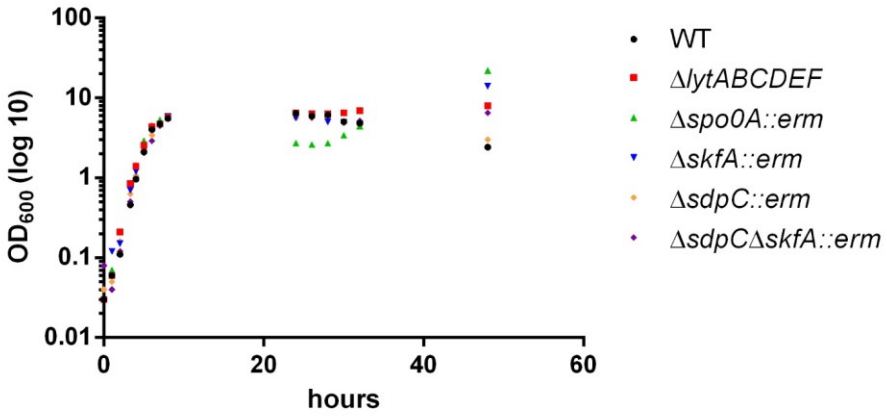

Figure 35 | Monitoring of growth for different *B. subtilis* strains. Wild type (black) as well as 168-Δ*sdpC::erm* (orange) showed a drop in OD measurement at 48 h after reaching stationary phase. In contrast 168-Δ*spo0A::erm* (green) and 168-Δ*skfA::erm* (blue) showed an increase in OD measurement. For 168-Δ*lytABC::neo*Δ*lytD::tet*Δ*lytE::cm*Δ*lytF::spec* (red) and 168-Δ*sdpC*Δ*skfA::erm* (purple) OD measurement remained the same after reaching early stationary phase at 24 h.

For the wild type, a continuous growth was observed for up to 24 h until an OD_{600} of 6.4 was reached and the cells entered stationary phase. Afterwards, the OD_{600} dropped to 2.4 after 48 h, which might indicate cell lysis (Figure 35 and Appendix Table 11). For 168-Δ*lytABC::neo*Δ*lytD::tet*Δ*lytE::cm*Δ*lytF::spec*, a continuous growth for up to 24 h until OD_{600} of 6.5 could be measured until the cells reached stationary phase. Then, the OD_{600} stagnated at 6.3 until 28 h of measurement and slightly increased afterwards to an OD_{600} of 7.9 after 48 h (Figure 35 and Appendix Table 11). For 168-Δ*spo0A::erm*, a continuous growth for up to 8 h until OD_{600} of 5.9 could be measured until the cells reached early stationary phase. Afterwards, the OD_{600} dropped at 2.7 until 28 h of measurement and increased afterwards to an OD_{600} of 22.0 after 48 h

(Figure 35 and Appendix Table 11). For 168-Δ*skfA::erm*, a continuous growth for up to 8 h until OD_{600} of 5.8 could be measured until the cells reached early stationary phase. Then, the OD_{600} stagnated at 5.7 until 26 h of measurement, slightly decreased afterwards to an OD_{600} of 4.6 after 32 h, but increased to an OD_{600} of 14.0 after 48 h (Figure 35 and Appendix Table 11). For 168-Δ*sdpC::erm*, a continuous growth for up to 8 h until OD_{600} of 5.6 could be measured until the cells reached early stationary phase. Then, the OD_{600} stagnated at 5.6 until 28 h of measurement and slightly decreased afterwards to an OD_{600} of 3.0 after 48 h, which might indicate cell lysis (Figure 35 and Appendix Table 11). For 168-Δ*sdpC*Δ*skfA::erm*, a continuous growth for up to 24 h until OD_{600} of 6.0 could be measured until the cells reached stationary phase. Then, the OD_{600} stagnated at around 6.0 until 48 h of measurement (Figure 35 and Appendix Table 11).

Due to the continuous growth and lack of cell lysis of the strain 168-Δ*lytABC::neo*Δ*lytD::tet*Δ*lytE::cm*Δ*lytF::spec*, the autolysins LytA, LytB, LytC, LytD, LytE, and LytF seem to play an important role in cannibalism. Additionally, SKF seems to influence cell lysis since 168-Δ*skfA::erm* showed continuous growth and lack of cell lysis, in contrast to SDP. Furthermore, a double mutant of the two toxins was shown to behave like the autolysin mutant. This indicates the importance of both processes, toxin release and autolysis, in cannibalism in *B. subtilis*.

4 Discussion

In this study, I identified and characterized the first known exo-*N*-acetylmuramidase (YbbC; renamed NamZ*)* and elucidated its role in the degradation of peptidoglycan fragments into single sugars, which may serve as carbon sources during nutrient limitation, such as cannibalistic growth (Müller *et al.* 2021). I further generated a cell wall labeling strain (*B. subtilis* 168-Δ*murQ*Δ*nagA*_pGP888-PAM) that is unable to catabolize peptidoglycan fragments via glycolysis and instead, directly shuttles these compounds into PGN synthesis via the anabolic recycling route of *Pseudomonas putida*, heterologously expressed from the responsible genes on a plasmid. This strain can now be used as a tool for studying cross-feeding of cell wall fragments in mixed cell populations. Additionally, I generated different autolysin mutants to study the role of those autolysins in cannibalism.

4.1 A unique exo-lytic *N*-acetylmuramidase is involved in peptidoglycan salvage in *B. subtilis*

The ability of *B. subtilis* to take up and utilize fragments of its own cell wall has previously been shown in our group (Borisova *et al.* 2016). In this process the peptidoglycan is degraded into single cell wall sugars *N*-acetylmuramic acid (MurNAc) and *N*-acetylglucosamine (GlcNAc), which are taken up and concomitantly are phosphorylated via the PTS-transporters MurP and NagP, respectively. MurNAc-6P serves as a substrate for the etherase MurQ which converts MurNAc-6P to GlcNAc-6P. Latter can be further metabolized and channeled either into glycolysis or peptidoglycan biosynthesis. The autolysins activated during cannibalism do not hydrolyze the peptidoglycan into single cell wall sugars. Therefore, *B. subtilis* must secret enzymes that allow to further degrade the cell wall fragments. In the recycling operon of *B. subtilis* the PTS-transporter MurP, the *N*-acetylmuramic acid-6-phosphate etherase MurQ and the regulator MurR are encoded together with the exo-*N*-acetyl-glucosaminidase NagZ and the *N*-acetylmuramyl-L-alanine amidase AmiE (Litzinger *et al.* 2010, Borisova *et al.* 2016). Additionally, the gene *ybbC* (renamed *namZ*), with previously unknown function is encoded in the operon, which supposably plays a role in degrading peptidoglycan fragments into single cell wall sugars.

In this study, *namZ* was identified as the gene encoding an exo-lytic *N*-acetyl-muramidase. This enzymatic entity had been described earlier by Del Rio and

colleagues, but the encoding gene remained unknown (Del Rio *et al.* 1973, Del Rio and Berkeley 1976). The mutant Δ*namZ* was grown until stationary phase and the supernatant was analyzed for accumulation products (Müller *et al.* 2021). HPLC-MS analysis of Δ*namZ* was compared to *B. subtilis* 168 wild type and Δ*nagZ* and revealed some minor differences (Figure 17). In summary, for supernatants of wild type and Δ*namZ*, the disaccharide MurNAc-GlcNAc did accumulate in small amounts only, whereas the amount for Δ*namZ* was twice as high in comparison. This is in agreement with the lack of an exo-*N*-acetylmuramidase entity that was characterized earlier by Del Rio and colleagues and supports assumption that *namZ* encodes this enzyme. In general, the low amount of accumulation product could be explained by the fact that *B. subtilis* may be able to take up MurNAc-GlcNAc into the cytoplasm as a disaccharide. A transporter with this function has been characterized for *S. aureus* (Kluj *et al.* 2018) and there is evidence that the transporter MurP of *B. subtilis* has a similar specificity (unpublished results). Furthermore, the trisaccharide MurNAc-GlcNAc-anhMurNAc accumulated in the supernatants of wild type, *ΔnamZ* and *ΔnagZ*, and the amounts differed significantly. The highest amounts were shown for *ΔnamZ*, further supporting its function as an exo-*N*-acetylmuramidase. For the wild type, only about half the amount accumulated in comparison to *ΔnamZ*, whereas almost no trisaccharide was found for *ΔnagZ* culture supernatant. In contrast, the disaccharides GlcNAc-anhMurNAc as well as GlcNAc-MurNAc did accumulate in the supernatant of Δ*nagZ* only. The lack of these both disaccharides GlcNAc-anhMurNAc and GlcNAc-MurNAc as accumulation products in the analyzed *ΔnamZ* supernatants could imply that they are used as substrates by NagZ. NamZ would thus be responsible for the generation of NagZ substrates in a manner that remains to be elucidated. Lastly, anhMurNAc accumulated in the supernatant of wild type and *ΔnamZ*, but not in the supernatant of Δ*nagZ*, indicating that anhMurNAc gets released from the reducing end of the peptidoglycan by the action of NagZ (Müller *et al.* 2021). Overall, these results show that NamZ and NagZ are jointly responsible for the cleavage of peptidoglycan. Moreover, the low amounts of accumulation products indicate that longer peptidoglycan fragments are released in the supernatant of cultures, which cannot be analyzed by the methods we used.

For the characterization of NamZ, the enzyme was heterologously expressed without its potential signal sequence, purified with a C-terminal His_6–tag and used on a variety of (chromogenic) substrates. It was shown that pNP-GlcNAc and oNP-Gal did not

serve as substrates, but pNP-MurNAc was specifically cleaved. Furthermore, the disaccharides MurNAc-GlcNAc and GlcNAc-MurNAc were used as potential substrates to investigate whether a terminal MurNAc at the non-reducing end is cleaved by NamZ. Via HPLC-MS analyses it could be shown, that MurNAc-GlcNAc but not GlcNAc-MurNAc did serve as a substrate, so NamZ specifically cleaves MurNAc from the non-reducing end and confirmed the assumption that NamZ is indeed an exo-*N*-acetylmuramidase. This suggests that NamZ is the exo-*N*-acetylmuramidase described by Del Rio.

Del Rio biochemically characterized the enzyme he had discovered, which is why the biochemical characterization of NamZ were also determined by its temperature and pH dependency and its kinetic parameters. It was shown that NamZ is most stable from 4°C to 37°C and at a pH range of 6.0 to 10.0, with a short-term maximal activity at 37°C and pH 6.0 to 8.0. These results are in agreement with Del Rio's characterization, where the exo was shown to be maximally stable and active at a pH of 8.0 (Del Rio and Berkeley 1976). Kinetic studies using pNP-MurNAc resulted in a maximal velocity v_{max} of 1.45 µmol min^{-1} mg^{-1} and a K_M of 0.125 mM, which is comparable to Del Rio's results with 4MU-MurNAc as substrate (v_{max} of 1.5 µmol min^{-1} mg^{-1} and a K_M of 190 µM) (Del Rio and Berkeley 1976). Kinetic studies using MurNAc-GlcNAc resulted in a maximal velocity v_{max} of 88.64 µmol min^{-1} mg^{-1} and a K_M of 3.59 mM. These parameters differ from Del Rio's results with MurNAc-GlcNAc as substrate (v_{max} of 16.29 µmol min^{-1} mg^{-1} and a K_M of 650 µM) (Del Rio and Berkeley 1976), so it seems like NamZ is more active but shows lower affinity to the used substrate. As a first saturation was reached at a MurNAc-GlcNAc concentration of 0.2 mM, kinetic parameters were also determined with substrate concentrations from 0.025 to 0.2 mM, resulting in a maximal velocity v_{max} of 5.99 µmol min^{-1} mg^{-1} and a K_M of 0.22 mM, which is more comparable to Del Rio's results. The reason for this difference remains unclear but could be due to the presence of components co-purified in our or Del Rio's substrate preparation that affect NamZ activity. A similar protocol was used to isolate MurNAc-GlcNAc, involving cleavage of peptidoglycan using the *N*-acetylglucosaminidase Atl^{Glc} from *S. aureus* followed by purification of MurNAc-GlcNAc by HPLC. The preparation varied insofar as we used peptidoglycan from *B. subtilis*, whereas Del Rio used PGN from *Micrococcus luteus* (Del Rio and Berkeley 1976). In addition, we removed the peptide stems from our substrate by using the amidase CwlC from *B. subtilis*, whereas Del Rio did not add any amidase and thus

only the endogenous amidase in the *M. luteus* preparation was present. However, even if our MurNAc-GlcNAc seems to be pure after purification by HPLC, it cannot be excluded that co-purified compounds from the cell wall may have affected the activity of NamZ.

NamZ's function as an exo-*N*-acetylmuramidase was also tested with purified peptidoglycan from *B. subtilis* as the substrate in an assay together with the exo-β-*N*-acetylglucosaminidase NagZ as well as the *N*-acetylmuramyl-L-alanine amidase AmiE from *B. subtilis*. Using HPLC-MS analysis it could be shown that the peptidoglycan is broken down into single cell wall sugars GlcNAc and MurNAc as well as peptides. As the amounts of products were rather small compared to the amount of substrate used, this indicates that PGN degradation is blocked by structural features within the peptidoglycan, such as de-*N*-acetylation. Presumably, the peptidoglycan is cleaved in an assembly of different autolysins (lytic transglycosylases, endo-β-*N*-acetyl-muramidases, and β-N-acetylglucosaminidases), releasing GlcNAc-MurNAc, GlcNAc-anhMurNAc, and MurNAc(-peptide)-GlcNAc as fragments. These can then be cleaved into the individual components of the PGN by NagZ, AmiE, and NamZ (Figure 36). These generated single cell wall sugars might serve as new carbon sources for cannibalistic cells to overcome nutrient limitation and delay sporulation.

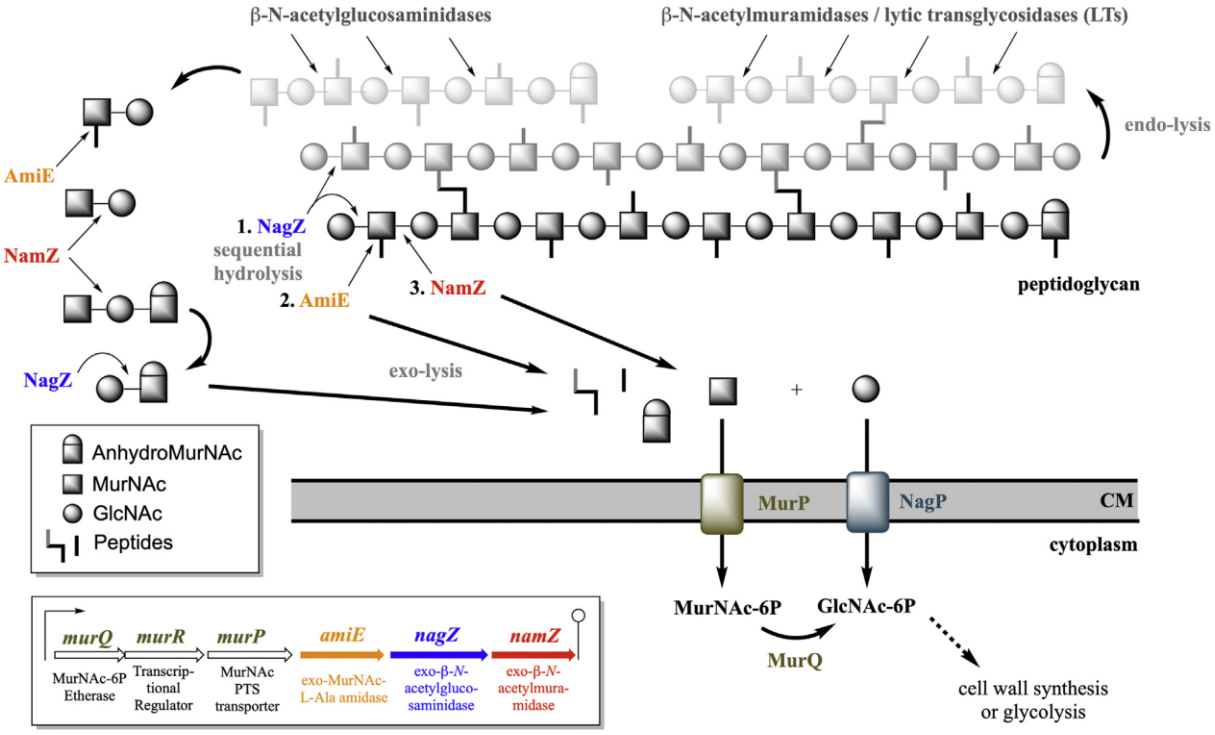

Figure 36 | Schematic of peptidoglycan recycling in *B. subtilis*. The exo-β-*N*-acetylglucosaminidase NagZ, the exo-N-acetylmuramyl-L-alanine amidase AmiE, and the exo-β-*N*-acetylmuramidase NamZ sequentially cleave GlcNAc, peptides, and MurNAc from peptidoglycan chains as well as from peptidoglycan fragments. NagZ cleaves GlcNAc from the non-reducing end, then AmiE cleaves the peptide stem of MurNAc, and then NamZ cleaves MurNAc from the non-reducing end. The peptdioglycan fragments originate from PGN chains by various autolysins, such as lytic transglycosylases, endo-β-*N*-acetylmuramidases, and β-*N*-acetylglucosaminidases. The released cell wall sugars can be taken up by B. subtilis through the MurP and NagP transporters, where they are phosphorylated to give MurNAc-6-P and GlcNAc-6-P. The action of the etherase MurQ converts MurNAc-6-P to GlcNAc-6-P, which can be introduced into either glycolysis or peptidoglycan synthesis. The figure was taken from (Müller *et al.* 2021).

Previously, it was shown by Litzinger *et al.* that NagZ is most active in late stationary phase (Litzinger *et al.* 2010). The published method for determining the time point of enzyme activity was successfully modified for use with a different substrate (pNP-GlcNAc). This modified method can now be used to characterize NamZ regarding the time point of highest activity. In this study, this experiment could not be performed as the substrate pNP-MurNAc was limited and would not have been sufficient for this purpose. Another aim of the modification of the method was the effect of the removal of MurQ, MurR and MurP of the recycling operon. The mutant *B. subtilis* 168-Δ*murQ*Δ*murR*Δ*murP* showed a permanently higher level of NagZ activity than the wild type. This suggests that the deletion of the regulator MurR influences the activity of NagZ and presumably also on the other two enzymes of the operon, AmiE and NamZ. To investigate the potentially increases activity of AmiE and NamZ, this method should

be repeated using substrates of those enzymes, e.g. MurNAc-peptides for AmiE and pNP-MurNAc for NamZ.

The presence of NamZ among different bacterial species was illustrated by constructing a phylogenetic tree (Figure 42 and (Müller *et al.* 2021)). NamZ was shown to be present mainly in the phylum *Bacteriodetes*, but also among Spirochetes, *Bacilli*, *Clostridia*, *Actinobacteria*, and *γ-proteobacteria*. Furthermore, it became clear that the presence of NamZ is related to the presence of the exo-β-*N*-acetylglucosaminidase NagZ, whereas NagZ also occurs alone. Furthermore, NamZ often co-occurs with the etherase MurQ. When MupG (Kluj *et al.* 2018), an exo-lytic 6-phospho-muramidase, is present, NamZ is absent, presumably because both enzymes have a complementary function. In species that exhibit the anabolic recycling route, such as *Pseudomonas*, NamZ is also absent in most cases. An exception to this is *Tannerella forsythia*. For this oral pathogen, it could be shown that it possesses three putative orthologs to NamZ of *B. subtilis* (Borisova *et al.* 2022). Two of those, TfNamZ1 and TfNamZ2, were characterized (Borisova *et al.* 2022) and could be identified as a disaccharide-forming exo-lytic β-*N*-acetylmuramidase (exo-disaccharidase, TfNamZ1), and as sole MurNAc monosaccharide-lytic exo-β-*N*-acetylmuramidase (TfNamZ2).

4.2 Tools for studying cross-feeding of cell wall fragments in mixed cell populations

I created strains and plasmids that can be used as tools to label the peptidoglycan and investigate the cross-feeding of strains in a mixed cell population. To allow peptidoglycan labeling, a strain was constructed that lacks the genes for shuttling peptidoglycan compounds into glycolysis but harboring *Pseudomonas putida* genes that allow their direct conversion to the peptidoglycan precursors UDP-GlcNAc and UDP-MurNAc. If this strain is first grown with labeled precursors MurNAc and GlcNAc, the label is exclusively incorporated in the peptidoglycan. Proof of successful integration can be provided by fluorescence microscopy. To demonstrate cross-feeding and flow of nutrients from one subpopulation to another, a combination of different mutant strains is required. Firstly, prey cells that lack the ability to act against emerging nutrient limitation, e.g. by missing the global regulator Spo0A, must be labeled with peptidoglycan compounds supplemented to the medium. Secondly, these cells are then grown in co-culture with a strain lacking the genes to shuttle peptidoglycan precursors into glycolysis but harboring genes from *Pseudomonas putida*, allowing direct conversion to the peptidoglycan precursors UDP-GlcNAc and UDP-MurNAc. Thereby, the flow of carbons can be shown, and it can be determined which fragments are taken up.

Aiming to show the uptake of recycled peptidoglycan fragments, the cell wall labeling strain 168-Δ*murQ*Δ*nagA*_pGP888-PAM was generated. In a first step, a mutant lacking the *N*-acetylmuramic acid-6-phosphate etherase MurQ and the *N*-acetylglucosamine-6-phosphate deacetylase NagA was generated, resulting in the strain 168-Δ*murQ*Δ*nagA*. By HPLC-MS analysis, it could be shown that MurNAc-6P and GlcNAc-6P accumulate intracellularly in this strain. This was in accordance with expectations, since deletion of the MurQ etherase prevents MurNAc-6P from being converted to GlcNAc-6P by cleavage of the lactate group. Thus, synthesis of new cell wall precursors by recycled MurNAc is no longer possible. Due to the deletion of the *N*-acetylglucosamine-6-phosphate deacetylase NagA, GlcNAc-6P cannot be de-acetylated to GlcN-6P and thus cannot be introduced into glycolysis.

To channel the accumulation products directly into peptidoglycan synthesis, the xylose-inducible plasmid pGP888-PAM was transformed, encoding the genes *mupP* (a *N*-acetylmuramic acid-6-phosphate phosphatase), *amgK* (a *N*-acetylmuramate/

N-acetylglucosamine kinase) and *murU* (a *N*-acetylmuramate α-1-phosphate uridylyl-transferase) of the anabolic cell wall recycling pathway from *Pseudomonas putida* (Gisin *et al.* 2013) into the 168-Δ*murQ*Δ*nagA* mutant resulting in the strain *B. subtilis* 168-Δ*murQ*Δ*nagA*_pGP888-PAM. MupP dephosphorylates MurNAc-6P and GlcNAc-6P, resulting in MurNAc and GlcNAc. AmgK phosphorylates both sugars at their C1 position. The resulting MurNAc α-1P and GlcNAc α-1P can be converted by the uridylyltransferases MurU and GlmU into UDP-MurNAc and UDP-GlcNAc, respectively, which are the precursors of the peptidoglycan (Figure 37).

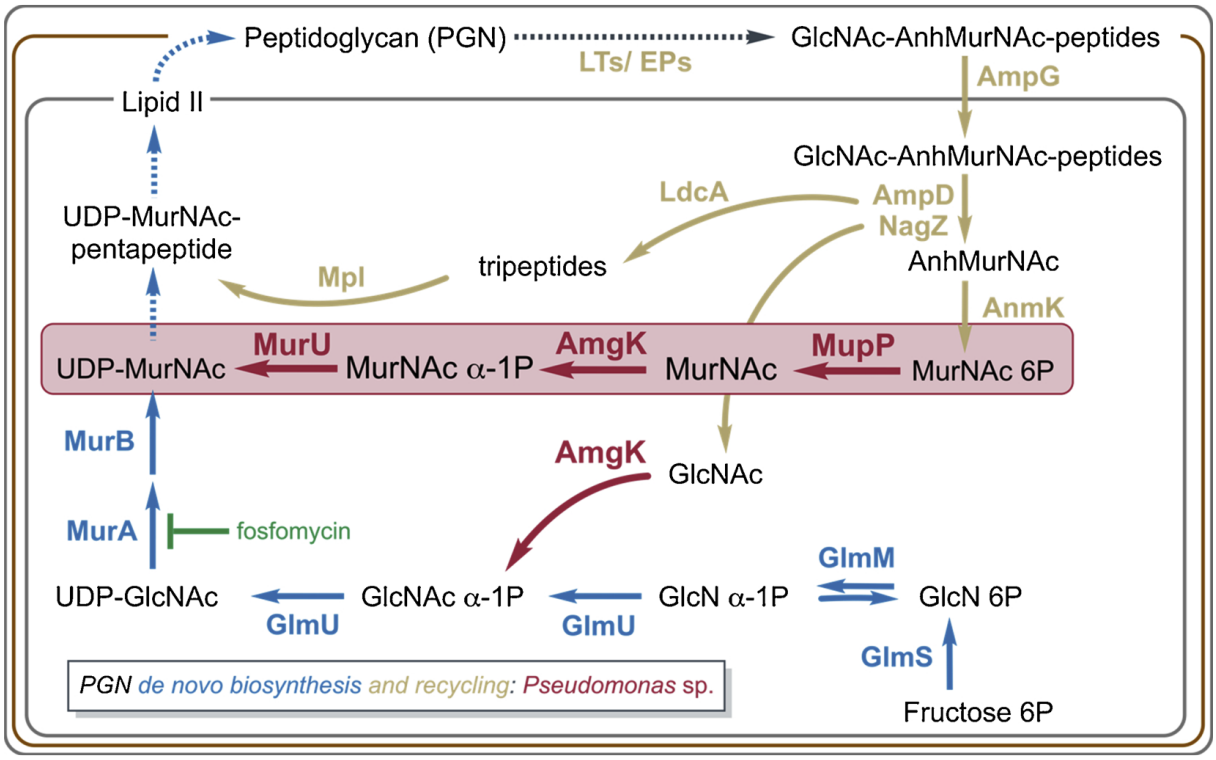

Figure 37 | Peptidoglycan recycling pathway in *Pseudomonas putida*. Lytic transglycosylases (LTs) and endopeptidases (EPs) release anhydromuropeptides (GlcNAc-AnhMurNAc-peptides), which are taken up into the cell by the transporter AmpG. Uptaken anhydromuropeptides are hydrolyzed by the β-*N*-acetylglucosaminidase NagZ, the amidase AmpD, and the carboxypeptidase LdcA to yield GlcNAc, AnhMurNAc, and the tripeptide Ala-Glu-mDAP. The resulting AnhMurNAc is phosphorylated by the kinase AnmK to MurNAc-6P. MurNAc-6P is dephosphorylated to MurNAc by the phosphatase MupP. On the one hand, the kinase AmgK phosphorylates the resulting MurNAc to MurNAc α-1P, which is uridylated by the uridylyltransferase MurU and introduced into the synthesis of cell wall precursors as UDP-MurNAc. Second, AmgK phosphorylates GlcNAc released by hydrolysis, which is also introduced into the synthesis of cell wall precursors. The figure was taken from (Mayer *et al.* 2019).

The strain 168-Δ*murQ*-Δ*nagA*_pGP888-PAM did not accumulate MurNAc-6P and GlcNAc-6P anymore when induced with xylose. Instead, low amounts of accumulating peptidoglycan synthesis intermediates, as MurNAc, the product of MupP activity, MurNAc-1P, the product of AmgK and UDP-MurNAc, the product of MurU could be

measured. Therefore, this strain indeed channels incorporated MurNAc and GlcNAc into peptidoglycan synthesis.

The usefulness of such a cell wall labeling strain has been previously demonstrated by Liang and colleagues (Liang *et al.* 2017). After deletion of the *N*-acetylmuramic acid 6-phosphate etherase MurQ in *E. coli*, they introduced the *P. putida* genes *amgK* and *murU* into the mutant and fluorescently labeled the PGN using “click” chemistry. It was shown that the strategy can be used for both Gram-negative and Gram-positive organisms. Liang and colleagues showed that PGN intermediates accumulated at the septal ring during cell division, providing insight into cell division in *E. coli*.

Feeding 168-Δ*murQ*-Δ*nagA*_pGP888-PAM with fluorescent precursors or radioactive or stable isotopes of MurNAc and GlcNAc would result in a labeled peptidoglycan. By HPLC-MS analysis, the percentage of externally taken up cell wall sugars in the peptidoglycan can be determined. Moreover, the cell wall labeling strain might also be used to show the flow of nutrients during cannibalism from prey to cannibalistic cells. Both cell wall sugars, MurNAc and GlcNAc, could serve as new carbon source for starving cells. By labeling Δ*spo0A* mutants, which serve as prey cells, grown in co-culture with wild type as well as the *B. subtilis* 168-Δ*murQ*-Δ*nagA* strain, the flow of carbons can be shown, and it can be determined which fragments are taken up. In addition, this cell wall labeling strain could be used to investigate whether other cell wall sugars, such as the linker region of WTA, are also taken up into cells and recycled.

4.3 Cannibalism

To investigate which autolysins are involved in cannibalism, different mutants were generated. The focus was on the autolysins LytC, LytD, LytE and LytF, since it had been shown that a quadruple mutant fails to be lysed (Lamsa *et al.* 2012). The double mutants lacking the global regulator *spo0A* as well as one of the major autolysins were generated earlier, resulting in the strains *B. subtilis* 168-Δ*lytC*Δ*spo0A::erm*, 168-Δ*lytD*Δ*spo0A::erm*, 168-Δ*lytE*Δ*spo0A::erm*, and 168-Δ*lytF*Δ*spo0A::erm* (Mühleck 2016). A spot assay was performed where wild type and mutants were compared. It could be shown that LytC, LytD and LytF do play a role in cannibalism but the phenotype could not reproducibly assessed, as in multiple experiments, the results were differed (Mühleck 2016).

Another strategy of investigate the autolysin function was to use fluorescently labeled strains in co-culture. Thus, the decrease of prey cells and the increase of cannibalistic cells could be monitored.

The fluorescence-labeled strains 168-*amyE::cfp* and 168-*amyE::yfp* were used for this purpose (Gunka *et al.* 2013). Fluorescence could be detected using a fluorescence microscope. To generate fluorescently labeled prey cells, the strain 168-*amyE::yfp* was used to generate mutants lacking the global regulator *spo0A*, as well as the autolyisns *lytC* and *lytD* which were replaced by an erythromycin resistance cassette. Replacement of the autolysins *lytE* and *lytF* in the strain 168-*amyE::yfp* with the erythromycin resistance cassette was unsuccessful. A possible reason for this could be the use of too little PCR product in the transformation. Since the same competent cells of 168-*amyE::yfp* were used for transformation as were used to generate the mutants 168-*amyE::yfp*Δ*spo0A::erm*, 168-*amyE::yfp*Δ*lytC::erm*, and 168-*amyE::yfp* Δ*lytD::erm*, a lack of competence of strain 168-*amyE::yfp* to take up the PCR product can be ruled out.

In order to co-culture the strains, continuous measurement of fluorescence during growth is an important factor. Since this is not feasible under the fluorescence microscope, the growth of the strains was studied in a spectrophotometer (Spark 10 M microplate reader, Tecan). However, the fluorescence of 168-*amyE::cfp* and 168-*amyE::yfp*Δ*spo0A::erm* was not measurable.

Therefore, to investigate the autolysin function in the cannibalistic growth of *B. subtilis* 168, the preparation of the fluorescently labeled autolysin mutants should

be successfully implemented. Furthermore, the double mutants 168-Δ*lytC*Δ*spo0A::erm*, 168-Δ*lytD*Δ*spo0A::erm*, 168-Δ*lytE*Δ*spo0A::erm*, and 168-Δ*lytF*Δ*spo0A::erm* should be marked fluorescently using the PCR product *amyE::yfp* and examined in a co-culture with 168-*amyE::cfp*. For this purpose, a strategy for successful fluorescence measurement in the spectrophotometer should be developed. For further experiments, the usage of a minimal medium with less intrinsic fluorescence than LB medium would be a new approach to solve this problem. In addition, measurement of OD_{600} during fluorescence measurement in the spectrophotometer to monitor the growth behavior of the strains would be beneficial.

Hence, which particular autolysins are involved in cannibalism could not be elucidated and the mechanism of how these autolysins are influencing the cannibalism-triggered autolysis remains unknown.

In addition to elucidating the autolysin role, the growth of different cannibalism mutants was observed. The aim was to show cell lysis of prey cells on the one hand and regrowth from cannibals due to released nutrients on the other hand. Therefore, cultures of different *B. subtilis* strains (wild type, 168-Δ*lytABC::neo* Δ*lytD::tet*Δ*lytE::cm*Δ*lytF::spec*, 168-Δ*spo0A::erm*, 168-Δ*skfA::erm*, 168-Δ*sdpC::erm*, and 168-Δ*sdpC*Δ*skfA::erm*) were grown in LB medium and growth was monitored continuously for 48 hours.

For the wild type, the population was expected to become heterogeneous with increasing nutrient deficiency, and that the prey cells became lysed by released toxins SDP and SKF, as well as activated autolysins, which would release nutrients for cannibalistic cells to use them as a food source to survive. Accordingly, a decrease in OD was expected with a subsequent re-increase due to the newly available nutrients. Cell lysis was observed by a decrease in OD after 24 hours, whereas the re-increase in OD could not be measured. The OD continued to decrease until the end of the measurement after 48 hours. For the autolysin mutant 168-Δ*lytABC::neo* Δ*lytD::tet*Δ*lytE::cm*Δ*lytF::spec*, the population was expected to become heterogeneous and to sense nutrient starvation. The cannibalistic cells should release the toxins and attack the prey cells. However, without the activated autolysins, fewer to no cells should lyse, releasing fewer to no nutrients for the cannibalistic cells. Accordingly, growth was expected to stagnate, as no decrease in OD should be monitored due to the absence of cell lysis, and no further growth of the cannibalistic

cells should be monitored due to the continued lack of nutrients. The measurements showed the expected result of stagnated growth after 24 hours. For the strain 168-Δ*spo0A::erm*, which is lacking the global regulator Spo0A, the population was expected not to differentiate into prey and cannibalistic cells because cannibalism genes cannot be activated without Spo0A. Therefore, a stagnation or a decrease in OD was expected after limitation of nutrients. In contrast to expectations, after a decrease in OD after 24 hours, the measurements showed a continuous re-increase in growth until the end of the measurements after 48 hours. For the toxin mutant 168-Δ*skfA::erm*, the population was expected to become heterogeneous and to sense nutrient starvation. The cannibalistic cells should release the toxin SDP even if SKF is missing and attack the prey cells. The presence of SDP should indirectly activate the autolysins leading to prey cell lysis and release of nutrients for the cannibalistic cells. Accordingly, a decrease in OD should be monitored due to cell lysis with a subsequent re-increase due to the newly available nutrients for cannibalistic cells. The measurements showed the expected result of decreased growth after 24 hours and a re-increase of OD until the end of the measurements after 48 hours. For the toxin mutant 168-Δ*sdpC::erm*, the population was also expected to become heterogeneous and to sense nutrient starvation. The cannibalistic cells should release the toxin SKF even if SDP is missing and attack the prey cells. As the presence of SKF alone should kill the prey cells but not activate the autolysins, as SDP most probably is responsible for the collapse of the PMF (Lamsa *et al.* 2012). So, no prey cell lysis and release of nutrients was expected. Accordingly, growth was expected to stagnate, as no decrease in OD should be monitored due to the absence of cell lysis, and no further growth of the cannibalistic cells should be monitored due to the continued lack of nutrients. The measurements showed a slight decrease in OD after 24 hours. For the toxin double mutant 168-Δ*sdpC*Δ*skfA::erm*, the population was expected to become heterogeneous and to sense nutrient starvation. However, as no toxins can be released in this mutant, the cannibalistic cells should not be able to attack the prey cells, leading to no indirect autolysin activation and therefore no cell lysis. The growth was expected to stagnate, as no decrease in OD should be monitored due to the absence of cell lysis, and no further growth of the cannibalistic cells should be monitored due to the continued lack of nutrients. The measurements showed the expected result of stagnated growth after 24 hours.

In summary, these observations strengthened the suspicion that the autolysins LytA, LytB, LytC, LytD, LytE, and LytF play an important role in cannibalism, because a mutant lacking these six autolysins did not show cell lysis. In addition, SKF was shown to influence cell lysis, in contrast to SDP. Furthermore, a double mutant of the two toxins was shown to behave like the autolysin mutant. This indicates the importance of both processes, toxin release and autolysis, in cannibalism in *B. subtilis*. It remains unclear why the wild type and spo0A mutant did not show the expected behavior in growth. For further experiments, the usage of a minimal medium lacking more nutrients from the beginning would be a new approach to solve this question.

The unique exo-*N*-acetylmuramidase enzyme, I identified in this study contributes to a sequential route of peptidoglycan hydrolysis in *B. subtilis*. It may be required by the cannibal cells during cannibalistic growth to feed on lysed cell walls of prey cells, although this study failed to clearly show that salvage actually occurs under these conditions. The obstacle for such experiments is that a flow from prey to cannibal cells must be shown and thus the cell types must be made distinguishable. Such experiments should be possible with the help of the mutant strains I engineered as tools, but which I have not been able to use in experiments myself. It is obvious that bacteria not only have defined strategies to grow under nutrient-rich conditions, but also defined metabolic routes under starvation conditions, and in *B. subtilis* one of these routes is cannibalistic growth. Given the large amounts of cell wall material released during the process of cell lysis in the decay phase and also during bacteriophage-induced lysis, cell wall material is clearly a fortuitous resource for many environmental bacteria.

5 Abbreviations

4MU-GlcNAc	4-methylumbelliferyl *N*-acetyl-β-D-glucosaminide
4MU-MurNAc	4-methylumbelliferyl β-*N*-acetylmuramic acid
Anh	anhydro
AUC	area under curve
BGSC	Bacillus Genetic Stock Center
bp	base pairs
BPC	base peak chromatogram
cps	counts per second
DNA	deoxyribonucleic acid
EIC	extracted ion chromatogram
GlcNAc	*N*-acetylglucosamine
h	hour(s)
HPLC(-MS)	high-performance liquid chromatography (coupled with mass spectrometry)
IPTG	isopropyl β-D-1-thiogalactopyranoside
kDa	kilodalton
LC-MS	liquid chromatography–mass spectrometry
LTA	lipoteichoic acid(s)
M	molar
min	minute(s)
ml	milliliter(s)
mM	millimolar
MurNAc	*N*-acetylmuramic acid
nm	nanometer
OD	optical density
oNP-Gal	oNP-Galactose (ortho-nitrophenyl-β-D-galactopyranoside)
PGN	peptidoglycan
PMF	proton motive force
pNP-GlcNAc	para-nitrophenyl-2-acetamido-2-deoxy-β-D-glucopyranoside
pNP-MurNAc	para-nitrophenyl-2-acetamido-3-O-(D-1-carboxyethyl)-2-deoxy-β-D-glucopyranoside
PTS	phosphotransferase system
rpm	rounds per minute
SDP	sporulation delay protein
SDS PAGE	sodium dodecyl sulfate polyacrylamide gel electrophoresis
SKF	sporulation killing factor
WTA	wall teichoic acid(s)

6 Symbols

°C	degree Celsius
Δ	genetic deletion
ΔΨ	transmembrane difference in electrical potential
ΔpH	difference between the intracellular pH and the extracellular pH
µ	micro
%	percent
α	alpha
β	beta

7 References

Amon, J. D., A. K. Yadav, F. H. Ramirez-Guadiana, A. J. Meeske, F. Cava and D. Z. Rudner (2020). "SwsB and SafA are required for CwlJ-dependent spore germination in *Bacillus subtilis*." J Bacteriol **202**(6).

Atrih, A., G. Bacher, G. Allmaier, M. P. Williamson and S. J. Foster (1999). "Analysis of peptidoglycan structure from vegetative cells of *Bacillus subtilis* 168 and role of PBP 5 in peptidoglycan maturation." J Bacteriol **181**(13): 3956-66.

Atrih, A. and S. J. Foster (1999). "The role of peptidoglycan structure and structural dynamics during endospore dormancy and germination." Antonie Van Leeuwenhoek **75**(4): 299-307.

Bagyan, I. and P. Setlow (2002). "Localization of the cortex lytic enzyme CwlJ in spores of *Bacillus subtilis*." J Bacteriol **184**(4): 1219-24.

Barreteau, H., A. Kovac, A. Boniface, M. Sova, S. Gobec and D. Blanot (2008). "Cytoplasmic steps of peptidoglycan biosynthesis." FEMS Microbiol Rev **32**(2): 168-207.

Barrett, D., T. S. Wang, Y. Yuan, Y. Zhang, D. Kahne and S. Walker (2007). "Analysis of glycan polymers produced by peptidoglycan glycosyltransferases." J Biol Chem **282**(44): 31964-71.

Bhavsar, A. P., L. K. Erdman, J. W. Schertzer and E. D. Brown (2004). "Teichoic acid is an essential polymer in *Bacillus subtilis* that is functionally distinct from teichuronic acid." J Bacteriol **186**(23): 7865-73.

Birnboim, H. C. and J. Doly (1979). "Rapid alkaline extraction procedure for screening recombinant plasmid DNA." Nucl. Acids Res. **7**: 1513-23.

Blackman, S. A., T. J. Smith and S. J. Foster (1998). "The role of autolysins during vegetative growth of *Bacillus subtilis* 168." Microbiology **144 (Pt 1)**: 73-82.

Boland, F. M., A. Atrih, H. Chirakkal, S. J. Foster and A. Moir (2000). "Complete spore-cortex hydrolysis during germination of *Bacillus subtilis* 168 requires SleB and YpeB." Microbiology (Reading) **146 (Pt 1)**: 57-64.

Borisova, M., K. Balbuchta, A. Lovering, A. Titz and C. Mayer (2022). "NamZ1 and NamZ2 from the oral pathogen *Tannerella forsythia* are peptidoglycan processing exo-beta-*N*-acetylmuramidases with distinct substrate specificities." J Bacteriol **204**(3): e0059721.

Borisova, M., R. Gaupp, A. Duckworth, A. Schneider, D. Dalügge, M. Mühleck, D. Deubel, S. Unsleber, W. Yu, G. Muth, M. Bischoff, F. Götz and C. Mayer (2016). "Peptidoglycan recycling in Gram-positive bacteria is crucial for survival in stationary phase." MBio **7**(5).

Bouhss, A., M. Crouvoisier, D. Blanot and D. Mengin-Lecreulx (2004). "Purification and characterization of the bacterial MraY translocase catalyzing the first membrane step of peptidoglycan biosynthesis." J Biol Chem.

Branda, S. S., J. E. Gonzalez-Pastor, S. Ben-Yehuda, R. Losick and R. Kolter (2001). "Fruiting body formation by *Bacillus subtilis*." Proceedings of the National Academy of Sciences of the United States of America **98**(20): 11621-6.

Branda, S. S., S. Vik, L. Friedman and R. Kolter (2005). "Biofilms: the matrix revisited." Trends Microbiol **13**(1): 20-6.

Braun, V. (1975). "Covalent lipoprotein from the outer membrane of *Escherichia coli*." Biochim Biophys Acta **415**(3): 335-77.

Brown, L., J. M. Wolf, R. Prados-Rosales and A. Casadevall (2015). "Through the wall: extracellular vesicles in Gram-positive bacteria, mycobacteria and fungi." Nat Rev Microbiol **13**(10): 620-30.

Brown, S., J. P. Santa Maria, Jr. and S. Walker (2013). "Wall teichoic acids of Gram-positive bacteria." Annu Rev Microbiol **67**: 313-36.

Cairns, L. S., L. Hobley and N. R. Stanley-Wall (2014). "Biofilm formation by *Bacillus subtilis*: new insights into regulatory strategies and assembly mechanisms." Mol Microbiol **93**(4): 587-98.

Calamita, H. G. and R. J. Doyle (2002). "Regulation of autolysins in teichuronic acid-containing *Bacillus subtilis* cells." Mol Microbiol **44**(3): 601-6.

Carballido-Lopez, R. and A. Formstone (2007). "Shape determination in *Bacillus subtilis*." Curr Opin Microbiol **10**(6): 611-6.

Chastanet, A., D. Vitkup, G. C. Yuan, T. M. Norman, J. S. Liu and R. M. Losick (2010). "Broadly heterogeneous activation of the master regulator for sporulation in *Bacillus subtilis*." Proc Natl Acad Sci U S A **107**(18): 8486-91.

Chen, R., S. B. Guttenplan, K. M. Blair and D. B. Kearns (2009). "Role of the sigmaD-dependent autolysins in *Bacillus subtilis* population heterogeneity." J Bacteriol **191**(18): 5775-84.

Cho, H., C. N. Wivagg, M. Kapoor, Z. Barry, P. D. A. Rohs, H. Suh, J. A. Marto, E. C. Garner and T. G. Bernhardt (2016). "Bacterial cell wall biogenesis is mediated by SEDS and PBP polymerase families functioning semi-autonomously." Nat Microbiol **1**: 16172.

Claverys, J. P. and L. S. Havarstein (2007). "Cannibalism and fratricide: mechanisms and raisons d'etre." Nat. Rev. Microbiol. **5**(3): 219-29.

Cleverley, R. M., Z. J. Rutter, J. Rismondo, F. Corona, H. T. Tsui, F. A. Alatawi, R. A. Daniel, S. Halbedel, O. Massidda, M. E. Winkler and R. J. Lewis (2019). "The cell cycle regulator GpsB functions as cytosolic adaptor for multiple cell wall enzymes." Nat Commun **10**(1): 261.

Cloud-Hansen, K. A., S. B. Peterson, E. V. Stabb, W. E. Goldman, M. J. McFall-Ngai and J. Handelsman (2006). "Breaching the great wall: peptidoglycan and microbial interactions." Nat Rev Microbiol **4**(9): 710-6.

Dalügge, D. (2015). Herstellung und Charakterisierung der markerlosen Deletionsmutante Δ*murQ* (Δ*ybbI*) in *Bacillus subtilis*, Master thesis.

De Boer, W. R., F. J. Kruyssen and J. T. Wouters (1981). "Cell wall turnover in batch and chemostat cultures of *Bacillus subtilis*." J. Bacteriol. **145**(1): 50-60.

Del Rio, L. A. and R. C. W. Berkeley (1976). "Exo-beta-*N*-acetylmuramidase - A novel hexosaminidase. Production by *Bacillus subtilis* B, purification and characterization." Eur J Biochem **65**(1): 3-12.

Del Rio, L. A., R. C. W. Berkeley, S. J. Brewer and S. E. Roberts (1973). "An enzyme from *Bacillus Subtilis* B with exo-beta-*N*-acetylmuramidase activity." FEBS Letters **37**(1): 7-9.

Demchick, P. and A. L. Koch (1996). "The permeability of the wall fabric of *Escherichia coli* and *Bacillus subtilis*." J Bacteriol **178**(3): 768-73.

DeWitt, T. and A. D. Grossman (2014). "The bifunctional cell wall hydrolase CwlT is needed for conjugation of the integrative and conjugative element ICEBs1 in *Bacillus subtilis* and *B. anthracis*." J Bacteriol **196**(8): 1588-96.

Diethmaier, C., N. Pietack, K. Gunka, C. Wrede, M. Lehnik-Habrink, C. Herzberg, S. Hubner and J. Stulke (2011). "A novel factor controlling bistability in *Bacillus subtilis*: the YmdB protein affects flagellin expression and biofilm formation." J Bacteriol **193**(21): 5997-6007.

Do, T., J. E. Page and S. Walker (2020). "Uncovering the activities, biological roles, and regulation of bacterial cell wall hydrolases and tailoring enzymes." J Biol Chem, 10.1074/jbc.REV119.010155.

Dobihal, G. S., Y. R. Brunet, J. Flores-Kim and D. Z. Rudner (2019). "Homeostatic control of cell wall hydrolysis by the WalRK two-component signaling pathway in *Bacillus subtilis*." Elife **8**.

Doyle, R. J. and A. L. Koch (1987). "The functions of autolysins in the growth and division of *Bacillus subtilis*." Crit. Rev. Microbiol. **15**(2): 169-222.

Doyle, R. J. and R. E. Marquis (1994). "Elastic, flexible peptidoglycan and bacterial cell wall properties." Trends Microbiol **2**(2): 57-60.

Driks, A. and R. Losick (1991). "Compartmentalized expression of a gene under the control of sporulation transcription factor sigma E in *Bacillus subtilis*." Proc Natl Acad Sci U S A **88**(22): 9934-8.

Duckworth, A. (2016). The *murQ* cell wall recycling operon of *Bacillus subtilis*, Dissertation, University of Tübingen.

Dworkin, J. and R. Losick (2005). "Developmental commitment in a bacterium." Cell **121**(3): 401-9.

Edwards, D. H. and J. Errington (1997). "The *Bacillus subtilis* DivIVA protein targets to the division septum and controls the site specificity of cell division." Mol Microbiol **24**(5): 905-15.

Egan, A. J., R. M. Cleverley, K. Peters, R. J. Lewis and W. Vollmer (2017). "Regulation of bacterial cell wall growth." FEBS J **284**(6): 851-67.

El Zoeiby, A., F. Sanschagrin and R. C. Levesque (2003). "Structure and function of the Mur enzymes: development of novel inhibitors." Mol Microbiol **47**(1): 1-12.

Ellermeier, C. D., E. C. Hobbs, J. E. Gonzalez-Pastor and R. Losick (2006). "A three-protein signaling pathway governing immunity to a bacterial cannibalism toxin." Cell **124**(3): 549-59.

Engelberg-Kulka, H., S. Amitai, I. Kolodkin-Gal and R. Hazan (2006). "Bacterial programmed cell death and multicellular behavior in bacteria." PLoS Genet **2**(10): e135.

Engelbrecht, A. (2016). Characterisation of exo-muramidases of *Bacillus subtilis* and *Tannerella forsythia*, Master thesis.

Fischer, K. E. and E. Bremer (2012). "Activity of the osmotically regulated *yqiHIK* promoter from *Bacillus subtilis* is controlled at a distance." J Bacteriol **194**(19): 5197-208.

Foster, S. J. (1991). "Cloning, expression, sequence analysis and biochemical characterization of an autolytic amidase of *Bacillus subtilis* 168 *trpC2*." J Gen Microbiol **137**(8): 1987-98.

Foster, S. J. (1993). "Analysis of *Bacillus subtilis* 168 prophage-associated lytic enzymes; identification and characterization of CWLA-related prophage proteins." J Gen Microbiol **139**(12): 3177-84.

Foster, S. J. and D. L. Popham (2002). Structure and synthesis of cell wall, spore cortex, teichoic acids, S-layers, and capsules. *Bacillus subtilis* and its closest relatives: From genes to cells. A. L. Sonenshein, J. A. Hoch and R. Losick. Washington, D.C., ASM Press**:** 21-41.

Fujita, M., J. E. Gonzalez-Pastor and R. Losick (2005). "High- and low-threshold genes in the Spo0A regulon of *Bacillus subtilis*." J Bacteriol **187**(4): 1357-68.

Fukushima, T., A. Afkham, S. Kurosawa, T. Tanabe, H. Yamamoto and J. Sekiguchi (2006). "A new D,L-endopeptidase gene product, YojL (renamed CwlS), plays a role in cell separation with LytE and LytF in *Bacillus subtilis*." J Bacteriol **188**(15): 5541-50.

Fukushima, T., T. Kitajima and J. Sekiguchi (2005). "A polysaccharide deacetylase homologue, PdaA, in *Bacillus subtilis* acts as an *N*-acetylmuramic acid deacetylase in vitro." J Bacteriol **187**(4): 1287-92.

Fukushima, T., T. Kitajima, H. Yamaguchi, Q. Ouyang, K. Furuhata, H. Yamamoto, T. Shida and J. Sekiguchi (2008). "Identification and characterization of novel cell wall hydrolase CwlT: a two-domain autolysin exhibiting *N*-acetylmuramidase and DL-endopeptidase activities." J. Biol. Chem. **283**(17): 11117-25.

Fukushima, T., N. Uchida, M. Ide, T. Kodama and J. Sekiguchi (2018). "DL-endopeptidases function as both cell wall hydrolases and poly-gamma-glutamic acid hydrolases." Microbiology (Reading) **164**(3): 277-86.

Fukushima, T., Y. Yao, T. Kitajima, H. Yamamoto and J. Sekiguchi (2007). "Characterization of new L,D-endopeptidase gene product CwlK (previous YcdD) that hydrolyzes peptidoglycan in *Bacillus subtilis*." Mol Genet Genomics **278**(4): 371-83.

Gilmore, M. E., D. Bandyopadhyay, A. M. Dean, S. D. Linnstaedt and D. L. Popham (2004). "Production of muramic delta-lactam in *Bacillus subtilis* spore peptidoglycan." J Bacteriol **186**(1): 80-9.

Gisin, J., A. Schneider, B. Nagele, M. Borisova and C. Mayer (2013). "A cell wall recycling shortcut that bypasses peptidoglycan *de novo* biosynthesis." Nat. Chem. Biol. **9**(8): 491-3.

Glauner, B., J. V. Höltje and U. Schwarz (1988). "The composition of the murein of *Escherichia coli*." J Biol Chem **263**(21): 10088-95.

González-Pastor, J. E. (2011). "Cannibalism: A social behavior in sporulating *Bacillus subtilis*." FEMS Microbiol Rev **35**(3): 415-24.

González-Pastor, J. E., E. C. Hobbs and R. Losick (2003). "Cannibalism by sporulating bacteria." Science **301**(5632): 510-3.

Goodell, E. W. (1985). "Recycling of murein by *Escherichia coli*." J Bacteriol **163**(1): 305-10.

Graham, L. L. and T. J. Beveridge (1994). "Structural differentiation of the *Bacillus subtilis* 168 cell wall." J Bacteriol **176**(5): 1413-21.

Gunka, K., L. Stannek, R. A. Care and F. M. Commichau (2013). "Selection-driven accumulation of suppressor mutants in *Bacillus subtilis*: the apparent high mutation frequency of the cryptic *gudB* gene and the rapid clonal expansion of *gudB(+)* suppressors are due to growth under selection." PLoS One **8**(6): e66120.

Gutierrez, J., R. Smith and K. Pogliano (2010). "SpoIID-mediated peptidoglycan degradation is required throughout engulfment during *Bacillus subtilis* sporulation." J Bacteriol **192**(12): 3174-86.

Hadi, T., U. Dahl, C. Mayer and M. E. Tanner (2008). "Mechanistic studies on *N*-acetylmuramic acid 6-phosphate hydrolase (MurQ): an etherase involved in peptidoglycan recycling." Biochemistry **47**: 11547-58.

Hamon, M. A. and B. A. Lazazzera (2001). "The sporulation transcription factor Spo0A is required for biofilm development in *Bacillus subtilis*." Molecular Microbiology **42**(5): 1199-209.

Hashimoto, M., S. Ooiwa and J. Sekiguchi (2012). "Synthetic lethality of the *lytE cwlO* genotype in *Bacillus subtilis* is caused by lack of D,L-endopeptidase activity at the lateral cell wall." J Bacteriol **194**(4): 796-803.

Hayashi, K. (1975). "A rapid determination of sodium dodecyl sulfate with methylene blue." Anal. Biochem. **67**(2): 503-6.

Hayhurst, E. J., L. Kailas, J. K. Hobbs and S. J. Foster (2008). "Cell wall peptidoglycan architecture in *Bacillus subtilis*." Proc Natl Acad Sci U S A **105**(38): 14603-8.

Höltje, J.-V. and B. Glauner (1990). "Structure and metabolism of the murein sacculus." Res. Microbiol. **141**(1): 75-89.

Höltje, J. V. (1998). "Growth of the stress-bearing and shape-maintaining murein sacculus of *Escherichia coli*." Microbiol Mol Biol Rev **62**(1): 181-203.

Höper, D., U. Völker and M. Hecker (2005). "Comprehensive characterization of the contribution of individual SigB-dependent general stress genes to stress resistance of *Bacillus subtilis*." J Bacteriol **187**(8): 2810-26.

Horsburgh, G. J., A. Atrih and S. J. Foster (2003a). "Characterization of LytH, a differentiation-associated peptidoglycan hydrolase of *Bacillus subtilis* involved in endospore cortex maturation." J Bacteriol **185**(13): 3813-20.

Horsburgh, G. J., A. Atrih, M. P. Williamson and S. J. Foster (2003b). "LytG of *Bacillus subtilis* is a novel peptidoglycan hydrolase: the major active glucosaminidase." Biochemistry **42**(2): 257-64.

Howell, A., S. Dubrac, K. K. Andersen, D. Noone, J. Fert, T. Msadek and K. Devine (2003). "Genes controlled by the essential YycG/YycF two-component system of *Bacillus subtilis* revealed through a novel hybrid regulator approach." Mol Microbiol **49**(6): 1639-55.

Jaeger, T. and C. Mayer (2008). "*N*-acetylmuramic acid 6-phosphate lyases (MurNAc etherases): role in cell wall metabolism, distribution, structure, and mechanism." Cell. Mol. Life Sci. **65**(6): 928-39.

Janes, B. K. and S. Stibitz (2006). "Routine markerless gene replacement in *Bacillus anthracis*." Infect Immun **74**(3): 1949-53.

Johnson, J. W., J. F. Fisher and S. Mobashery (2013). "Bacterial cell-wall recycling." Ann N Y Acad Sci **1277**: 54-75.

Jolliffe, L. K., R. J. Doyle and U. N. Streips (1981). "The energized membrane and cellular autolysis in *Bacillus subtilis*." Cell **25**(3): 753-63.

Kemper, M. A., M. M. Urrutia, T. J. Beveridge, A. L. Koch and R. J. Doyle (1993). "Proton motive force may regulate cell wall-associated enzymes of *Bacillus subtilis*." J Bacteriol **175**(17): 5690-6.

Kim, L., A. Mogk and W. Schumann (1996). "A xylose-inducible *Bacillus subtilis* integration vector and its application." Gene **181**(1-2): 71-6.

Kim, S. J., J. Chang and M. Singh (2014). "Peptidoglycan architecture of Gram-positive bacteria by solid-state NMR." Biochim Biophys Acta, 10.1016/j.bbamem.2014.05.031.

Kluj, R. M., P. Ebner, M. Adamek, N. Ziemert, C. Mayer and M. Borisova (2018). "Recovery of the Peptidoglycan Turnover Product Released by the Autolysin Atl in Staphylococcus aureus Involves the Phosphotransferase System Transporter MurP and the Novel 6-phospho-N-acetylmuramidase MupG." Front Microbiol **9**: 2725.

Kobayashi, K., I. P. Sudiarta, T. Kodama, T. Fukushima, K. Ara, K. Ozaki and J. Sekiguchi (2012). "Identification and characterization of a novel polysaccharide deacetylase C (PdaC) from *Bacillus subtilis*." J Biol Chem.

Koch, A. L. (1986). "The pH in the neighborhood of membranes generating a protonmotive force." J Theor Biol **120**(1): 73-84.

Koch, A. L. and R. J. Doyle (1985). "Inside-to-outside growth and turnover of the wall of Gram-positive rods." J Theor Biol **117**(1): 137-57.

Kodama, T., H. Takamatsu, K. Asai, K. Kobayashi, N. Ogasawara and K. Watabe (1999). "The *Bacillus subtilis yaaH* gene is transcribed by SigE RNA polymerase during sporulation, and its product is involved in germination of spores." J Bacteriol **181**(15): 4584-91.

Kodama, T., H. Takamatsu, K. Asai, N. Ogasawara, Y. Sadaie and K. Watabe (2000). "Synthesis and characterization of the spore proteins of *Bacillus subtilis* YdhD, YkuD, and YkvP, which carry a motif conserved among cell wall binding proteins." J Biochem **128**(4): 655-63.

Kraigsley, A. M. and S. E. Finkel (2009). "Adaptive evolution in single species bacterial biofilms." FEMS Microbiol Lett **293**(1): 135-40.

Krulwich, T. A., G. Sachs and E. Padan (2011). "Molecular aspects of bacterial pH sensing and homeostasis." Nature Reviews Microbiology **9**(5): 330-43.

Kuroda, A., Y. Asami and J. Sekiguchi (1993). "Molecular cloning of a sporulation-specific cell wall hydrolase gene of *Bacillus subtilis*." J Bacteriol **175**(19): 6260-8.

Kuroda, A., M. Imazeki and J. Sekiguchi (1991). "Purification and characterization of a cell wall hydrolase encoded by the *cwlA* gene of *Bacillus subtilis*." FEMS Microbiol Lett **65**(1): 9-13.

Laemmli, U. K. (1970). "Cleavage of structural proteins during the assembly of the head of bacteriophage T4." Nature **227**: 680-5.

Lamsa, A., W. T. Liu, P. C. Dorrestein and K. Pogliano (2012). "The *Bacillus subtilis* cannibalism toxin SDP collapses the proton motive force and induces autolysis." Mol Microbiol **84**(3): 486-500.

Lazarevic, V., P. Margot, B. Soldo and D. Karamata (1992). "Sequencing and analysis of the *Bacillus subtilis lytRABC* divergon: a regulatory unit encompassing the structural genes of the *N*-acetylmuramoyl-L-alanine amidase and its modifier." J Gen Microbiol **138**(9): 1949-61.

Lewis, K. (2000). "Programmed death in bacteria." Microbiol Mol Biol Rev **64**(3): 503-14.

Liang, H., K. E. DeMeester, C. W. Hou, M. A. Parent, J. L. Caplan and C. L. Grimes (2017). "Metabolic labelling of the carbohydrate core in bacterial peptidoglycan and its applications." Nat Commun **8**: 15015.

Litzinger, S., A. Duckworth, K. Nitzsche, C. Risinger, V. Wittmann and C. Mayer (2010). "Muropeptide rescue in *Bacillus subtilis* involves sequential hydrolysis by beta-*N*-acetylglucosaminidase and *N*-acetylmuramyl-L-alanine amidase." J Bacteriol **192**(12): 3132-43.

Liu, W. T., Y. L. Yang, Y. Xu, A. Lamsa, N. M. Haste, J. Y. Yang, J. Ng, D. Gonzalez, C. D. Ellermeier, P. D. Straight, P. A. Pevzner, J. Pogliano, V. Nizet, K. Pogliano and P. C. Dorrestein (2010). "Imaging mass spectrometry of intraspecies metabolic exchange revealed the cannibalistic factors of Bacillus subtilis." Proc Natl Acad Sci U S A **107**(37): 16286-90.

Longchamp, P. F., C. Mauel and D. Karamata (1994). "Lytic enzymes associated with defective prophages of *Bacillus subtilis*: sequencing and characterization of the region comprising the *N*-acetylmuramoyl-L-alanine amidase gene of prophage PBSX." Microbiology (Reading) **140 (Pt 8)**: 1855-67.

López, D., H. Vlamakis, R. Losick and R. Kolter (2009). "Cannibalism enhances biofilm development in *Bacillus subtilis*." Mol Microbiol **74**(3): 609-18.

Margot, P. and D. Karamata (1992). "Identification of the structural genes for *N*-acetylmuramoyl-L-alanine amidase and its modifier in *Bacillus subtilis* 168: inactivation of these genes by insertional mutagenesis has no effect on growth or cell separation." Mol Gen Genet **232**(3): 359-66.

Margot, P., C. Mauel and D. Karamata (1994). "The gene of the *N*-acetylglucosaminidase, a *Bacillus subtilis* 168 cell wall hydrolase not involved in vegetative cell autolysis." Mol. Microbiol. **12**(4): 535-45.

Margot, P., M. Pagni and D. Karamata (1999). "*Bacillus subtilis* 168 gene *lytF* encodes a gamma-D-glutamate-meso-diaminopimelate muropeptidase expressed by the alternative vegetative sigma factor, sigmaD." Microbiology (Reading) **145 (Pt 1)**: 57-65.

Margot, P., M. Wahlen, A. Gholamhoseinian, P. Piggot and D. Karamata (1998). "The *lytE* gene of *Bacillus subtilis* 168 encodes a cell wall hydrolase." J Bacteriol **180**(3): 749-52.

Mauck, J., L. Chan and L. Glaser (1971). "Turnover of the cell wall of Gram-positive bacteria." J Biol Chem **246**(6): 1820-17.

Mauck, J. and L. Glaser (1970). "Turnover of the cell wall of *Bacillus subtilis* W-23 during logarithmic growth." Biochem Biophys Res Commun **39**(4): 699-706.

Mayer, C. (2012) "Bacterial cell wall recycling." eLS, doi: 10.1002/9780470015902.a0021974.

Mayer, C., R. M. Kluj, M. Mühleck, A. Walter, S. Unsleber, I. Hottmann and M. Borisova (2019). "Bacteria's different ways to recycle their own cell wall." Int J Med Microbiol, 10.1016/j.ijmm.2019.06.006: 151326.

McGivney, E., L. C. Han, A. Avellan, J. VanBriesen and K. B. Gregory (2017). "Disruption of autolysis in *Bacillus subtilis* using TiO_2 nanoparticles." Scientific Reports **7**.

McKenney, P. T. and P. Eichenberger (2012). "Dynamics of spore coat morphogenesis in *Bacillus subtilis*." Mol Microbiol **83**(2): 245-60.

Meeske, A. J., E. P. Riley, W. P. Robins, T. Uehara, J. J. Mekalanos, D. Kahne, S. Walker, A. C. Kruse, T. G. Bernhardt and D. Z. Rudner (2016). "SEDS proteins are a widespread family of bacterial cell wall polymerases." Nature **537**(7622): 634-8.

Mengin-Lecreulx, D., L. Texier, M. Rousseau and J. van Heijenoort (1991). "The *murG* gene of *Escherichia coli* codes for the UDP-*N*-acetylglucosamine: *N*-acetylmuramyl-(pentapeptide) pyrophosphoryl-undecaprenol *N*-acetylglucosamine transferase involved in the membrane steps of peptidoglycan synthesis." J Bacteriol **173**(15): 4625-36.

Molle, V., M. Fujita, S. T. Jensen, P. Eichenberger, J. E. González-Pastor, J. S. Liu and R. Losick (2003). "The Spo0A regulon of *Bacillus subtilis*." Molecular Microbiology **50**(5): 1683-701.

Moriyama, R., A. Hattori, S. Miyata, S. Kudoh and S. Makino (1996). "A gene (*sleB*) encoding a spore cortex-lytic enzyme from *Bacillus subtilis* and response of the enzyme to L-alanine-mediated germination." J Bacteriol **178**(20): 6059-63.

Morlot, C., T. Uehara, K. A. Marquis, T. G. Bernhardt and D. Z. Rudner (2010). "A highly coordinated cell wall degradation machine governs spore morphogenesis in *Bacillus subtilis*." Genes Dev **24**(4): 411-22.

Mühleck, M. (2016). Konstruktion von Mutanten zur Untersuchung des Kannibalismus in *Bacillus subtilis* 168, Master thesis.

Müller, M., M. Calvert, I. Hottmann, R. M. Kluj, T. Teufel, K. Balbuchta, A. Engelbrecht, K. A. Selim, Q. Xu, M. Borisova, A. Titz and C. Mayer (2021). "The exo-beta-*N*-acetylmuramidase NamZ from *Bacillus subtilis* is the founding member of a family of exo-lytic peptidoglycan hexosaminidases." J Biol Chem **296**: 100519.

Nakano, M. M., M. A. Marahiel and P. Zuber (1988). "Identification of a genetic locus required for biosynthesis of the lipopeptide antibiotic surfactin in *Bacillus subtilis*." J Bacteriol **170**(12): 5662-8.

Nandy, S. K., P. M. Bapat and K. V. Venkatesh (2007). "Sporulating bacteria prefers predation to cannibalism in mixed cultures." FEBS Lett. **581**(1): 151-6.

Neuhaus, F. C. and J. Baddiley (2003). "A continuum of anionic charge: structures and functions of D-alanyl-teichoic acids in Gram-positive bacteria." Microbiol Mol Biol Rev **67**(4): 686-723.

Nugroho, F. A., H. Yamamoto, Y. Kobayashi and J. Sekiguchi (1999). "Characterization of a new sigma-K-dependent peptidoglycan hydrolase gene that plays a role in *Bacillus subtilis* mother cell lysis." J Bacteriol **181**(20): 6230-7.

Paredes-Sabja, D., P. Setlow and M. R. Sarker (2011). "Germination of spores of *Bacillales* and *Clostridiales* species: mechanisms and proteins involved." Trends Microbiol **19**(2): 85-94.

Park, J. T. and T. Uehara (2008). "How bacteria consume their own exoskeletons (turnover and recycling of cell wall peptidoglycan)." Microbiol Mol Biol Rev **72**(2): 211-27.

Pasquina-Lemonche, L., J. Burns, R. D. Turner, S. Kumar, R. Tank, N. Mullin, J. S. Wilson, B. Chakrabarti, P. A. Bullough, S. J. Foster and J. K. Hobbs (2020). "The architecture of the Gram-positive bacterial cell wall." Nature **582**(7811): 294-7.

Perego, M. (1993). Integrational Vectors for genetic manipulation in *Bacillus subtilis*. Bacillus subtilis and Other Gram-Positive Bacteria. J. A. H. a. R. L. A.L. Sonenshein, 10.1128/9781555818388.ch42**:** 615-24.

Pérez Morales, T. G., T. D. Ho, W.-T. Liu, P. C. Dorrestein and C. D. Ellermeier (2013). "Production of the cannibalism toxin SDP is a multistep process that requires SdpA and SdpB." Journal of bacteriology **195**(14): 3244-51.

Piggot, P. J. and D. W. Hilbert (2004). "Sporulation of *Bacillus subtilis*." Current opinion in microbiology **7**(6): 579-86.

Popham, D. L. and P. Setlow (1993). "Cloning, nucleotide sequence, and regulation of the *Bacillus subtilis pbpE* operon, which codes for penicillin-binding protein 4* and an apparent amino acid racemase." J Bacteriol **175**(10): 2917-25.

Priest, F. G. (1993). Systematics and ecology of *Bacillus*. *Bacillus subtilis* and other Gram-positive bacteria: biochemistry, physiology, and molecular genetics. A. L. Sonenshein, J. A. Hoch and R. Losick. Washington, D.C., American Society for Microbiology**:** 3-17.

Psylinakis, E., I. G. Boneca, K. Mavromatis, A. Deli, E. Hayhurst, S. J. Foster, K. M. Varum and V. Bouriotis (2005). "Peptidoglycan *N*-acetylglucosamine deacetylases from *Bacillus cereus*, highly conserved proteins in *Bacillus anthracis*." J Biol Chem **280**(35): 30856-63.

Rashid, M. H., M. Mori and J. Sekiguchi (1995). "Glucosaminidase of *Bacillus subtilis*: cloning, regulation, primary structure and biochemical characterization." Microbiology **141 (Pt 10)**: 2391-404.

Regamey, A. and D. Karamata (1998). "The *N*-acetylmuramoyl-L-alanine amidase encoded by the *Bacillus subtilis* 168 prophage SP beta." Microbiology (Reading) **144 (Pt 4)**: 885-93.

Reith, J. and C. Mayer (2011). "Peptidoglycan turnover and recycling in Gram-positive bacteria." Appl Microbiol Biotechnol **92**(1): 1-11.

Rice, K. C. and K. W. Bayles (2008). "Molecular control of bacterial death and lysis." Microbiol Mol Biol Rev **72**(1): 85-109, table of contents.

Rodrigues, C. D., K. A. Marquis, J. Meisner and D. Z. Rudner (2013). "Peptidoglycan hydrolysis is required for assembly and activity of the transenvelope secretion complex during sporulation in *Bacillus subtilis*." Mol Microbiol **89**(6): 1039-52.

Rogers, H. J. (1974). "Peptidoglycans (mucopeptides): structure, function, and variations." Ann N Y Acad Sci **235**(0): 29-51.

Salzberg, L. I., L. Powell, K. Hokamp, E. Botella, D. Noone and K. M. Devine (2013). "The WalRK (YycFG) and sigma(I) RsgI regulators cooperate to control CwlO and LytE expression in exponentially growing and stressed *Bacillus subtilis* cells." Mol Microbiol **87**(1): 180-95.

Sanchez, S., C. M. Dunn and D. B. Kearns (2021). "CwlQ is required for swarming motility but not flagellar assembly in *Bacillus subtilis*." J Bacteriol **203**(10).

Schaub, R. E. and J. P. Dillard (2017). "Digestion of peptidoglycan and analysis of soluble fragments." Bio-Protocol **7**(15).

Scheffers, D. J., L. J. Jones and J. Errington (2004). "Several distinct localization patterns for penicillin-binding proteins in *Bacillus subtilis*." Mol Microbiol **51**(3): 749-64.

Scheurwater, E., C. W. Reid and A. J. Clarke (2008). "Lytic transglycosylases: bacterial space-making autolysins." Int J Biochem Cell Biol **40**(4): 586-91.

Schleifer, K. H. and O. Kandler (1972). "Peptidoglycan types of bacterial cell walls and their taxonomic implications." Bacteriol Rev **36**(4): 407-777.

Schönert, S. (2004). Maltose-und Maltodextrin-Verwertung in *Bacillus subtilis*. Dissertation, University of Konstanz.

Schumacher, M. A., J. Lee and W. Zeng (2016). "Molecular insights into DNA binding and anchoring by the *Bacillus subtilis* sporulation kinetochore-like RacA protein." Nucleic Acids Res **44**(11): 5438-49.

Sekiguchi, J., K. Akeo, H. Yamamoto, F. K. Khasanov, J. C. Alonso and A. Kuroda (1995). "Nucleotide sequence and regulation of a new putative cell wall hydrolase gene, *cwlD*, which affects germination in *Bacillus subtilis*." J Bacteriol **177**(19): 5582-9.

Shank, E. A., V. Klepac-Ceraj, L. Collado-Torres, G. E. Powers, R. Losick and R. Kolter (2011). "Interspecies interactions that result in *Bacillus subtilis* forming biofilms are mediated mainly by members of its own genus." Proc Natl Acad Sci U S A **108**(48): E1236-43.

Shida, T., H. Hattori, F. Ise and J. Sekiguchi (2000). "Overexpression, purification, and characterization of *Bacillus subtilis N*-acetylmuramoyl-L-alanine amidase CwlC." Biosci Biotechnol Biochem **64**(7): 1522-5.

Silhavy, T. J., D. Kahne and S. Walker (2010). "The bacterial cell envelope." Cold Spring Harb Perspect Biol **2**(5): a000414.

Smith, T. J., S. A. Blackman and S. J. Foster (1996). "Peptidoglycan hydrolases of *Bacillus subtilis* 168." Microb Drug Resist **2**(1): 113-8.

Smith, T. J., S. A. Blackman and S. J. Foster (2000). "Autolysins of *Bacillus subtilis*: multiple enzymes with multiple functions." Microbiology **146 (Pt 2)**: 249-62.

Smith, T. J. and S. J. Foster (1995). "Characterization of the involvement of two compensatory autolysins in mother cell lysis during sporulation of *Bacillus subtilis* 168." J Bacteriol **177**(13): 3855-62.

Sudiarta, I. P., T. Fukushima and J. Sekiguchi (2010a). "*Bacillus subtilis* CwlP of the SP-{beta} prophage has two novel peptidoglycan hydrolase domains, muramidase and cross-linkage digesting DD-endopeptidase." J Biol Chem **285**(53): 41232-43.

Sudiarta, I. P., T. Fukushima and J. Sekiguchi (2010b). "*Bacillus subtilis* CwlQ (previous YjbJ) is a bifunctional enzyme exhibiting muramidase and soluble-lytic transglycosylase activities." Biochem Biophys Res Commun **398**(3): 606-12.

Suzuki, T. and Y. Tahara (2003). "Characterization of the *Bacillus subtilis ywtD* gene, whose product is involved in gamma-polyglutamic acid degradation." J Bacteriol **185**(7): 2379-82.

Tan, I. S. and K. S. Ramamurthi (2014). "Spore formation in *Bacillus subtilis*." Environ Microbiol Rep **6**(3): 212-25.

Teufel, T. (2019). Aufreinigung von Zellwandfragmenten zur Analyse des Peptidoglykanrecyclings bei Bakterien, Master thesis.

Uehara, T. and J. T. Park (2008). Peptidoglycan recycling. EcoSal-*Eschericia coli* and *Salmonella*: Cellular and Molecular Biology. Washington, D.C., ASM Press, EcoSal Plus 2013; doi:10.1128/ecosalplus.4.7.1.5.

van Heijenoort, J. (2001). "Formation of the glycan chains in the synthesis of bacterial peptidoglycan." Glycobiology **11**(3): 25R-36R.

Vermassen, A., S. Leroy, R. Talon, C. Provot, M. Popowska and M. Desvaux (2019). "Cell wall hydrolases in bacteria: Insight on the diversity of cell wall amidases, glycosidases and peptidases toward peptidoglycan." Front Microbiol **10**: 331.

Visweswaran, G. R., K. Leenhouts, M. van Roosmalen, J. Kok and G. Buist (2014). "Exploiting the peptidoglycan-binding motif, LysM, for medical and industrial applications." Appl Microbiol Biotechnol **98**(10): 4331-45.

Vollmer, W. and U. Bertsche (2008). "Murein (peptidoglycan) structure, architecture and biosynthesis in *Escherichia coli*." Biochim Biophys Acta **1778**(9): 1714-34.

Vollmer, W., D. Blanot and M. A. de Pedro (2008a). "Peptidoglycan structure and architecture." FEMS Microbiol Rev **32**(2): 149-67.

Vollmer, W., B. Joris, P. Charlier and S. Foster (2008b). "Bacterial peptidoglycan (murein) hydrolases." FEMS Microbiol Rev **32**(2): 259-86.

Walter, A. and C. Mayer (2019). Peptidoglycan Structure, Biosynthesis, and Dynamics During Bacterial Growth. Extracellular Sugar-Based Biopolymers Matrices. E. Cohen and H. Merzendorfer. Cham, Springer International Publishing, 10.1007/978-3-030-12919-4_6**:** 237-99.

Warth, A. D. and J. L. Strominger (1971). "Structure of the peptidoglycan from vegetative cell walls of Bacillus subtilis." Biochemistry **10**(24): 4349-58.

Wheeler, R., R. D. Turner, R. G. Bailey, B. Salamaga, S. Mesnage, S. A. Mohamad, E. J. Hayhurst, M. Horsburgh, J. K. Hobbs and S. J. Foster (2015). "Bacterial Cell Enlargement Requires Control of Cell Wall Stiffness Mediated by Peptidoglycan Hydrolases." MBio **6**(4): e00660.

Yamaguchi, H., K. Furuhata, T. Fukushima, H. Yamamoto and J. Sekiguchi (2004). "Characterization of a new Bacillus subtilis peptidoglycan hydrolase gene, yvcE (named cwlO), and the enzymatic properties of its encoded protein." J Biosci Bioeng **98**(3): 174-81.

Yamamoto, H., S. Kurosawa and J. Sekiguchi (2003). "Localization of the vegetative cell wall hydrolases LytC, LytE, and LytF on the Bacillus subtilis cell surface and stability of these enzymes to cell wall-bound or extracellular proteases." J Bacteriol **185**(22): 6666-77.

Zheng, L., W. Abhyankar, N. Ouwerling, H. L. Dekker, H. van Veen, N. N. van der Wel, W. Roseboom, L. J. de Koning, S. Brul and C. G. de Koster (2016). "Bacillus subtilis Spore Inner Membrane Proteome." J Proteome Res **15**(2): 585-94.

8 Appendix

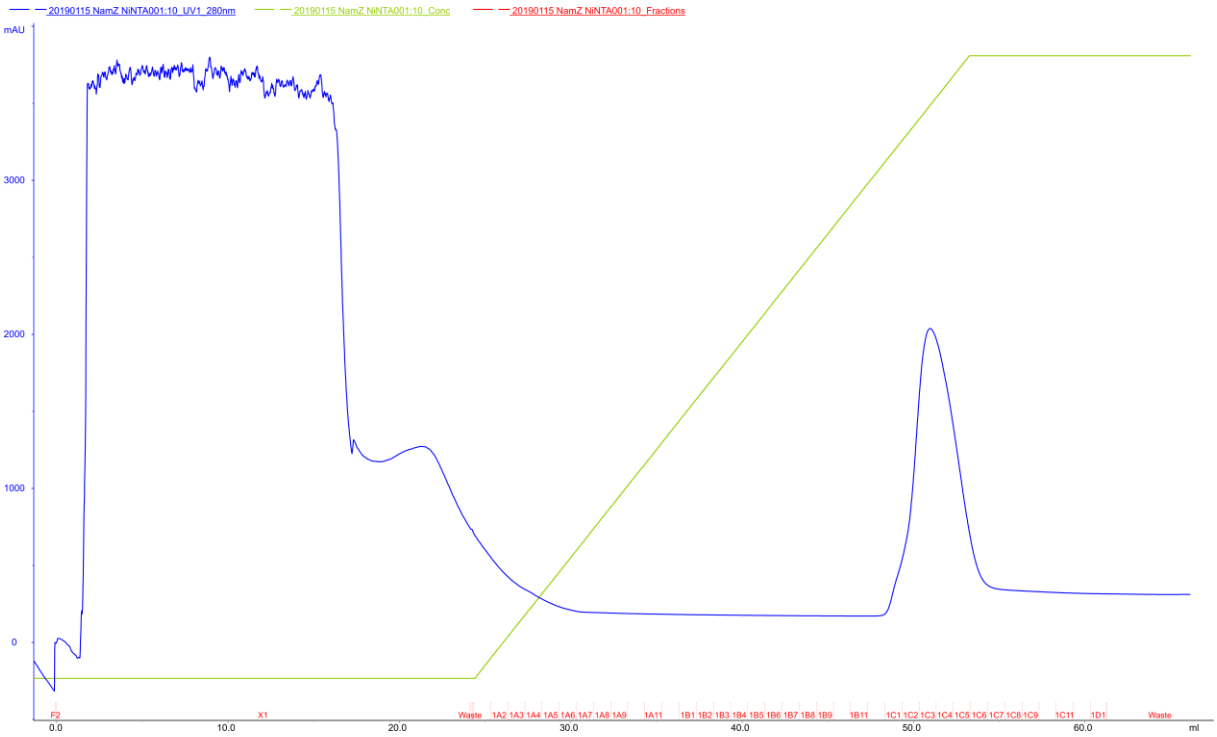

Figure 38 | Elution profile of Ni^{2+}-chromatography of NamZ

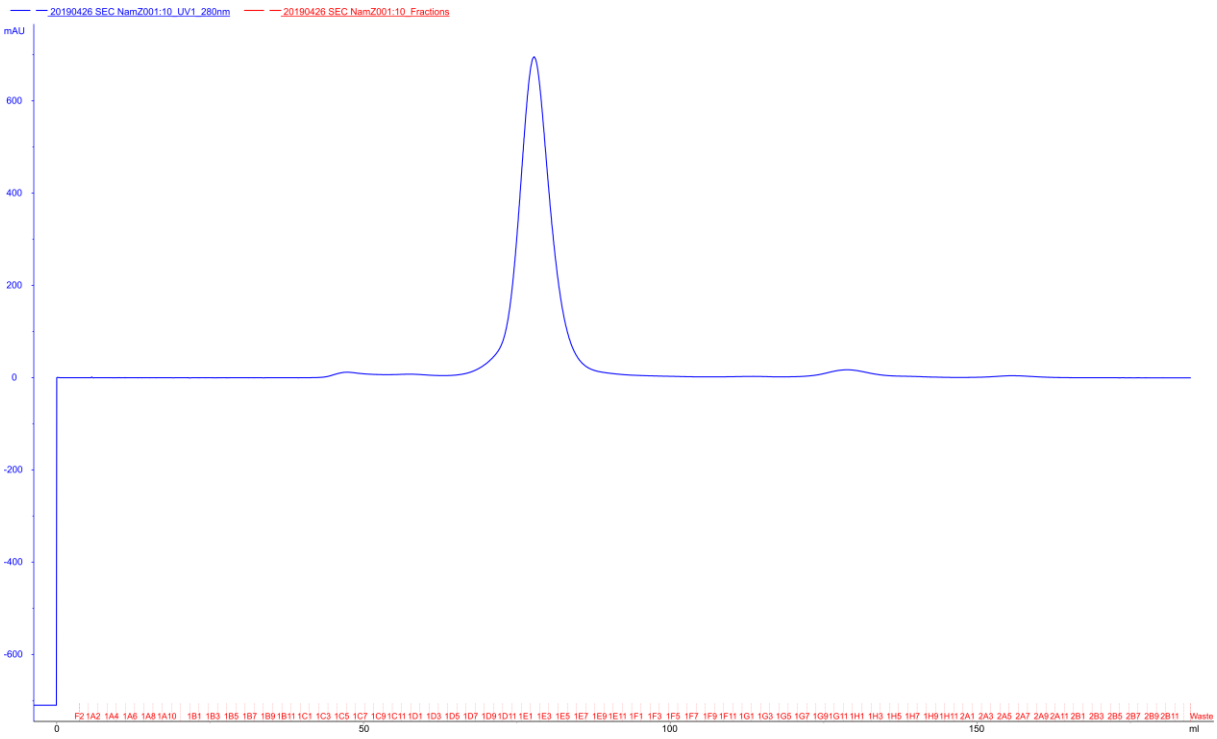

Figure 39 | Elution profile of size exclusion chromatography of NamZ

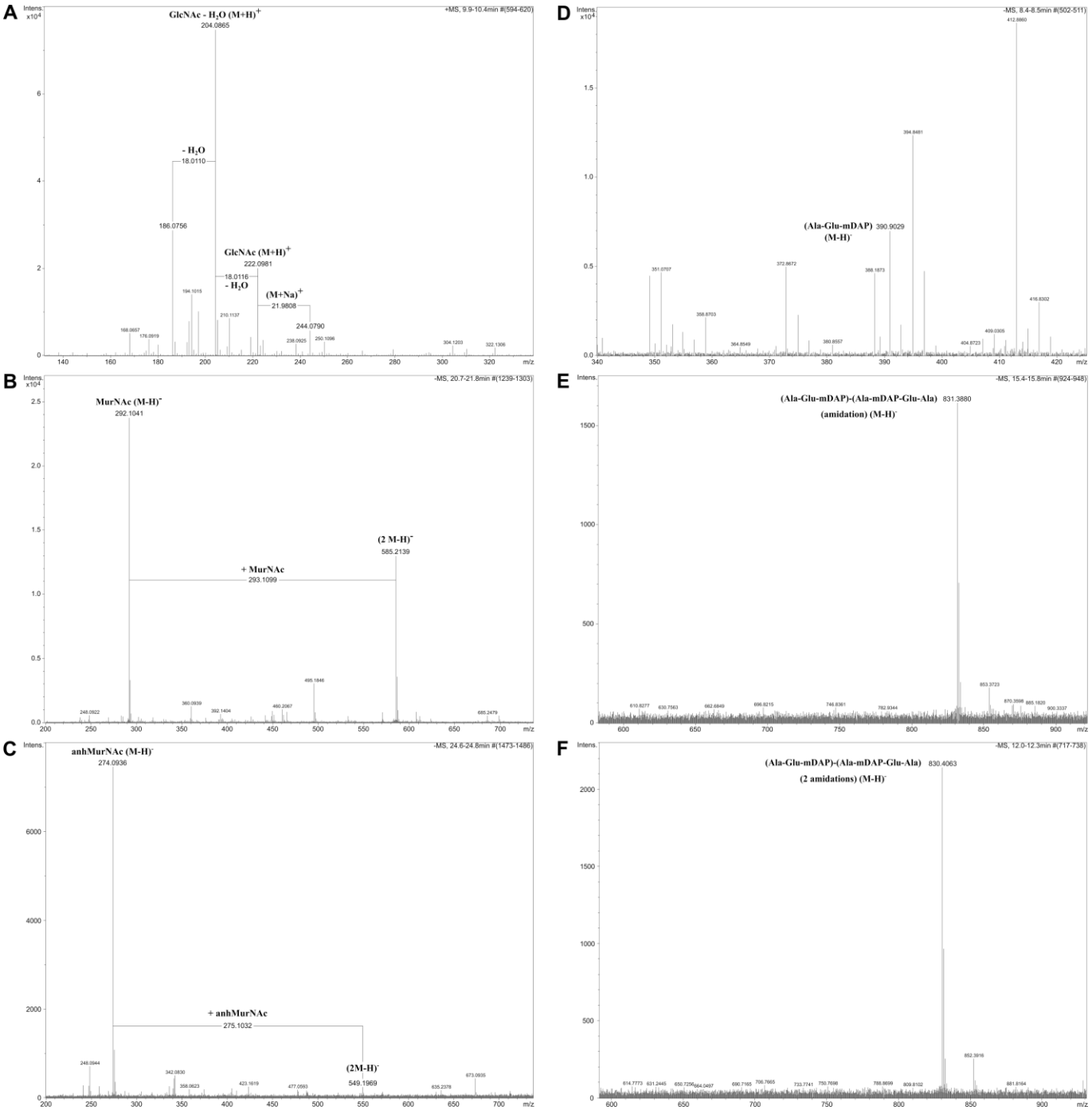

Figure 40 | Mass spectra of HPLC-MS analysis of sequential digest of *B. subtilis* peptidoglycan with NagZ, AmiE and NamZ. The following cell wall sugars and peptides could be identified: **(A)** GlcNAc was identified by measured mass of $(M+H)^+$ 222.098 m/z. Additionally, product masses for sodium adduct $(M+H)^+$ 244.079 m/z and water elimination appeared. **(B)** MurNAc was identified by measured mass of $(M-H)^-$ 292.104 m/z. Additionally, product mass for MurNAc dimer appeared (2 M-H)$^-$ 585.214 m/z. **(C)** AnhMurNAc was identified by measured mass of $(M-H)^-$ 274.094 m/z. Additionally, product mass for anhMurNAc dimer appeared (2 M-H)$^-$ 549.197. **(D)** Tripeptide with one amidation was identified by measured mass of $(M-H)^-$ 388.187 m/z. **(E)** Tri-tetrapeptide with two amidations was identified by measured mass of $(M-H)^-$ 830.406 m/z. **(F)** Tri-tetrapeptide with one amidation was identified by measured mass of $(M-H)^-$ 831.388 m/z. All products of sequential digest are shown as extracted ion chromatograms (EIC).

Table 11 | OD_{600} values for growth of cannibalistic mutants in LB medium.

h	wild type	168-Δ*lytABC::neo*Δ*lytD::tet* Δ*lytE::cm*Δ*lytF::spec*	168-Δ*spo0A::erm*	168-Δ*skfA::erm*	168-Δ*sdpC::erm*	168-Δ*sdpC*Δ*skfA::erm*
1	0.06	0.06	0.07	0.12	0.05	0.04
2	0.11	0.21	0.21	0.15	0.16	0.12
3	0.46	0.85	08.5	0.70	0.63	0.50
4	0.96	1.40	1.44	1.20	1.06	1.00
5	2.10	2.55	2.90	2.25	2.20	2.05
6	4.00	4.30	4.50	4.10	3.40	2.90
7	4.70	4.70	5.30	4.50	4.90	4.50
8	5.50	5.70	5.90	5.80	5.60	5.50
24	6.40	6.50	2.70	5.60	5.60	6.00
26	5.90	6.30	2.60	5.70	5.60	6.00
28	6.10	6.30	2.70	5.00	5.50	5.70
30	5.00	6.50	3.40	4.90	4.80	4.80
32	4.80	6.90	4.40	4.60	4.50	5.10
48	2.40	7.90	22.00	14.00	3.00	6.50

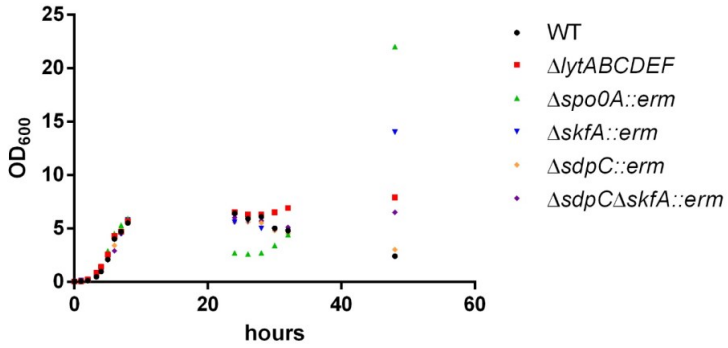

Figure 41 | Monitoring of growth of different *B. subtilis* strains. OD measurements are shown without logarithmic calculation.

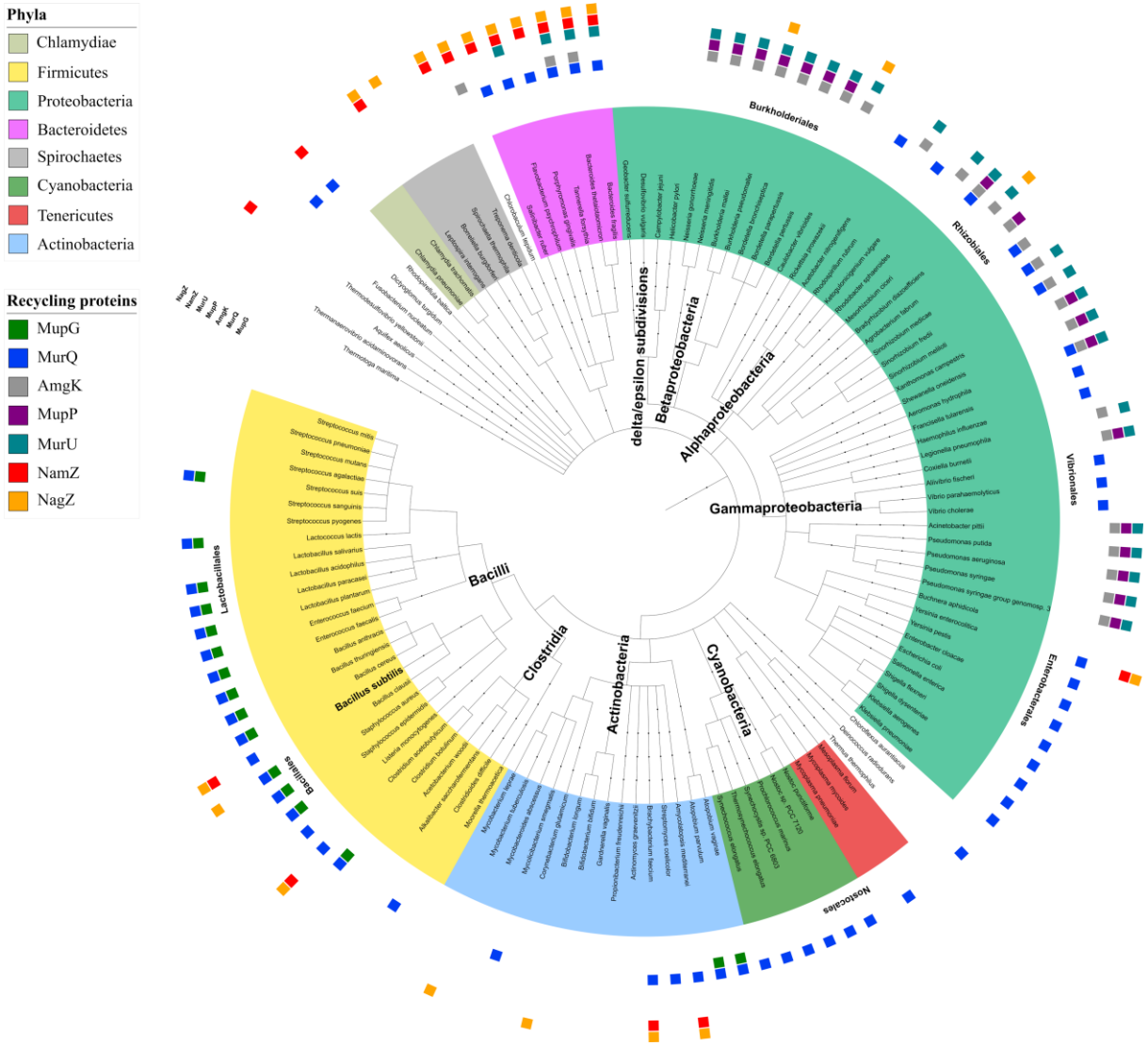

Figure 42 | Phylogenetic tree depicting the distribution of NamZ as well as other peptidoglycan recycling-associated proteins (Müller *et al.* 2021)**.**

Danksagung

An dieser Stelle ein großes Dankeschön an all diejenigen, ohne die diese Arbeit nicht zustande gekommen wäre.

Zuerst möchte ich mich bei meinem Doktorvater Prof. Dr. Christoph Mayer für die Betreuung dieser Arbeit bedanken. Danke für die Möglichkeit mein Thema nach meiner Masterarbeit in deiner Arbeitsgruppe weiterzuführen. Danke für all die fachlichen Ratschläge, hilfreichen Anregungen, wissenschaftlichen Diskussionen und deine freundliche Art.

Des Weiteren möchte ich mich herzlich bei Prof. Dr. Karl Forchhammer dafür bedanken, dass er sich als zweiter Berichterstatter zur Verfügung gestellt hat.

Für die finanzielle Unterstützung bedanke ich mich beim GRK 1708 und der Deutschen Forschungsgesellschaft.

Ein großes Dankeschön an die gesamte AG-Mayer mitsamt aller Ehemaligen für das Schaffen einer großartigen Atmosphäre, das offene Ohr bei Fragen und Problemen und die Anregungen und Ratschläge in den Seminaren. Danke an Marina Borisova-Mayer, Isabel Hottmann, Robert Kluj, Simon Friz, Axel Walter, Katja Balbuchta, Alicia Engelbrecht und Tim Teufel für die Unterstützung bei dieser Arbeit, die großartige Zeit im Labor, die Kaffeepausen, die vielen Ratschläge und die Erlebnisse auch außerhalb des Labors!

Ich danke auch den besten Freunden, die man sich wünschen kann. Ihr habt, mich während dieser Zeit durch Hochs und Tiefs begleitet, unterstützt, die Motivation hochgehalten und die Abstinenz an Wochenenden einfach akzeptiert.

Besonderen Dank an meine Eltern, die mich immer unterstützt und an mich geglaubt haben. Danke, dass ihr immer hinter mir gestanden seid; ohne euch und eure Unterstützung wäre ich niemals so weit gekommen.

Vielen Dank Benni, dass du immer an mich geglaubt hast, mir den Rücken freigehalten hast und mit mir im selben Boot sitzt. Danke für alles!